Tomas Bata University in Zlín
Faculty of Technology

Doctoral Thesis

Binder Systems for Powder Injection Moulding

Polymerní pojiva pro vstřikování práškových materiálů

Davit Bleyan

Submitted to Tomas Bata University in Zlin
Faculty of Technology
Zlin 2015

Doctoral study programme: P2808 Chemistry and Materials Technology
2808V006 Technology of Macromolecular Substances

Supervisor: Prof. Ing. Berenika Hausnerová, Ph.D.

Keywords: powder injection moulding; binder system; debinding; specific interactions; adhesion; thermogravimetric analysis; FTIR; calorimetry; contact angle

Klíčová slova: vstřikování práškových materiálů, pojivo, odstraňování pojiva, specifické interakce, adheze, termogravimetrická analýza, FTIR, kalorimetrie, kontaktní úhel.

CONTENTS

ABSTRACT

Powder injection moulding (PIM) is a net shape, multi-stage production technique for manufacturing complex geometry parts in high production volumes. PIM process involves four main production stages: mixing, injection moulding, debinding and sintering. For such multi-stage processing technique, the deliberate choice of component materials can significantly reduce the defect formations during consequent stages, as well as positively influence the energy efficiency, while reducing processing time.

The aim of the thesis was to study the role of particular binder components and their interactions with mould channel walls, for development of a novel, environmentally friendly feedstocks.

For novel binder systems polyethylene glycol was used as plasticiser which allowed using water for solvent debinding, instead of highly reactive chemicals (acetone, hexane, heptane). Different molecular weight PEGs served for balancing the initial weight loss during thermal debinding, ensuring gradual binder extraction. The use of carnauba wax as another binder component was motivated by the aim to lower the mixing temperatures, which is crucial for using advanced reactive fillers such as titanium. Further, it allowed replacing the synthetic backbone polymers by eco-friendly renewable natural components, increasing the environmental sustainability of this technology. The debinding characteristics of newly composed feedstocks were studied using thermogravimetric analysis. The results have shown that carnauba wax exhibited superior debinding properties compared to polyethylene and paraffin wax, with gradual thermal extraction up to late debinding stage.

Further, alongside carnauba wax, another novel binder – acarawax was considered as a substitute for polyolefins. In order to study the feedstocks in detail, the adhesion between binder system components, as well as binders, powders and the mould materials was investigated. Contact angle analysis was performed, and using acid base model, surface energies were evaluated. Binders showed similar values with only exception of PEG and to some extent acrawax which exhibited much higher surface energies and polar component values. Among mould materials the heat-treated steel showed the highest value of surface energy, and noticeably higher polar component too. For the ceramic powders Al_2O_3 and ZrO_2 the obtained values were rather similar.

For studying the interactions and chemical mechanism occurring within binder system, the components were substituted with their low molecular analogues. The specific interactions of the substitutes were evaluated using combined FTIR and analogue calorimetry. The highest cross interaction values suggesting strong interactions were obtained for analogues of PEG and acrawax.

This study provides an important understanding of the role of particular binder system components and their interactions, which will allow to precisely balancing the feedstock composition, positively influencing the energy efficiency and processing properties of a PIM cycle.

ABSTRACT IN CZECH

Vstřikování práškových materiálů (PIM) je velkoobjemový, vícestupňový proces pro výrobu přesných kovových a keramických dílů komplexních tvarů. Proces PIM se skládá ze čtyř etap: míchání, vstřikování, odstraňování pojiva a slinování. U vícestupňové technologie je rozdílnými požadavky vyplývajícími z jednotlivých výrobních fází komplikován výběr vhodných materiálů.

Cílem této práce je sestavit novou, ekologicky přijatelnější recepturu polymerního pojiva a přispět k porozumění úlohy jednotlivých pojivových složek v PIM směsi, jejich vzájemných interakcí, i interakcí s prášky a materiály používanými pro konstrukci vstřikovacích forem.

Pro nové systémy pojiva byl použit jako plastifikátor polyetylénglykol (PEG), který je odstranitelný rozpouštěním ve vodě (narozdíl od běžně využívaných parafínických vosků chemicky odstranitelných v acetonu, hexanu či heptanu). Různé molekulové hmotnosti PEG byly testovány i z hlediska bilancování hmotnostních úbytků během tepelného odstraňování pojiva.

Použití karnaubského vosku jako další pojivové složky bylo motivováno snahou snížit teplotu míchání PIM směsí, což má zásadní význam pro použití pokročilých reaktivních prášků jako jsou titanové slitiny. Dále je takto umožněno nahrazení tzv. páteřní (backbone) pojivové složky (termoplastické nebo termosetické) ekologicky přijatelnějšími substancemi, což zvýší ekologickou šetrnost této technologie.

Charakteristiky odstraňování pojiva nových systémů byly studovány pomocí termogravimetrické analýzy. Výsledky potvrdily, že karnaubský vosk vykazuje pozvolnější odstraňování ve srovnání s nízkohustotním polyetylénem či parafínickým voskem.

Adheze mezi jednotlivými komponenty pojiva, prášky (Al_2O_3 a ZrO_2) a materiály používanými na výrobu vstřikovacích forem byla zkoumána prostřednictvím měření kontaktního úhlu. V této fázi výzkumu byla testována možnost využití další nové pojivové složky –acrawaxu (N, N'-Etylén Bis-stearamid). Byla provedena analýza povrchových energií s tím, že nejnižší byly vypočítány pro nitridované a TiN kalené povrchy, zatímco zušlechtěný povrch vykázal nejvyšší hodnoty povrchové energie i výrazně vyšší hodnoty jejího polárního komponentu. Pro keramické prášky byly hodnoty povrchové energie přibližně stejné. Pojiva se v hodnotách povrchových energií též příliš nelišila, jedinou výjimkou byl PEG, který vykázal výrazně vyšší hodnoty povrchové energie i hodnoty jejího polárního komponentu.

Pro studium interakcí mezi jednotlivými pojivovými komponenty (PEG, karnaubský vosk a acrawax) bylo použito nízkomolekulárních analogů. Specifické interakce analogů byly vyhodnoceny pomocí FTIR a kalorimetrie. Interakce analogů PEG a acrawaxu byly přibližně dvakrát silnější, než je tomu u dvojice analogů PEG-karnaubský vosk.

Tato studie představuje důležitý příspěvek k porozumění úlohy jednotlivých komponentů PIM pojiv, které umožní přesně vyvážit složení systému, a následně tak pozitivně ovlivnit zpracovatelské vlastnosti PIM procesu.

LIST OF PAPERS

The following papers are included in the presented doctoral thesis.

I **Polyolefin Backbone Substitution in Binders for Low Temperature Powder Injection Moulding Feedstocks**
Hausnerova, B.; Kuritka, I.; Bleyan, D.
Molecules 2014, *19*, 2748-2760.

II **Specific Interactions of Low Molecular Weight Analogues of Carnauba Wax and Polyethylene Glycol Binders of Ceramic Injection Moulding Feedstocks**
Bleyan, D.; Svoboda, P.; Hausnerova, B.
Ceramics International 2015, *41*, 3975-3982.

III **The Development of Powder Injectionmoulding Binders: A Quantification of Individual Components' Interactions**
Bleyan, D.; Hausnerova, B.; Svoboda, P.
Powder Technology 2015, 286, 84-89.

IV **Surface Adhesion between Ceramic Injection Molding Feedstocks and Processing Tools**
Bleyan, D.; Hausnerova, B.; Kasparkova, V.; Pata V.
Submitted to Ceramics International

V **PIM Binder System with Advanced Adhesion**
Hausnerova, B.; Bleyan, D.
Patent Application Submitted

1. THEORETICAL BACKGROUND

1.1. Binder role in particular PIM steps

Powder injection moulding (PIM) is a challenging technique derived from plastic injection moulding, delivering complex and high precision parts by a multi-stage powder forming process [1]. It gains a superior attention, since it plays a crucial role for production of medical, dental, aerospace, and automotive in high production volumes with low time consumption and processing cost. Parts produced by PIM can be composed of carbon steels, low alloy steels, stainless steels, low expansion alloys, tool steels, soft magnetic alloys, super alloys, and ceramics.

This technique is also known for reduction of production waste and cost, since parts are manufactured close to their theoretical net weight. The combination of various operations makes PIM cost efficient and is often recognized as a technology having minimal negative ecological impact, compared to other manufacturing techniques (casting or machining). PIM is of a crucial importance for modern manufacturing industry, since without it many applications would be more expensive or, in some cases would simply be impossible to be manufactured by other means of fabrications [2].

During PIM process a powder (at 55 – 70 vol.%) is mixed with binder system to create a homogeneous feedstock, which is pelletized and moulded into the desired shape (Figure 1) [3]. After parts are moulded, the binder system is extracted using solvent and/or thermal debinding. Debound parts are sintered at elevated temperatures (up to 1650 °C in case of ceramics) to adhere powder particles at molecular level to near the theoretical density [4,5]. Figure 2 shows the appearance of PIM feedstock and a turbocharger rotor made using PIM technology.

Having different role at each processing stage, the binder system often has contradictory or inconsistent requirements to its composition, since it must ensure agglomeration-free sufficient wetting and uniform distribution of powder particles within feedstock during mixing, and provide the feedstock with moderate viscosity during injection moulding at low temperatures [3]. Fail to reach those properties will result in separation, segregation, and agglomeration [6]. Then, during early debinding it must have steady thermal degradation properties and high fluidity to create a pore network within the part to ensure defect free extraction of a backbone binder at late debinding stage. Lack of successful extraction of the binder may result in cracks, voids, distortions, non-uniform shrinkage and warping in the final products [7-9]. At the same time, backbone binder component must remain in a small amount up to early sintering stage, to retain the shape of the part before powder particles are bonded. Such a multi-step processing approach necessarily requires high accuracy, especially on early phases, since fault during composing the feedstock cannot be eliminated during consequential stages [10].

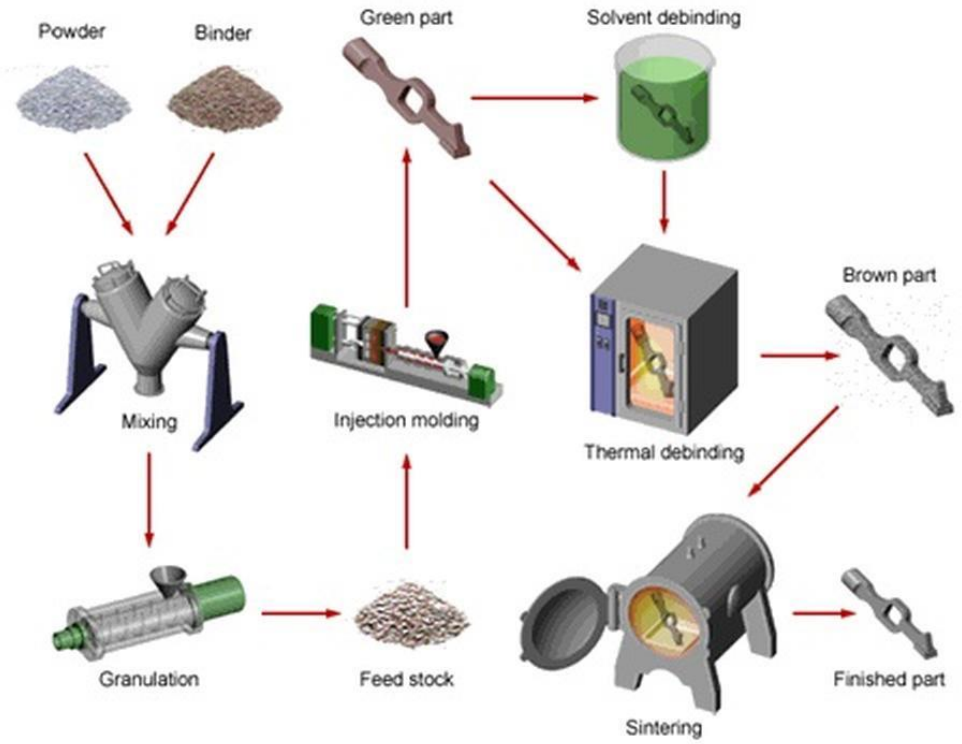

Figure 1. Powder injection moulding process [3].

Due to complexity of their role, PIM binder systems consist of various polymers, waxes and processing aids [11]. In PIM, polyolefins such as polyethylene (PE) and polypropylene (PP) are widely used as binder system backbones [4], while paraffin wax (PW) often serves as a plasticiser together with small amount of processing aid, typically stearic acid (SA) [12].

Figure 2. Pelletized PIM feedstock (left) and turbocharger rotor made using PIM technology (right) [13].

1.1.1. Mixing

In PIM the mixing stage is of a crucial importance, since the inconsistencies in the feedstock cannot be eliminated during any of the consequent processing stages. Various mixing techniques and equipment are used in PIM. The Z-blade mixers and twin extruders are commonly used. The mixing of the powder and the binder should result in a homogeneous product, and ensure sufficient powder particle coating with the binder, avoiding uneven distribution and particle agglomeration [3]. Mixing must be processed above melting temperatures of the binder components for ensuring uniform coating of all powder particles. Uniformity of the feedstock is required in order to control the moulding stage and the shrinkage behaviour. The inconsistent mixing may result in voids, cracks and distortions in moulded parts which lead to warping and non-uniform shrinkage of the sintered parts [14].

Specific binder system components such as SA can highly influence the mixing stage. Li *et al.* [15] investigated effect of different SA content in feedstock based on 17-4PH stainless steel and paraffin wax-based binder. It was found that a tailored content of SA can decrease the viscosity of the feedstock and improve the dispersability of the powder and increase the critical solid loading due to the enhancement of interactions between the powder and the binder. The FTIR measurements showed that chemical adsorption occurs between SA and powder surface after mixing, reinforcing the interacting force between the powder and the binder. The experiments [16] showed that about 5 wt.% of SA is the optimal amount for improving the wettability of the binder and enhancing the processing properties of the feedstock. Other researchers confirm the positive effect of using 5 wt.% of SA such as improved wettability and better rheological stability [17].

Fan *et al.* [18] studied the effect of SA on feedstock mixing and particle size distribution. The results showed that addition of 1 % SA leads to easier mixing and better feedstock fluidity, and is able to noticeably improve the compatibility of the powder and the binder. Figure 3 shows the schematic diagrams of torque evolution during feedstock mixing for a) feedstock without SA and b) feedstock with SA. It was found that at lower temperatures (<125 °C), the feedstock containing SA has improved rheological performance over the feedstock without SA, whereas at higher temperatures (>125 °C) the situation is vice versa. This work also claims that addition of SA can reduce the temperature required for injection moulding and such feedstocks are more suitable for feedstocks based on ultrafine powders.

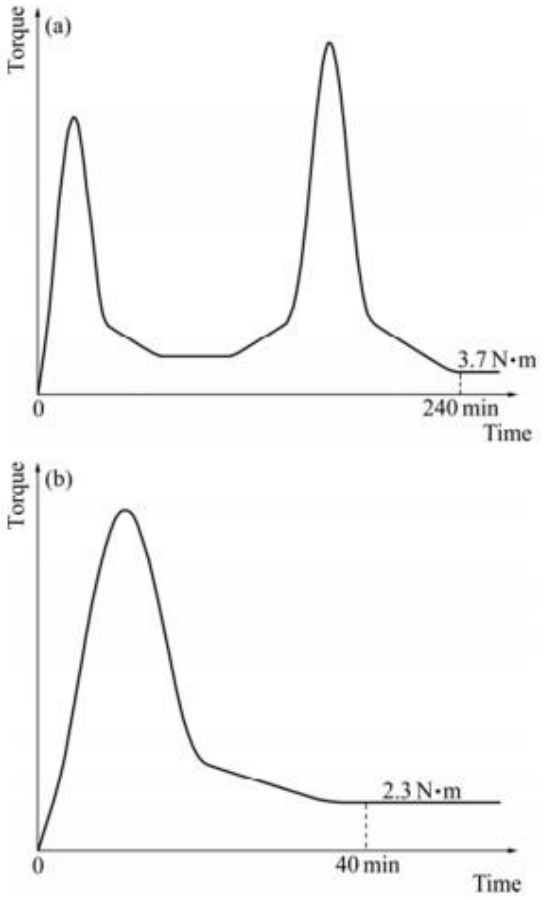

Figure 3. Schematic diagrams of torque evolution during feedstock mixing: a) feedstock without SA; b) feedstock containing SA [18].

1.1.2. Injection moulding

The injection moulding parameters highly depend on the binder composition. The moulding process can be characterized by the moulding pressure: high pressure injection moulding (HPIM) and low pressure injection moulding (LPIM) [19]. HPIM is suitable for the feedstocks containing thermoplastic backbones in their binder systems, and usually it is carried out at the temperatures 120 to 220 °C. LPIM is used for the feedstocks based on paraffin wax or water soluble binders at the temperatures below 100 °C.

Hausnerova *et al.* [20] studied feedstock based on aluminum oxide and multicomponent water-soluble polymer binder by examining the pressure-volume-temperature (PVT) characteristic. In high-pressure moulding process the feedstock is in pressurized melt form, which can be characterized with flow behaviour and compressibility. The hydroscopic fine alumina powder and binder, sensitive to destabilization in water, often result in high viscosity, which can be reduced with dispersants and lubricating agents. In this study only 1 wt.% of oleic acid lowered the viscosity, enhanced the processing properties and ensured the mouldability of the feedstock.

Ahn *et al.* [21] have investigated feedstocks composed of powder with different combinations of binder systems and a binder system with different combinations of powder systems, with an objective to optimize functions such as binder system composition, feedstock composition, part geometry and injection moulding process. The influence of the powder/binder combinations on the rheological behaviour and thermal stability of powder were evaluated. The characterization of the feedstocks and the simulation analyse revealed that the injection moulding pressure-related parameters such as wall shear stress, injection pressure, and clamping force were dependent rather on the binder system, than on the powder characteristics, in the range of particle attributes studied. For the temperature-related parameters such as melt front temperature difference and cooling time, binder selection was also found to be more critical than powder selection.

1.1.3. Debinding

Prior taking the moulded parts to sintering temperatures, the binder must be removed from the components without disrupting their shape. When binder is heated, it softens often resulting in inability to withstand the stresses arising from gravity, temperature gradients or internal vapour pockets [22]. Lack to meet the required debinding properties may result in defects such as blistering, cracks, slumping and deformations, as well as moulded components would have poor mechanical properties and show dimensional distortions.

Also, it should be noticed that a size of moulded compound depends exponentially on time needed for removing the binder system [23]. Two general debinding routs are identified based on a thermally activated process or solvent extraction [3]. Other types such as catalytic debinding or vacuum debinding are also used and investigated, but even in such cases the removal is thermally activated (Table 1).

Table 1. Overview of debinding methods [3].

Debinding	Solvent	Immersion
		High pressure
		Thermally assisted
	Thermal	Diffusion
		Permeation
		Wicking

1.1.3.1. Solvent debinding

Use of complex binder systems with various types of components often results in a need of multistep processing. Solvent debinding methods evolved as an alternative for removing the binder, reducing the risks of defect formation found in thermal debound parts [24]. During solvent debinding process each fraction of the binder system can be removed using various solvents [25]. Often used solvents include organic compounds such as acetone, hexane, heptane, octane or trichloroethane as well as water [26-28]. The use of heated solvent may considerably increase the extraction rate. At the point where a soluble fraction of the binder has been removed, a network of interconnected pores is created within the moulded part [29]. The following thermal cycle employed to remove the remaining binder can be as short as 3 to 4 h [30].

Solvent debinding can be expressed in four consequential steps [31]: (1) solvent molecules penetrate into the binder, transforming into swollen gels; (2) gel disintegrates, becoming in a state of a solution; (3) solution diffuses from the centre towards the surface; (4) solution is diluted from the surface into a solvent bath.

Binder removal using solvent debinding can cause a raw of issues connected with binder swelling and softening. The extent of the polymer crystallinity and cross-linking partly determine the solvent polymer interactions [30]. The evolution of the effect of swelling on dimensional changes was investigated for wax-polymer binder system solvent debound in heptane [31]. Measuring the dimensional changes using laser dilatometry at various solvent temperatures, it was found that shrinkage also occurs at the end of the debinding run. The stress concentrations from shrinkage may result in cracking or distortions. Meanwhile it is suggested that using higher solvent temperatures may minimize the chance of cracking [32].

Majority of organic solvents used for solvent debinding is flammable, carcinogenic and ecologically unfriendly. To eliminate their use, water soluble PEG can be introduced to binder systems [33]. In such systems the debinding starts with water diffusing into PEG, turning it into a gel (Figure 4). In case that the attraction between PEG and water molecules is larger than the interactions between polymers, second stage of binder dissolution can occur. At this stage gel disintegrates into a solution, where the absorbed water content can be defined as equilibrium water content (*EWC*) [34]. It is noticed that the dissolution of PEG starts when the water concentration in PEG gel is larger than the *EWC* of PEG.

$$EWC = \frac{\text{weight of swollen gel} - \text{weight of dry gel}}{\text{weight of swollen gel}}$$

At the intermediate stage the PEG molecules swell gradually to form gel from the surface towards the centre of the part, when the PEG molecules came into contact with water and the swell forces the part to expand continuously [33]. As it can be seen, the interconnected pore channels are formed, which can serve as escape paths for decomposed gas during subsequent thermal debinding for insoluble binders components.

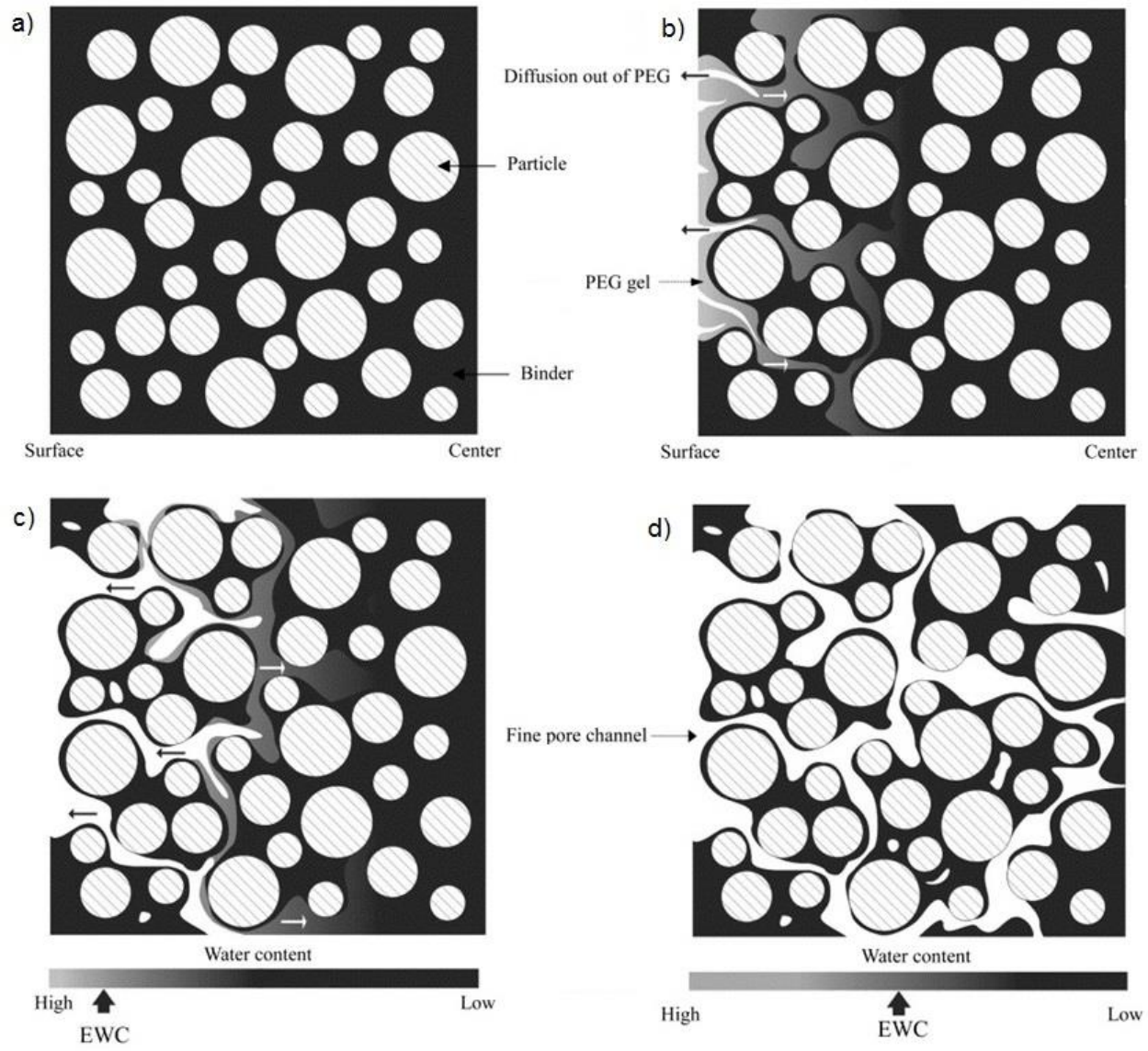

Figure 4. Schemas of binder distributions at the (a) as-moulded, (b) initial, (c) intermediate and (d) final stages of solvent debinding based on water extraction [33].

1.1.3.2. Thermal debinding

Due to its simplicity, thermal debinding is a core process widely used for a binder removal [3]. During this stage the moulded component is heated at a slow rate, allowing gradual evaporation of the major binder fraction (at first a low molecular weight), creating a network of pores within the part. For binder systems with a single binder component, the binder decomposes at the binder-gas interface and the evolving gas diffuses or penetrates from the centre towards the surface of the compound through the inter-particle voids. The rate of vapour removal from the compact will depend on the frequency of collisions between molecules or molecular impact with the pore walls.

The thermal debinding cycle includes three main stages. First stage involves thermal expansion of powder and binder, where the binder melts. The thermal expansion difference between powder and binder may result in a pressure build up. Depending on the amount of pressure and the thickness of the part, it can lead to a slumping. Multicomponent binder systems are composed in order to accommodate this effect, since different components have different thermal characteristics, meaning that while one component of binder system is melting, the other one retains the part shape. At the second stage, the increased temperature results in evaporation of a low molecular weight component at the surface. Using capillary forces liquid binder travels from the centre of the part towards the surface where it evaporates. This process results in formation of a pore network, which allows faster evaporation within the part and escape of vapours. In case the binder is extracted too quickly, cracking and blistering will occur. During the final, third stage, thermal decomposition of binder takes place at higher temperatures. The created network of pores allows faster removal of remaining binder without a risk of cracking or blistering.

Three different transport mechanisms are defined for thermal debinding: diffusion, permeation and wicking. For compounds with small pore sizes, the debinding rate is diffusion-controlled. Compounds with larger pore sizes tend to a permeation controlled debinding, while the pore size is defined by the particle size and particle size distribution. For short debinding times, high pressure gradients and high debinding temperatures will deliver larger gaseous phase volumes and higher diffusion rates. Using components with large particle sizes may highly enhance the binder extraction rate. Wicking controlled debinding is based on the flow of the softened binder due to capillary action promoted by a substrate. As for gaseous transport by diffusion or permeation, larger particle sizes in the compact promote faster debinding, since the binder is removed in the liquid state, varying the debinding time linearly. Since the viscosity decreases with increasing temperatures, higher debinding temperatures may noticeably shorten the required debinding time. It was also found that the heating rates can be accelerated by increase of the boiling point of the binder system components [35].

An example of a stepwise thermal debinding designed for carbonyl iron feedstock with binder system including LDPE, AW, SA and diethyl phthalate (DEP) can be seen on Figure 5 [36]. In order to analyse the thermal debinding behaviour of the feedstock, TGA must be carried out [36-38]. Figure 6 shows the TGA curves of stainless 316L steel based feedstock with binder system consisting of PP/PW/SA [39]. From the plot two decomposition steps can be distinguished; at first, due to their low molecular weight, PW and SA decomposed in the range from 180 to 350 °C,

following with the second step in range from 350 °C to 460 °C, which corresponds to decomposition of higher molecular weight PP.

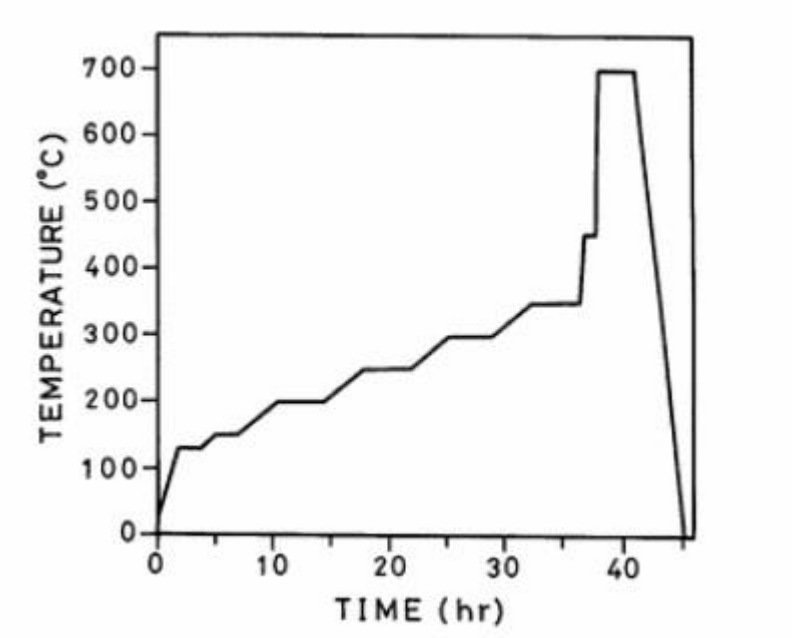

Figure 5. Thermal debinding schedule designed for LDPE/AW/SA/DEP binder system [36].

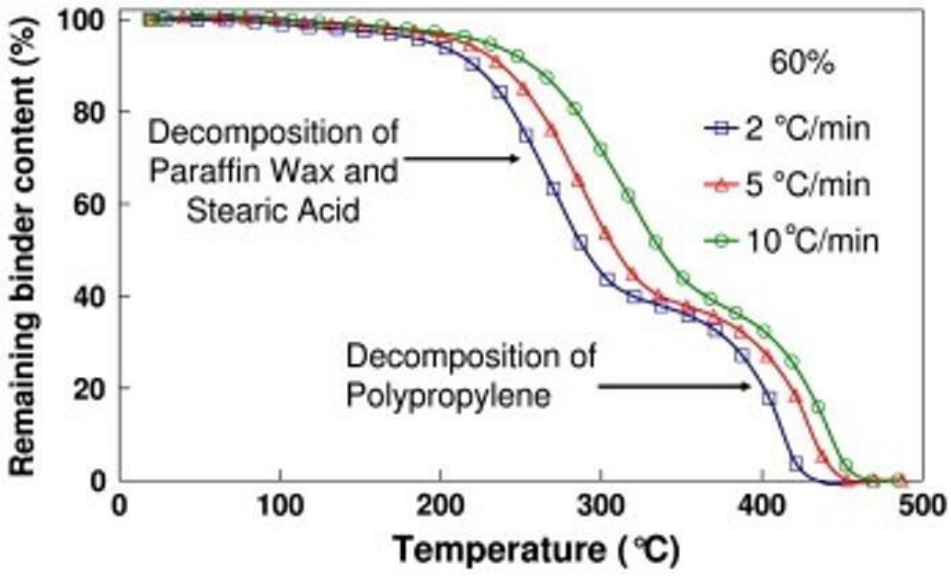

Figure 6. Remaining binder content curves vs. temperature at different heating rates for 316L stainless steel in argon atmosphere [39].

1.1.4. Sintering

Sintering is a thermal treatment for bonding the particles into a coherent, predominantly solid structure via mass transport events which often occur on the atomic scale [3]. Figure 7 shows the sintering stages starting with the loose powder and subsequent sintering in each of the three stages. The initial open pore structure and high porosity are consumed by interparticle neck growth, grain growth, and pores shrinkage, with eventual formation of closed spherical pores in the final stage [40].

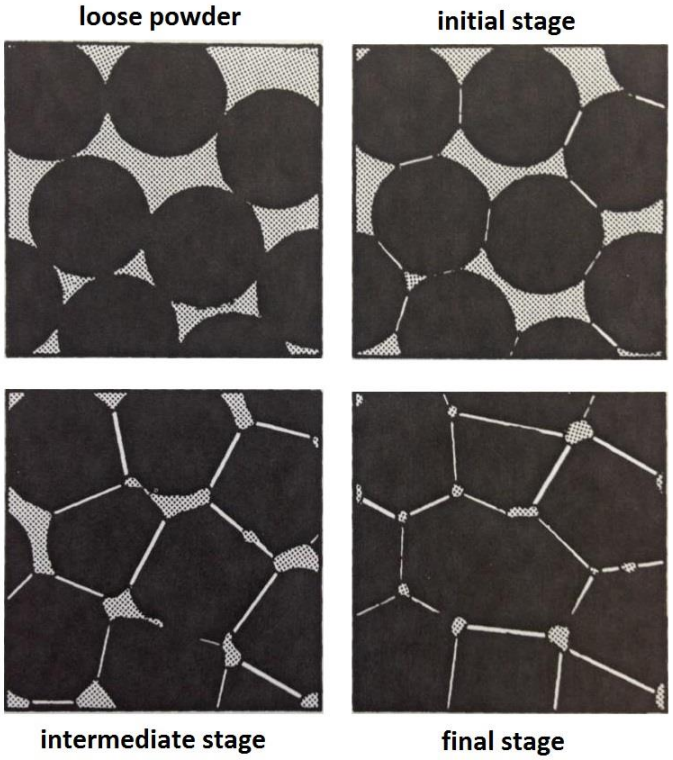

Figure 7. The stages of the particle sintering [40].

It is typical for particles to sinter bonds together when they are heated to relatively high temperatures. Sintering can be carried out in vacuum or under various gas atmospheres, depending on the type of the material. The common iron powders are sintered at the temperatures around 1200 °C, while higher temperatures (up to 1650 °C) can be employed for titanium and tungsten based feedstocks under vacuum, argon, hydrogen or nitrogen atmospheres. Besides the powder shape and size, an important role in early sintering stage plays the binder backbone, which must hold the particles in their place until they can be still bonded at higher temperatures.

1.2. Properties and application requirements for binders

1.2.1. Binder system

As already stated, the binder system is of a crucial interest in PIM, since it provides the processing properties to the feedstock and determines whether composition can be applied. Typical binder system includes a backbone, plasticizer and processing aid. Table 2 shows examples of polymers, waxes and processing aids employed in composing the binder system.

Table 2. Properties of commonly used PIM binder system components [41].

Name	Abbreviation	Density ISO 1133 [g/cm³]	Melting Temperature [°C]	Molecular Weight [g/mol]	Role
Polyethylene	PE	0.918	108	250000	Backbone
Polypropylene	PP	0.946	170	440000	Backbone
Polystyrene	PS	1.05	240	400000	Backbone
Ethylene-vinyl acetate	EVA	0.934	96	60000	Backbone
Poly(methyl methacrylate)	PMMA	1.18	160	30000	Backbone
Paraffin wax	PW	0.9	58	400	Plasticizer
Stearic acid	SA	0.85	70	284	Processing aid

The role of each component is defined according to its physical properties. The proper choice of a binder system components and their content is highly important in order to grant the feedstock sufficient wetting and lubrication, low viscosity and steady degradation properties [42].

1.2.1.1. Backbones

The role of backbones in feedstock is to remain in brown (debound) parts until late debinding and early sintering stage to hold the powder particles together before they can be sintered at higher temperatures. Thermoplastic polymers such as PP, PE, LDPE and HDPE are of a common use in PIM [43-45]. It has been shown [46] that higher molecular weight HDPE provides better dimensional stability and enhances the quality of green parts. In contrast, usage of LDPE results in favourable flow behaviour of feedstock giving advantages for the injection moulding stage. Meanwhile, due to their high molecular weight (over 250000 g/mol) polyolefins having relatively high viscosity and poor adhesion to polar powders, always require use of additional processing aids.

Poly(methyl methacrylate) is a polymer of high-average molecular weight which is often used together with PEG, providing stiffness and strength to the mouldings [47-50]. Furthermore, Singh *et al.* [51] showed that increasing the content of PMMA in a binder system containing PC and PMMA lowers the degradation temperatures linearly (Figure 8).

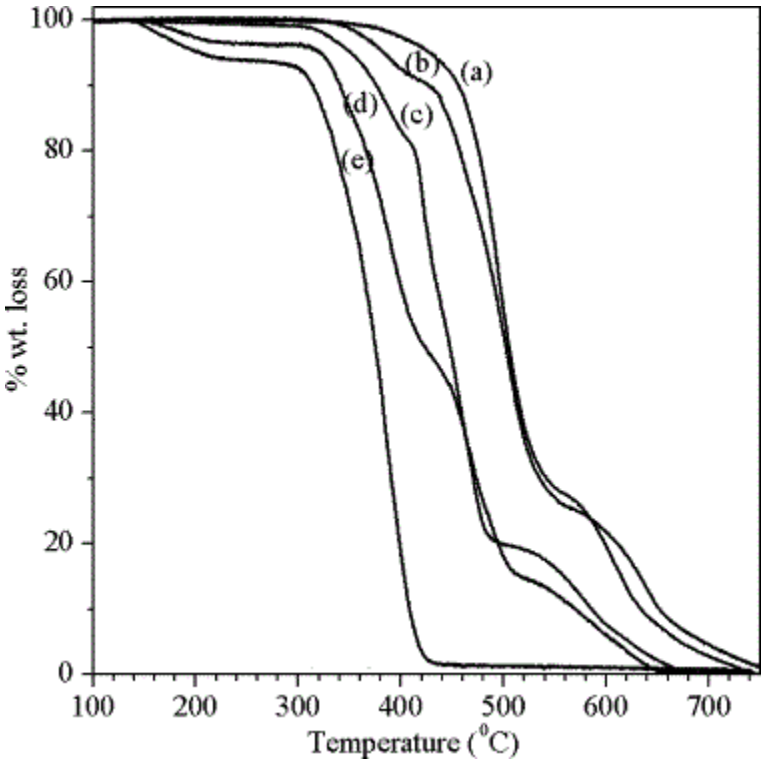

Figure 8. TGA curve of PC/PMMA blends: (a) pure PC, (b) PC/10PMMA,(c) PC/30PMMA, (d) PC/50PMMA blend, and (e) pure PMMA [51].

1.2.1.2. Plasticizers

In binder systems, paraffin wax (PW) often stands next to thermoplastic binders as a plasticizer. In such a feedstock it usually represents a major component of binder system (up to 65 wt.%) [52]. Processing of feedstocks containing PW can be highly time consuming, requiring two stage debinding, solvent extraction in hexane followed by thermal treatment under vacuum or argon atmosphere to possibly minimize the carbon and oxygen contents within moulded parts [53].

PEG is a water soluble plasticizer used in PIM. It is employed extensively in PIM process to eliminate the use of organic solvents, such as acetone and heptane, which are flammable and raise many ecological concerns. The solubility of PEG is highly affected by temperature. Use of low molecular weight PEGs (PEG 1000, PEG 1500) in binders, besides improving wetting and viscoelastic characteristics, highly advances the early debinding stage [54]. Rapidly melting at low temperatures (37 – 43 °C), it ensures sufficient pore formation during solvent debinding for

subsequent defect-less removal of remaining binder components [55]. The use of higher molecular weight PEG (PEG 8000) prevents binder separation and strengthens the mouldings [56].

1.2.1.3. Processing aids

Small amount (< 5 wt.%) of processing aid – Stearic acid (SA) can be often seen in feedstock compositions. Due to its particular structure, SA significantly reduces the friction force among the powder particles, allowing them to be distributed much more easily [57]. SA also enhances the adhesion between binder and powder particles by lowering the surface energy [58]. This results in improved mixing process and tailors the powder loading [59].

Another surfactant – oleic acid (OA) can be also seen used in binder systems [20,60] as processing aid. The comparative study of SA, OA and 12-hydroxystearic acid (HSA) effect on the flow behaviour of alumina feedstock, done by Tseng [61], showed that systems including SA exhibited superior pseudoplastic flow behaviour and lower viscosity over the systems with OA and HSA. Also, it was found that the yield stress and viscosity decrease proportionally with the increase in SA fraction. Meanwhile, another research done by Li *et al.* [15] discovered that excessive SA concentration (above 5 wt.%) can lead to multilayer coverage of the particles surface, and it has rather limited effect on further lowering the viscosity.

1.3. Interactions between feedstock components and feedstock components with mould channel walls

In PIM, the feedstock plays crucial role, determining the success or failure of the complex processing chain. The investigation of the interactions between feedstock components and mould materials is essential for injection moulding step.

1.3.1. Interactions between powder and binder system components

In PIM the interactions of powder and binder system components should be studied, based on a concern of powder/binder separation [62-64]. This phenomenon occurs during injection moulding stage due to non-uniform shear rates near the mould channel wall interface, leading to particle rotation and aggregation in the central plateau of the channel flow [65]. To avoid this, study of the cause of feedstock slip at the channel wall must be performed, while this parameter depends on both, feedstock components, as well as on the material of the channel and its surface treatment. In order to evaluate the parameter, the interfacial adhesion between two must be studied. The adhesion can be evaluated from the surface tensions of tested materials and their contact angles.

Yang *et al.* [66] studied the surface tensions together with the contact angles of PP, HDPE, PS and PMMA melts. The contact angle between PS, PMMA and mould materials were measured using sessile drop technique. The tangent of the included angle between the drop contour line and the solid surface line was calculated from the contact angle, as showed in Figure 9, where Υ_{SL} interfacial tension between solid and liquid, Υ_{LG} interfacial tension between liquid and gas or

vapour, Υ_{SG} interfacial tension between solid and gas or vapour, θ contact angle. The experimental results were used to build a mathematical model representing the relationship between surface tension and temperature of polymer melts. The increase of inter-force between melt–solid molecules was found to be higher than that between melt–melt molecules, suggesting that the internal molecules of melt will squeeze into a melt interface layer. The relation curves between the surface tension and time of four melts are achieved at a specific temperature. This study showed, that the surface tensions increase gradually, and reach static values with the increasing time, and the melt interface layer tends to extend leading to the smaller contact angle, and thus better wettability.

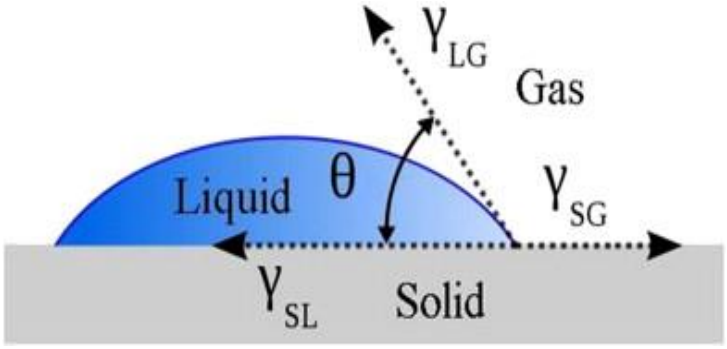

Figure 9. Contact angle at the liquid–gas–solid interface, where θ is degree of contact angle, Υ_{SL}, Υ_{LG}, Υ_{SG} are solid/liquid, liquid/gas, solid/gas interfacial tensions respectively [mN/m] [67].

Michalski *et al.* [68] investigated various methods for calculation of surface free energy of PVC/EVA polymer blends. The contact angles of standard liquids on the polymers have been measured at 20 °C inside a thermostatized ambient chamber by the sessile drop method. The testing liquids included water, glycerol, formamide, ethylene glycol, diiodomethane and a-bromonaphtalene. Van Oss treatment (Lifshitz and electron donor–electron acceptor components of surface free energy) and the Owens–Wendt treatment (dispersive and nondispersive components of surface free energy) calculation methods were used. According to the obtained results, the surface free energy were found to be greatly dependent on the calculation method and on the number of standard liquids used for contact angle measurements. All the calculation methods were in good agreement for the surface free energy of PVC, while by increasing the EVA content in the blends, a contradiction between the methods was found. Author suggests that there is not a definite solution for the calculation of solid surface free energy and development of existing models are required for achieving consistency in calculations of such important physicochemical quantities.

Ucar *et al.* [69] studied surface properties of ethylene vinyl acetate (EVA), polyvinyl acetate (PVAc) and high density polyethylene (HDPE) blends using contact angle analysis and X-ray photoelectron spectroscopy. Tested EVA samples varied in content of vinyl acetate (VA) in the range 12 to 33 wt.%. Thin layers of each blend were prepared from their xylene solutions at high temperatures by a dip coating technique. Static and dynamic contact angle measurements were carried out using grade water, methylene iodide, ethylene glycol and formamide liquids. The

obtained data showed that increase of polar hydrophilic VA in blend content resulted in a decrease of the water equilibrium contact angles.

1.3.2. Interactions between feedstock components and mould channel walls

Number of researchers have studied the liquid/solid interface interactions, via rheological approaches [70,71]. Silberzan *et al*. [72] reported on spreading behaviour of high molecular weight and low molecular weight polymers on high energy surfaces using optical microscopy and ellipsometry. The results showed that on the same kind of surfaces low molecular weight polymers exhibited more rapid spreading rate than the polymers with high molecular weight.

Schonhor *et al.* [73] studied the kinetics of wetting of high-energy (aluminum, mica) and low-energy (Teflon) surfaces by polyethylene and ethylene-vinyl acetate copolymer melts using contact angle measurements. However, the study concludes that the mechanism of wetting of liquids remained unknown, as well as no empirical rate law of wetting process could be evaluated.

In PIM, one of the main concern for studying liquid/solid interface interactions is the wall slip phenomenon [74,75]. Wall slip occurs when feedstock does not adhere to the mould channel walls, while instead moves in a narrow stream in a solid phase, and can be the main cause of jetting and raw of defects in the moulded parts, including weld lines and uneven shrinkage.

Krauss *et al.* [76] investigated the rheological behaviour of alumina feedstock with different loading levels (55-59 vol.%) by means of capillary rheometry. The multicomponent binder system used was based on PEG, polyvinylbutyral and SA. The measurements were performed at the temperatures 175, 180 and 185 °C. The results showed that feedstock with the lowest loading level (55 vol.%) exhibited the lowest viscosity, and has least chances of wall slip and jetting.

Often simulations and modelling are used for broader understanding of wall slip phenomenon. Pearson *et al.* [77] suggested that the ratio of molecule size to the wall surface roughness scale is of a key importance. For the cases where molecular size is smaller than the wall roughness scale, no effective slip can occur, while for the large macromolecules, slip is more likely to occur.

Jabbarzadeh *et al.* [78] studied the effect of wall roughness on the wall slip using a molecular dynamics simulation. Obtained results indicated that the wall slip increases with the size of molecules and the wall roughness period, while it decreases with increasing wall roughness amplitude, which was in agreement with the Pearson's theory.

Nevertheless, the analysis of interactions between feedstock components and mould channel walls are very scarce, and in order to precede in the research, the microstructure fluid-solid interface must be studied [79].

1.3.3. Interactions between binder system components

Complexity of demands on binder systems has always been a challenge for composing advanced feedstocks, since the required processing properties are usually achieved by using a

binder system consisting out of 3 to 5 different polymers, waxes and processing aids. This diversity of components makes it extremely difficult to study the complete and individual reaction pathways and chemical mechanisms occurring within such a system [80]. There are number of approaches for studying the binder systems. Rheological analysis using capillary rheometry is one of the most common measure of determining whether binder system is applicable, while dismissing is an investigation of interactions of particular binder components [81].

The degree of interactions between the polymers can influence the energy efficiency in applications by thermal storage of energy as sensible or latent heat in compounds, which go through phase changes near the required operating temperatures [82]. For investigation of specific interactions of nonpolar polymers such as PW and PE's (HDPE, LDPE and LLDPE), differential scanning calorimetry (DSC) and atomic force microscopy (AFM) has been used [83].

Melting point depression analysis via the Flory–Huggins approximation for thermodynamic mixing of two components was used to obtain the interaction parameters between PW and PE's. It has been found [83] that HDPE, LDPE and LLDPE are partially miscible with PW, with HDPE/PW having the weakest miscibility. Due to the influence of miscibility on the thermal behaviour of PW, it is suggested to use HDPE in PE/PW form-stable phase change materials in order to maintain the energy saving behaviour of PW.

Singh *et al.* [51] studied the specific interactions in partially miscible polycarbonate (PC) and poly (methyl methacrylate) (PMMA) blend. Different weight ratios of PC/PMMA blends were prepared by solution casting method using tetrahydrofuran as a solvent. Blends have been characterized using thermogravimetric analysis (TGA), DSC, FTIR and powder X-ray diffraction techniques. Obtained results suggested the presence of specific interactions between the PC and PMMA phases in the blends.

Sudhakar *et al.* [84] reported on miscibility of chitosan and PEG blend using a buffer solution. By collecting the FTIR spectra for polyblend films and polymers it was observed that by increasing the amount of PEG the O–H stretch peak tends to lower peak wavenumbers, serving as an evidence of blend components miscibility. Doulabi *et al.* [85] studied the miscibility of PEG and chitosan by using acetate buffer solution for different blend compositions. The viscosity, density, and refractive index were measured in order to quantify the interaction parameters. The results showed that the components at 80 % or higher chitosan concentration were miscible by means of intermolecular hydrogen-bonding interaction between hydroxyl groups of polyethylene glycol fumarate with amino and hydroxyl groups of chitosan.

Meanwhile, study of polymer interactions is a challenging and highly time consuming task requiring advanced knowledge, which also leads to proposal of numerical models to predict the feedstock properties [86-89]. Polymer–polymer miscibility guide developed by the group of Coleman and Painter [90] is one of the early predictive approaches, while mathematical models predicting the feedstock properties can never replace full, case specific research. There is a noticeable lack of efforts in studying the interactions between the binder system components, while the understanding of the interactions between binders system component can be the key for development of a novel binder system with advanced processing properties, making the feedstock highly robust and significantly shortening the overall processing time.

The substitution of polymers by their low molecular analogues can be used where the specific interactions between polymers cannot be studied by other means. This technique allows to eliminate the majority of self-interactions during cross-interaction measurements, which is not possible for polymer – polymer interactions evaluation [91].

1.3.3.1. Substitution of binder system components

Only few studies have considered the substitution of polymers with their low molecular analogues for investigation of specific interactions between theoretically immiscible polymers [91,92].

French *et al.* [93] employed the exothermic mixes of chemical analogue of poly(vinyl phenol) with analogues of polyacetal and poly(ethylene oxide) suggesting miscibility for the blends of poly(vinyl phenol) with polyacetal and with poly(ethylene oxide). It was found that the interaction parameter corresponding to the poly(vinyl phenol) and the poly(ethylene oxide) analogue mixtures is in agreement with the interaction parameter reported for the polymer mixtures, which was based on the melting point depression of poly(ethylene oxide) in blends with poly(vinyl phenol). Strong hydrogen bonding between phenol and ether groups in these analogue mixtures were observed using FTIR. It was predicted that a rather wide range of styrene-vinyl phenol copolymers would exhibit miscibility with polyacetal via application of the binary interaction model.

Svoboda *et al.* [91] investigated the miscibility window in the blends of poly(ε-caprolactone) and poly(styrene-co-acrylonitrile). Components were substituted by their low molecular weight analogues and corresponding to monomers of each polymer, since respective homopolymer pairs are not miscible. FTIR and calorimetric measurements were carried out for studying the interactions within the miscibility window in detail. Combination of FTIR measurements together with other techniques is often used for studying the specific interactions, where the shift of peaks is assumed as an evidence of a partial miscibility [94-96]. Analogue calorimetry is widely used as a tool for rationalizing and extending the results of polymer-polymer miscibility [97-99] and number of researchers reported on successful use of both (FTIR and calorimetry) for quantifying and evaluating the specific interactions [100-102].

In interaction studies, FTIR measurements are used as a tool for observing the peak shift for blend functional group. In order to calculate the self-interaction energy values low molecular analogues, ethylbenzene (EB) and propionitrile (PN) were diluted at 1 % concentration in buffer solution (hexane, decalin), and the peak shift is measured, Figure 10. For liquid–liquid interactions, the peak shift of O–H stretch bounding to lower wavenumber can serve as an evidence of present interactions. Svoboda et al. [91] gives a simple binary interaction model as one possible explanation for the miscibility window behaviour, based on consideration of an intramolecular interaction within the copolymer, in addition to intermolecular ones.

Bourara *et al.* [103] reported on FTIR peak shift in the hydroxyl region of blends of Poly(4-vinylphenol) (PVPh)/Poly(vinyl methyl ketone) (PVMK) blends in different ratios, Figure 11. It

can be seen that the absorbance of initially observed hydroxyl-hydroxyl associated stretching peak at 3361 cm^{-1} of pure PVPh decreases gradually and shifts slightly to a higher frequency with the increase of the PVMK content in the blend. This can be explained by formation of the hydrogen bonding that may occur between hydroxyl groups of PVPh and carbonyl groups of PVMK. Landry *et al.* [92] investigated the miscibility between polystyrene polymers containing potential hydrogen bond donor groups and other polymers that are good hydrogen bond acceptors. The thermodynamics of mixing of low molecular analogues of chosen organic polymers of interest were studied using calorimetric analysis. In blends which included both, substitute liquids and polymers, the strengths of the interactions with the acids were found to be different for esters and amides. Authors suggest that for forming miscible blends with strong, self-associating hydrogen bond donors, the preference must be set towards stronger bases, since the stronger interaction between the acid and the base helps to break up the self-associations. In this study [92] differential scanning calorimetry, together with infrared spectroscopy and optical transparency was used in order to investigate the miscibility of composed blends. The evaluation of interactions for the substitute liquids is thus considered useful for predicting the miscibility occurring between the corresponding polymers.

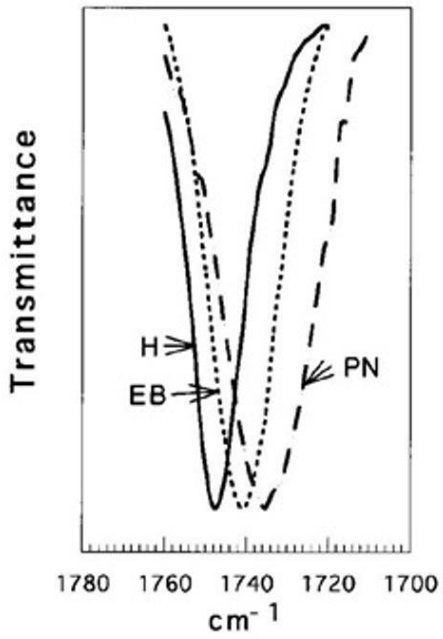

Figure 10. FTIR peaks of the carbonyl group C=O stretch of PP (1% solution) in hexane (H), ethylbenzene (EB), and propionitrile (PN) [91].

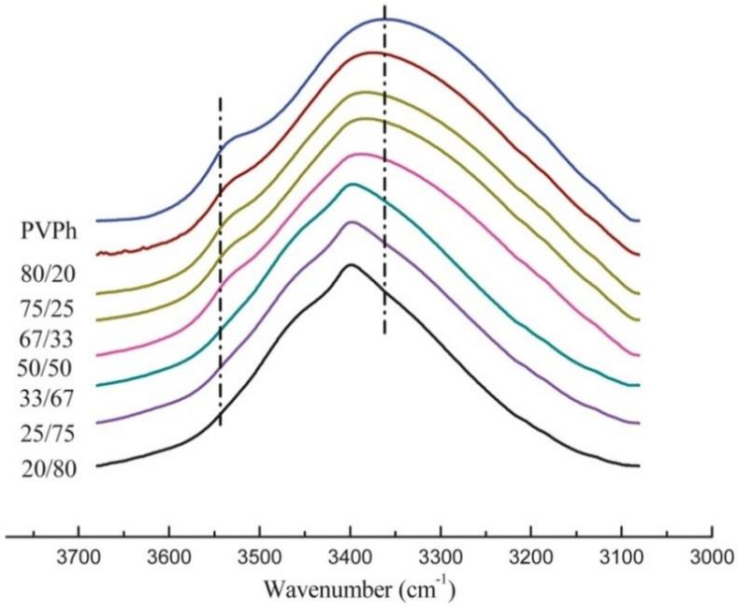

Figure 11. FTIR spectra of Poly(4-vinylphenol)/Poly(vinyl methyl ketone) blends in the 3050–3580 cm^{-1} region [103].

2. AIM AND METHODOLOGY OF THE WORK

Aim of this doctoral thesis is to study the role of particular binder components and their interactions in Powder Injection Moulding. The research will be focused on possibility of substituting common backbone polymers with novel compounds which can enhance overall processing properties, while remaining environmentally friendly.

Organic waxes will be considered, as well as low molecular weight binder components. The polar waxes should provide improved adhesion to the powder, which is crucial especially for superfine fillers. Simultaneously, they can be manufactured at lower temperatures, which is advantageous for energy consumption throughout the PIM process and for reactive powders as titanium alloys.

Polyethylene glycols with various molecular weights should provide advantage of early formation of pore network in moulded parts and enhance the debinding properties. In order to investigate the processing properties, feedstocks with different binder components ratio and varying in powder loading will be composed. The solvent debinding will be carried out using temperature controlled water bath in order to study extraction rate of the soluble binder components. Thermogravimetric analysis will serve as a major tool for understanding the thermal debinding characteristics of newly formed feedstocks. Obtained data should spread light on connections between feedstock powder loading, binder composition and binder extraction rate.

Literature search has shown that there is a lack of studies on interactions of binder systems components. Due to difficulty of studying the complete and individual reaction pathways and chemical mechanisms occurring within polymer blends, components will be substituted with their low molecular weight analogues. The interactions of substitutes will be investigated by means of FTIR and calorimetry. Dilution of low molecular analogues in non-interacting solution will be used for calculating the self-interaction energies. The amount of peak shift within functional group will indicate the presence of interactions. Obtained data from both FTIR and analogue calorimetry will allow a quantitative evaluation of specific interactions. This technique allows eliminating of the majority of self-interactions during cross-interaction measurements, which is not possible for polymer – polymer interaction evaluation.

Furthermore, another widely accepted concern of PIM process is the separation of powder and binder components during injection moulding stage. One of the factors is the adhesion of binder system to the mould channel walls resulting in significantly higher shear rates, initiating phase separation. In order to study the interaction between feedstock components and mould channel walls, contact angle analysis will be applied.

The results should contribute to understanding the role of particular binder components allowing to precisely balance the binder system composition for novel PIM feedstocks with advanced processing properties, while minimizing the negative ecological impact of technological cycle due to usage of eco-friendly components.

3. DISCUSSION OF THE RESULTS

Literature search showed [104-106] that waxes such as carnauba wax (CW) and acrawax (AW) have a perspective of taking over the role of backbone in binder systems, which can highly advance feedstocks with reactive fillers widely used in biomedical applications, and requiring low temperature processing [107].

First, low density polyethylene (LDPE) served as a main backbone component for comparison, since it has low molecular weight (compared to other binders from polyolefin group) and is broadly utilized in many binder systems [4,45,83].

Table 3 shows the compositions and powder loadings of 22 newly composed feedstocks. Use of polyethylene glycol was motivated based on some reports [108-111] on successful application in binder systems, and its compatibility with wide range of binder components, as well as referring to its environmentally friendly nature, which allows to eliminate the need of using number of chemicals during solvent debinding.

The study of the effect of different molecular weight of polyethylene glycols (PEG) on the feedstock showed that high amount of low molecular PEG 1000 enhances the initial debinding stage, since having low molecular weight and low melting temperature it was first to be extracted by evaporation from the surface of the specimen. Further, this process creates network of pores that serve as escape paths for components with higher molecular weight, which propagate towards the specimen surface ensuring quicker debinding with low risk of defect formations.

To investigate the role of PEG molecular weight, comparative study has been done for two contrasting feedstocks based on LDPE. Feedstocks (F10) with equal fraction of LDPE and PW (30 wt.%), large amount of highest molecular weight PEG used – PEG6000 (39 wt.%) and 1 wt.% SA was compared with feedstock (F14) with similar amount of PW (30 wt.%), lower amount of LDPE (20 wt.%) and PEG6000 (22 wt.%), with additional 10 wt.% PEG1000 and 15 wt.% PEG4000, as well as 3 wt.% SA. The results revealed that lower molecular weight PEG's in feedstock (F14) exhibited more gradual early stage debinding, compared to feedstock (F10) with single PEG6000 (Figure 12 and Figure 13).

Feedstock with 10 wt.% of PEG1000 and 20 wt.% of PEG4000 (F14) developed a gradual slope of initial weight loss, which is at temperatures above 200 °C linked to evaporation of volatile degradation products of higher molecular weight components (PW, LDPE).

In contrast, feedstock without low molecular PEG in its composition (F10), exhibited sharp slope, which can be referred as an initial sharp weight loss (Figure 12). For both feedstocks F10 and F14 (Figures 12 and 13) full extraction of the binder system was observed at 456 and 448 °C, respectively. For the feedstocks with PW as a backbone and high amount of PEG6000 (F17, F18), TGA curve exhibited sharp initial drop starting at 174 and 172 °C, and reaching 10.03 and 12.68 wt.% weight loss already at 208 and 209 °C, respectively. This tendency can result in cracks and distortions in the debound parts, and thus should be avoided [7-9].

Table 3. Novel feedstock compositions (data derived from Paper I).

Code	LDPE	PW	PEG1000	PEG4000	PEG6000	SA	ϕ_m
	wt.%	wt.%	wt.%	wt.%	wt.%	wt.%	wt.%
F1	20	20	10	39	10	1	84.7
F2	10	30	10	39	10	1	85.2
F3	20	20	10	39	10	1	85.2
F4	40	-	20	39	-	1	85.2
F5	40	-	10	25	20	5	85.2
F6a	40	10	-	20	29	1	85.2
F6b							85.5
F6c							85.9
F6d							86.5
F7a	40	10	-	10	39	1	85.2
F7b							85.5
F7c							85.8
F8a	50	-	-	10	39	1	85.2
F8b							85.5
F8c							85.8
F9	20	30	-	20	29	1	85.5
F10	30	30	-	-	39	1	85.2
F11	35	30	-	15	19	1	85.2
F12	30	40	-	12	13	5	85.6
F13	31	33	-	15	16	5	85.2
F14	20	30	10	15	22	3	85.5
F15	25	36	10	10	16	3	85.2
F16	20	10	20	20	27	3	85.2

Code	CW	PW	PEG1000	PEG4000	PEG6000	SA	ϕ_m
	wt.%	wt.%	wt.%	wt.%	wt.%	wt.%	wt.%
F17	-	45	-	-	50	5	84.7
F18	-	40	-	15	40	5	84.2
F19	25	30	-	20	20	5	84.5
F20	35	20	10	10	20	5	84.2
F21	40	10	10	12	25	3	84.2
F22	40	10	10	14	25	1	85.2

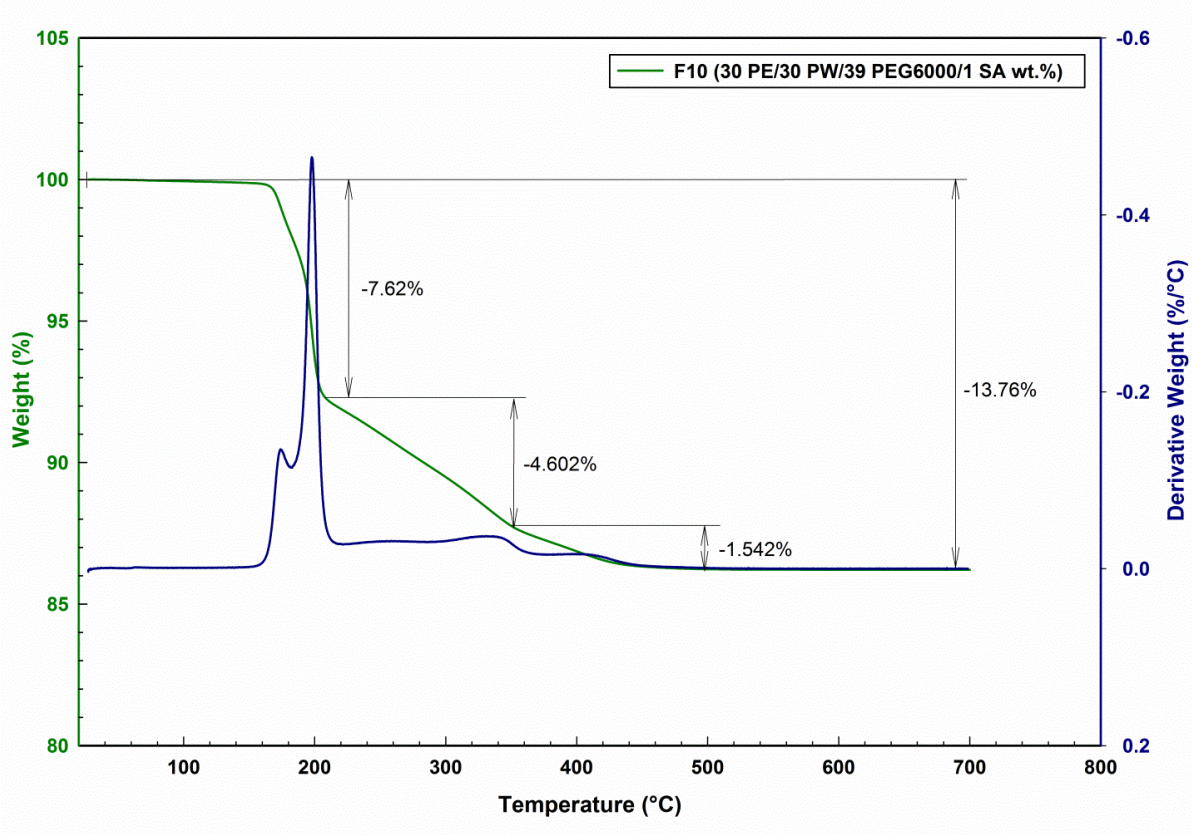

Figure 12. TGA weight loss and corresponding derivative curve for F10 (30 LDPE/30 PW/39 PEG6000/1 SA wt.%) (Paper I).

The feedstocks composed using 25 to 40 wt.% of CW (F19-F22) together with combination of different molecular weight PEG and SA, developed a slight decrease at the first degradation stage with a gradual transition to the second stage and kept this tendency until late debinding. In this respect, the second stage represents the extraction of CW, where the exhibited moderate decline is connected with the narrow setting range of CW. Furthermore, CW is composed of a mixture of linear chain esters, alcohols, acids and hydrocarbons and exhibits small linear expansion in temperature range 22–52 °C compared to other waxes [112,113]. This is an example of possibility to exclude unwanted rapid drop by proper choice of component's mass distribution. The collected data of total mass loss has shown that full binder extraction was achieved for all examined feedstocks.

Meanwhile, solvent debinding was performed for selected feedstocks in order to ensure faster thermal debinding with lower chances of defect formation [54,108]. As expected, a significant weight drop was observed for the samples with high vol.% of low molecular PEG binders and vice versa, feedstocks with low wt.% of PEG showed smaller weight loss, Table 4. The thermal debinding of the solvent debound feedstocks allowed to analyse and compare results with previously collected data for solely thermal debinding. As it can be noticed from Table 4, the

low temperature peaks diminished, as well as the mass loss proportions have changed, which can be explained by the selectivity of the water debinding which removes water-soluble components. Further, the peaks seem to be slightly shifted towards lower temperatures indicating easier mass removal from the fired body in this temperature region. This suggests that the water debinding created pore network within the specimen body by removal of the soluble part of the binder system.

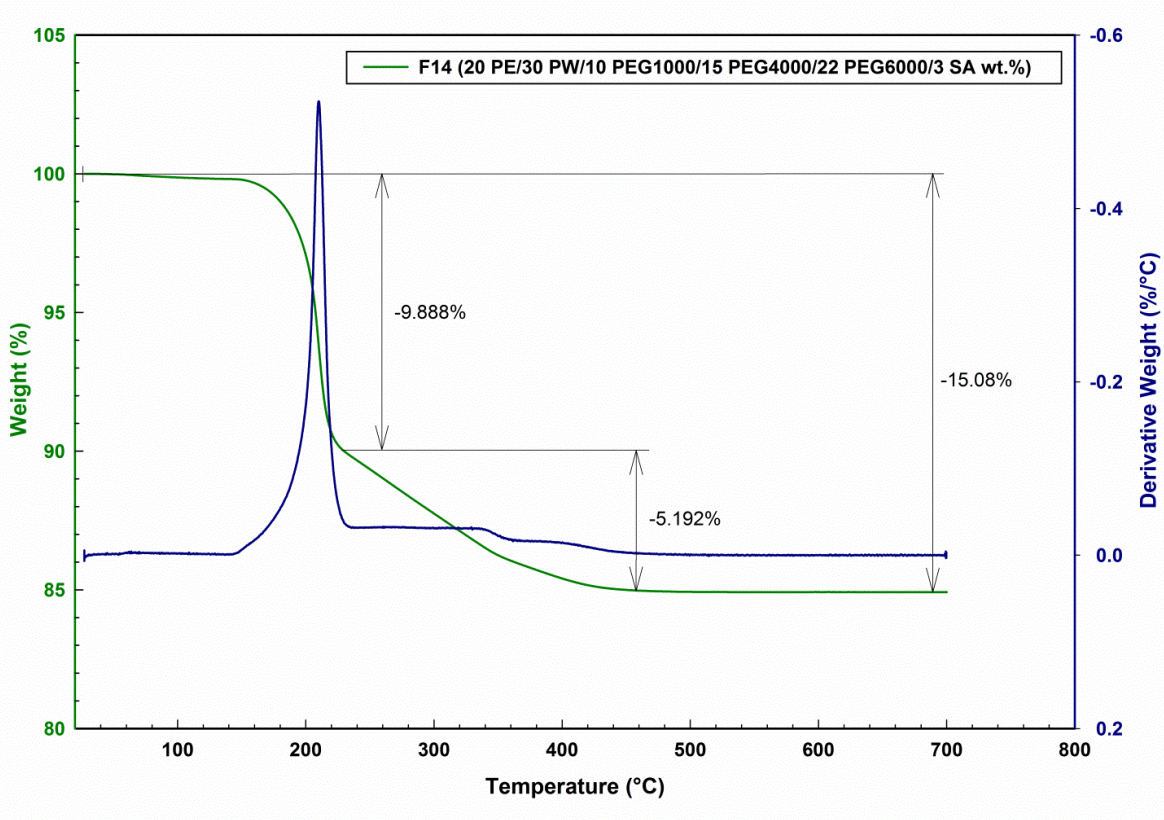

Figure 13. TGA weight loss and corresponding derivative curve for F14 (20 LDPE/30 PW/10 PEG1000/15 PEG4000/22 PEG6000/3 SA wt.%) (Paper I).

Furthermore, feedstocks with high vol.% of LDPE and PW showed a hydrophobic behaviour, while the correlation of extraction efficiency with PW rather than with LDPE tends towards the role of PW as the key blocking agent in the analysed compositions, which can be explained by better miscibility of the low molecular compounds with other component of the binder system.

The thermal debinding involves three main processes: evaporation, thermal degradation and oxidative degradation. High molecular weight components (polyolefins) are subjected to thermal degradation by random polymer chain scission, while the low molecular weight compounds or fragments of polymers are mainly evaporated by propagation towards the specimen surface.

Table 4. Weight loss peaks in wt.% during thermal debinding for initial solvent extracted feedstocks (data derived from Paper I).

Feedstock	Peak 1		Peak 2		Peak 3	
	[°C]	[wt.%]	[°C]	[wt.%]	[°C]	[wt.%]
F2	210	0.93	225	5.75	487	4.86
F6a	200	2.43	364	11.4	475	1.91
F7a	170	2.48	-	-	477	13.52
F9	170	1.33	250	6.1	480	3.56
F10	220	0.16	229	5.77	490	4.44
F14	199	0.89	220	6.57	494	4.64
F16	175	1.17	252	10.1	449	4.19
F22	208	1.8	230	6.37	467	5.35

For PEG, the polymer degradation process is based on a diminution of chain length and reduction in molecular weight, resulting from the bond scission in the backbone of the macromolecules similar to linear polymers.

The peak degradation temperatures and corresponding mass losses are showed in Table 5. As it can be seen the debinding proceeded in 3 to 4 steps. The earliest mass loss for LDPE based feedstocks F4 and F16, was observed at 171 °C by 0.33 and 0.23 wt.% respectively, while for the CW/PW based composition F18 it took place at 172 °C by only 0.12 wt.%. Full binder extraction was observed for all samples, earliest at 442 °C for PW based feedstocks F17, F18 and latest at 473 °C for LDPE based feedstocks F5 and F6a.

Further, by depicting a plot of mass losses vs temperature (Figure 14), one may observe, that feedstocks based on CW/PW exhibited stable, gradual mass loss throughout all temperature range, compared to the feedstock based solely on LDPE or PW.

From observed results one may conclude, that high content of PEG in feedstock, significantly lowers the initial thermal degradation temperatures, serving as a bridge between early and late debinding stages.

Overall, novel feedstocks based on Al_2O_3 high compressible superground powder and polyolefin backbone substitutes - paraffin wax and carnauba wax showed that novel components ensure gradual extraction throughout all range of processing temperatures Figure 14, as well as remain within green part until the late debinding stage.

Table 5. Thermal degradation peaks in percentage of weight loss (data derived from Paper I).

Feedstock	Peak 1		Peak 2		Peak 3		Peak 4	
	[°C]	[wt.%]	[°C]	[wt.%]	[°C]	[wt.%]	[°C]	[wt.%]
F1	185	0.36	223	11.61	-	-	455	4.98
F2	180	0.19	215	11.92	-	-	447	4.8
F3	175	0.51	215	10.09	-	-	465	5.77
F4	171	0.33	223	10.15	348	4.33	469	2.11
F5	175	0.21	238	9.35	349	4.53	473	2.2
F6a	176	0.15	251	8.82	352	4.97	473	2.18
F6b	184	0.15	234	7.77	338	4.9	472	2.21
F6c	192	0.17	243	8.47	348	4.17	470	1.82
F6d	192	0.14	230	7.8	338	4.42	457	1.95
F7a	189	0.11	242	8.11	356	3.92	462	1.94
F7b	197	0.31	240	8.62	341	4.14	471	2.14
F7c	194	0.19	238	8.21	335	4.34	453	2.1
F8a	181	0.15	232	7.67	348	6.38	454	2.67
F8b	185	0.19	237	7.34	349	5.1	446	2.23
F8c	188	0.18	234	6.9	344	5.3	450	2.34
F9	180	0.23	204	7.51	352	4.48	459	1.29
F10	189	0.22	205	7.63	350	4.6	456	1.54
F11	205	0.32	-	-	354	13.9	462	1.95
F12	201	0.29	245	7.62	348	4.62	460	1.85
F13	207	0.35	251	8.29	349	4.88	455	1.96
F14	176	0.36	219	9.52	-	-	448	5.16
F15	203	0.38	248	9.25	348	4.04	455	1.74
F16	171	0.23	200	9.88	-	-	458	5
F17	174	0.18	208	10.03	-	-	442	4.64
F18	172	0.12	209	12.68	-	-	442	4.51
F19	190	0.16	231	9.07	-	-	460	6.42
F20	194	0.17	245	8.89	341	4.56	458	2.16
F21	189	0.16	-	-	346	13.71	460	2.08
F22	195	0.23	247	8.74	345	4.45	459	1.91

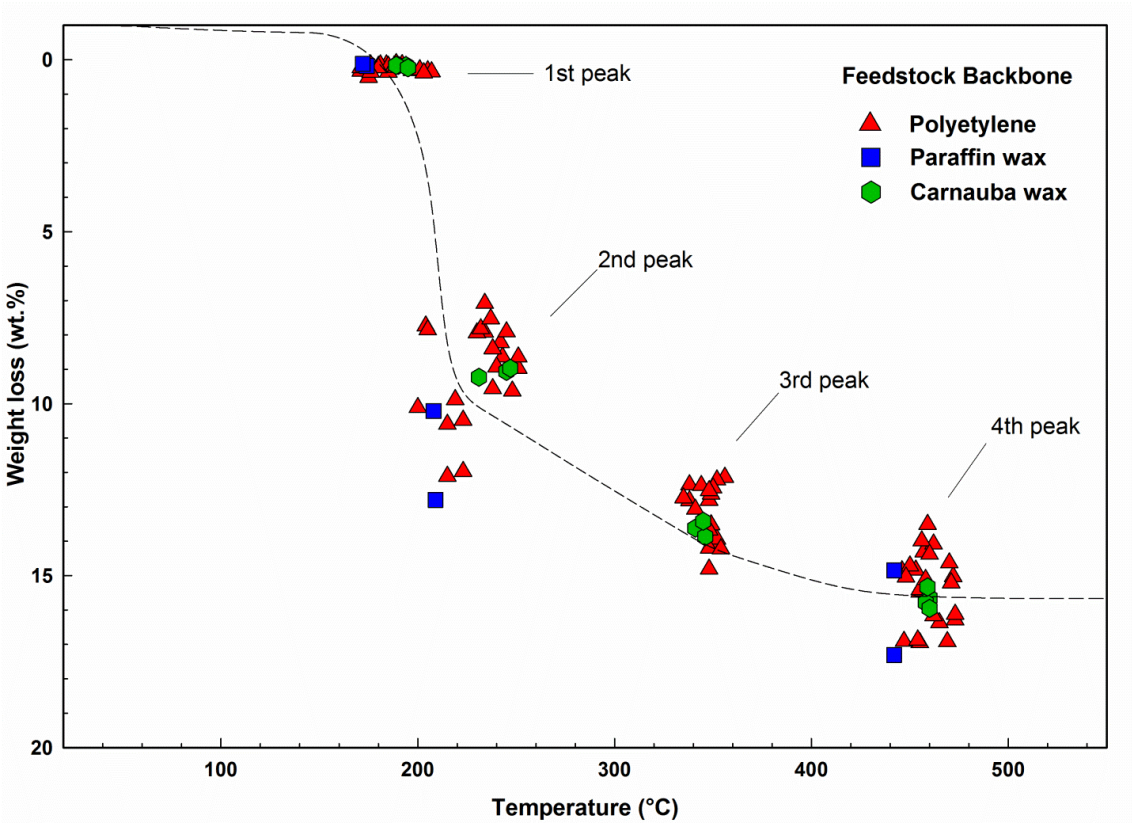

Figure 14. Thermal degradation peaks of tested feedstocks (data derived from Paper I).

To extend the knowledge required for composing novel feedstocks further, the interactions between feedstock components and mould materials were studied.

Tested materials included LDPE, PW, CW, AW, SA, as well as Al_2O_3 and ZrO_2 powders. Four most often used treatments of steel were considered for channel walls of an injection mold: hardened, hardened TiN, nitridized and heat-treated.

The surface energy was determined by measurements of contact angles of three test liquids set (deionized water, ethylene glycol and diiodomethane) using the SEE (Surface Energy Evaluation) system for both feedstocks and mould materials.

The obtained values of contact angles are showed in Table 6. As expected the measured contact angles are lowest with diiodomethane and highest with water, with exception of both ceramic powders with the lowest contact angles for ethyleneglycol. The low contact angles measured for PEG 6000 with all testing liquids could be explained by the hydrophilicity of its surface. It is well known that as the contact angle decreases, the tendency of the binder to spread over the powder particle increases, hence resulting in a better wettability [114].

Contact angles for CW and SA exhibited very similar values in water, and crosswise for the remaining testing liquids. Lower intrinsic viscosities and higher polarities make the low molecular weight surface active agents more effective in reducing the feedstock viscosity, compared to the ones with high molecular weight. SA offers excellent adhering to the powder surface, fully coating the particles and preventing powder aggregation. Meanwhile, the interlinking

strength between binder components is weak, due to the short chain lengths of the low molecular weight surface active agent as SA, which can result in necking during plastic forming [115].

In order to enhance the interlinking strength between binder components a polymer having suitable functional groups in each repeating unit can be effective, improving as well the adhesion to the powder surface. From the materials tested, PEG showing the lowest contact angles, is the most suitable one for this role. Further, PEG has strong interactions with AW, while AW itself exhibited values of contact angles similar to PW, where no adhesion is expected.

Table 6. Contact angles of tested mould–die materials, powers and binders (Paper IV).

Name	Ethylene glycol [°]	Diiodomethane [°]	Water [°]
Mould die material			
Hardened	60.9	50.2	72.7
Hardened TiN	57.5	51.7	77.3
Nitridized	71.3	59.8	96.6
Heat-treated	79.9	57.0	78.1
Ceramic powder			
Al_2O_3	23.0	40.6	60.5
ZrO_2	35.6	39.1	67.7
Binder			
LDPE	56.0	44.5	85.8
PW	76.3	52.8	114.1
PEG6000	23.7	22.2	24.0
CW	51.9	64.1	94.6
AW	90.7	57.8	108.8
SA	64.9	52.4	94.9

The free surface energy for acid-base model were calculated for unpolar Lifshitz-van der Waals component $\gamma^{(LW)}$, electron-donor (γ^-), electron-acceptor (γ^+), polar component $\gamma^{(AB)}$, as well as $\gamma^{(total)}$ representing the sum of unpolar and polar components are showed in Table 7.

Hydrogen bonding is the primarily agent which enhances the adhesion of binder components onto the powder surface via Lewis acid-base reactions [116]. The adsorption of the binder components onto the powder surface is competitive such that patterns similar to the Langmuir adsorption and desorption isotherms usually take place [117].

Table 7. Calculated free surface energies components (J/m^2) for tested mould-die materials, binder components and ceramic powders (Paper IV).

Material	$\gamma^{(total)}$ [a]	$\gamma^{(LW)}$ [b]	$\gamma^{(AB)}$ [c]	$\gamma^{(+)}$ [d]	$\gamma^{(-)}$ [e]
Mold die material					
Hardened	40.7	34.1	6.5	0.5	21.6
Hardened TiN	33.7	33.3	0.4	0	12.3
Nitridized	28.9	28.7	0.3	0	1.8
Heat-treated	53.4	30.3	23.1	4.2	31.9
Ceramic powder					
Al_2O_3	47.2	39.3	7.9	1	15.7
ZrO_2	44.4	40.1	4.4	0.4	12
Binder					
LDPE	38.2	37.3	0.9	0.1	3.4
PW	33.1	32.7	0.4	0	1.4
PEG 6000	64.7	47.1	17.6	1.1	72
CW	33.8	33.2	0.6	0.1	1
AW	33.6	29.8	3.7	2.1	1.7
SA	33.5	32.9	0.6	0.1	1

[a] Sum of unpolar and polar components. [b] Lifshitz-van der Waals component. [c] Polar component. [d] Electron-donor. [e] Electron-acceptor.

The results showed lowest total surface energy for nitridized and hardened TiN surfaces, which have similar dispersion and polar components. In contrast, the heat-treated surface showed the highest value of surface energy of 55.4 J/m^2 and noticeably higher polar component 23 J/m^2, compared to nitridized and hardened TiN surfaces (0.4 J/m^2). Meanwhile, the dispersion part of surface energy was similar to other tested surface modifications. Figure 15 shows the differences

in $\gamma^{(total)}$ for tested mould-die materials. It can be seen that heat-treated sample exhibits an exceptional behaviour.

The surface properties are another major factor which influences the adhesion analysis influence, since the liquid penetrating the porous surface may result in an artificially lower contact angles. Due to this, the tested surfaces have been analysed using contactless scanner in order to exclude the effect of surface structure affecting the calculated adhesion values. Calculated roughness profiles R_z (μm) of the tested powders and mould-die materials are showed in Table 8.

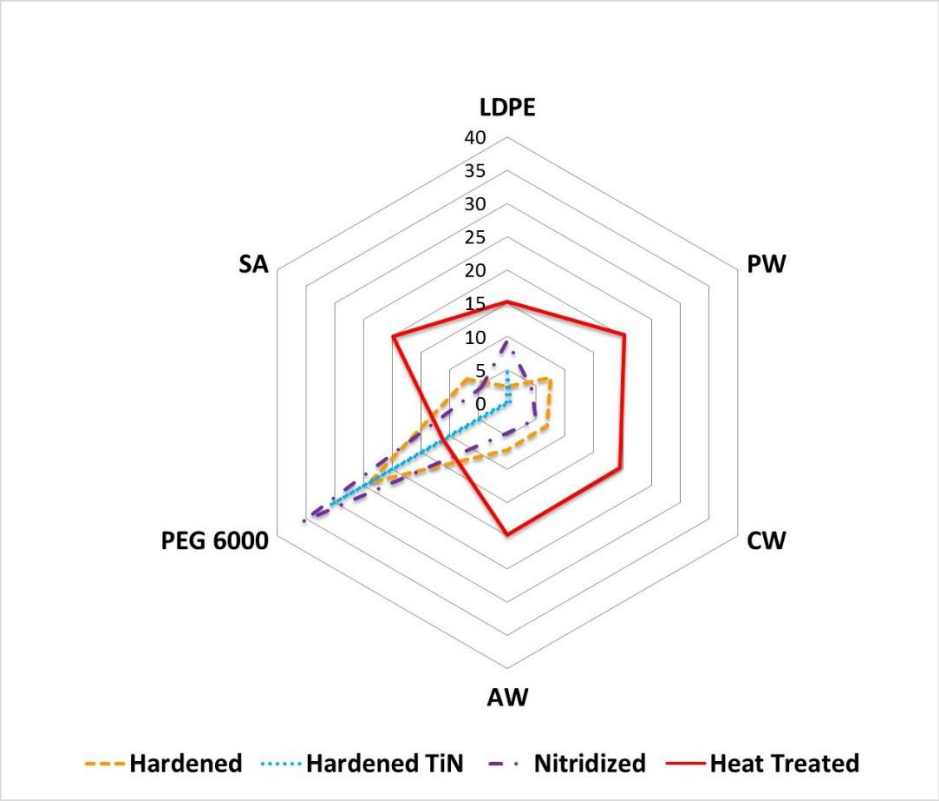

Figure 15. The differences of $\gamma^{(total)}$ between polymer binders and mould-die materials.

For the ceramic powders, the obtained surface characteristics were rather similar, with 44 and 47 J/m^2 of $\gamma^{(total)}$ for ZrO_2 and Al_2O_3, respectively, with alumina having also slightly higher polar component of surface energy.

Calculated $\gamma^{(total)}$ differences for respective powders and binder components are showed in Figure 16. The values are about 3 J/m^2 higher for (PW, LDPE, AW, CW, SA) and lower for PEG for Al_2O_3 powder compared to ZrO_2 sample.

Surface characteristics of binders showed values of $\gamma^{(total)}$ similar to other tested materials ranging from 34 to 38 J/m^2. Further, the polar components exhibited similar values (below 1 J/m^2), except for acrawax, where the polar component $\gamma^{(ab)}$ was higher of 3.7 J/m^2.

Table 8. Roughness profiles R_z (μm) of the tested powders and mould-die materials (Paper IV).

Material	Mean	Std dev	Min	Max
Ceramic powder				
Al_2O_3	2.90	0.451	1.89	4.15
ZrO_2	2.68	0.387	1.90	4.00
Mold die material				
Heat-treated	3.24	0.371	2.44	4.68
Hardened	4.00	1.060	2.09	8.02
Hardened TiN	3.22	0.445	2.23	4.50
Nitridized	3.72	0.675	2.68	5.97

From all tested binders, only PEG 6000 showed highly different values of surface energy (64.7 J/m^2) with polar component of 17.6 J/m^2, which can be explained by its chemical composition. A polar surfaces show only γ^{LW} with very low or full absence of polar component and as a rule their total surface energy is lower compared those with both polar and unpolar components of γ (metals).

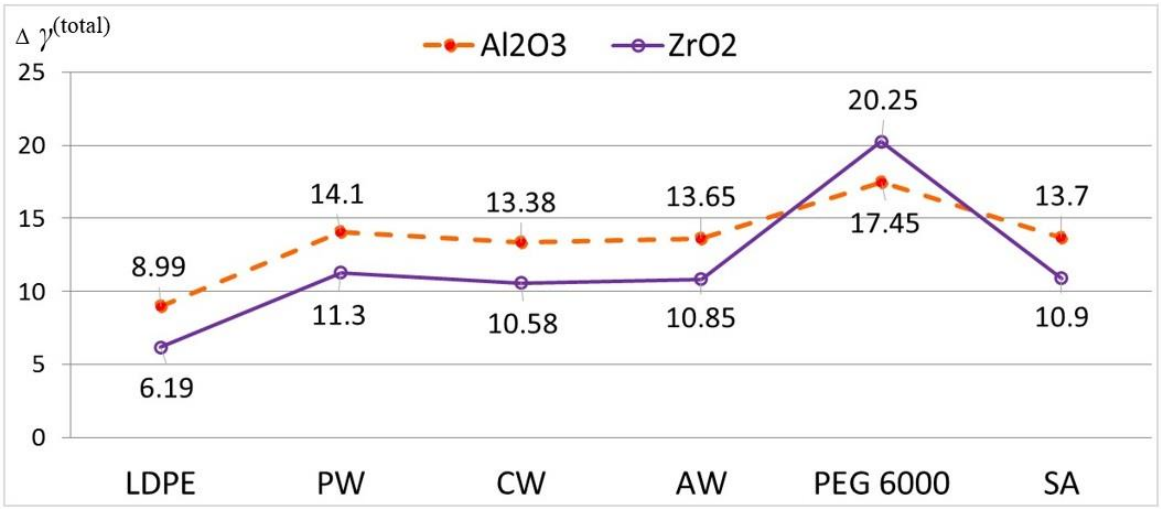

Figure 16. The differences of $\gamma^{(total)}$ between polymer binders and ceramic powders.

The complexity of chemical mechanisms occurring within the binder system requires further deep investigation [80]. Furthermore, in the cases where the specific interactions between polymers cannot be studied by other means, the substitution of polymers by their low molecular

analogues can be applied. Such technique allows to eliminate majority of self-interactions during cross-interaction measurements, which is not possible for polymer – polymer interactions analysis.

Scheme 1 shows an example of substitution of binder system components with their low molecular analogues. This technique provided advantage of neglecting self-interactions of polymers, which is one of the major concerns in studies of miscibility of polymer-polymer blends. Much smaller self-interactions of low molecular substitutes allowed precise calculation of present interactions. As showed in Table 9, polyethylene glycol (PEG) was substituted by 2-ethoxyethanol (2ET) and diethylene glycol monoethyl ether (DGME), carnauba wax (CW) by amyl butyrate (AM) and butyl valerate (BV), and acrawax (AW) by methylacetamide (NMA) low molecular analogues.

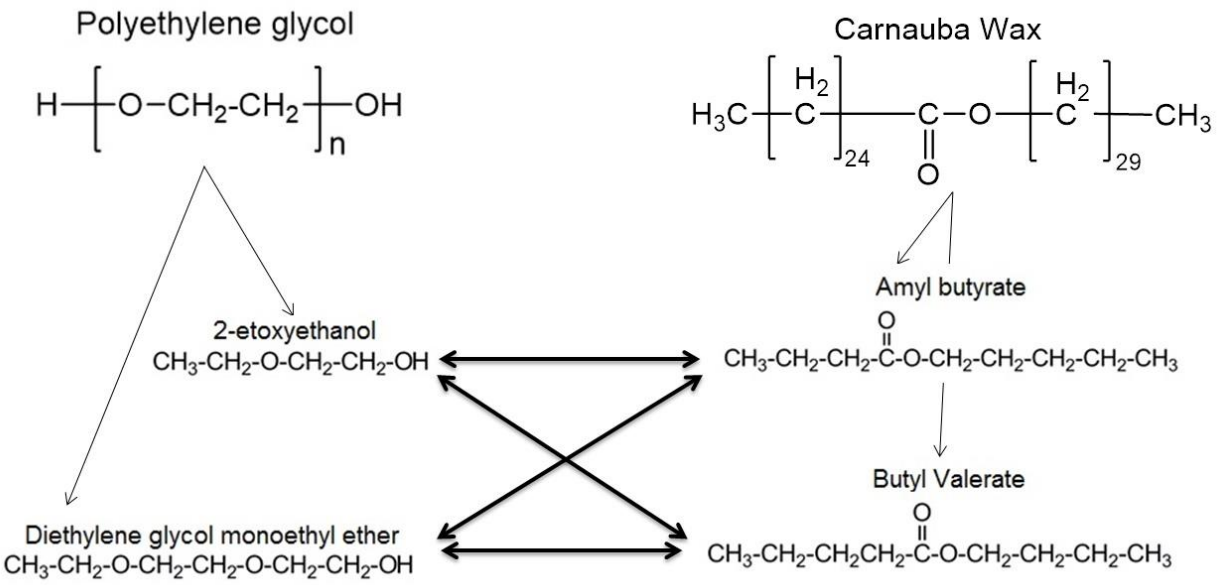

Scheme 1. Substitution of polyethylene glycol (PEG) and carnauba wax (CW) with low molecular analogues (data derived from Paper II).

The quantitative analysis of interactions was based on assumption that change of Van der Waals intermolecular interactions accompanying mixing is negligible (e.g. mixing of hexane and heptane) and all contributions to the heat of mixing are due to specific acid-base interactions, as well as that all organic liquids (except for saturated hydrocarbons) make the specific self-association based on electron donor (basic) and electron acceptor (acid) sites of one molecule [118].

Further, it was assumed that molecules are self-associated in $X - X$ pairs consisting of two molecules by the acid-base interaction and all $X - X$ interactions are broken in the case of high dilution, where all dissociated X molecules form new $X - Y$ interactions and molecules Z (saturated hydrocarbons) do not have any acid-base self-associations and do not form acid-base interactions with another molecule (X or Y).

Table 9. Self-interaction and association energies of low molecular analogues [J/mol] (derived from Paper II and Paper III).

Binder		PEG		CW		AW
	Low-molecular analogue	2ET	DGME	AM	BV	NMA
PEG	2ET	11861	-	5008	6471	9659
	DGME	-	16236	3793	3011	7139
CW	AM	5560	4162	5264	-	5899
	BV	6784	3294	-	4132	6353
AW	NMA	10624	7846	5382	5810	2308

Dilution at different concentrations gave an important understanding of the progress of peak shift and allowed to define the optimal rate at which the peak shift is complete. Figure 17 reveals that shift of carbonyl C–O stretching peak for 2ET diluted in hexane at initial 40 % allows to observe development of a peak shoulder, which progressively grows at 20 and 12 %, reaching magnitude equal to original 1119 cm^{-1} peak at 6 % concentration and 1131 cm^{-1}.

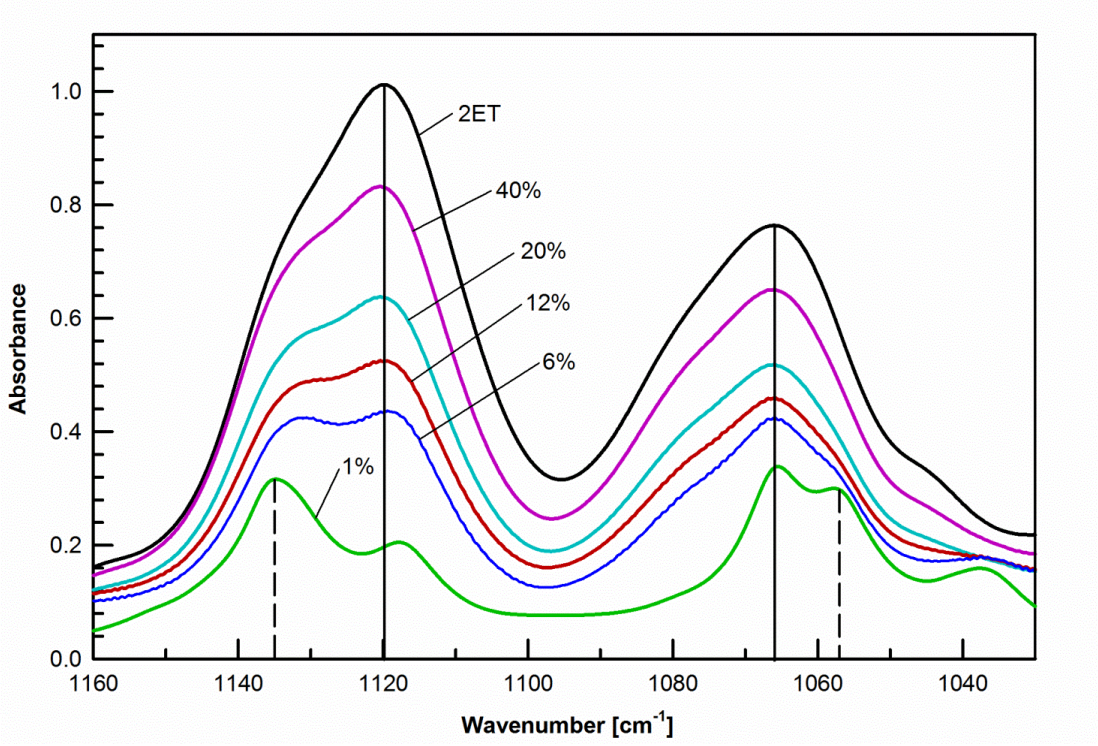

Figure 17. Shift of FTIR peaks for C–O bonding of 40, 20, 12, 6 and 1 % of 2-ethoxyethanol (2ET) in hexane (Paper II and Paper III).

This observation suggests that at 6 % concentration half of 2ET molecules are already isolated by the hexane. For the dilution at 1 % concentration the magnitude of 1131 cm^{-1} peak suggests that the majority of the 2ET molecules are surrounded by the hexane (molecules are separated), even though the small peak at 1119 cm^{-1} is a hint of a presence of small amount of self-interaction pairs which can be neglected. Moreover, due to the asymmetry of the C–O bonding in 2ET (Figure 18), second peak shift was also observed at 1065 cm^{-1}, with minor shoulder for 12 and 6 %, and prominent peak at 1056 cm^{-1} for 1 % dilution. The asymmetry of C–O bonding for 2ET can be explained by intramolecular vibrations created due to the presence of additional –OH in chemical structure of 2ET [119].

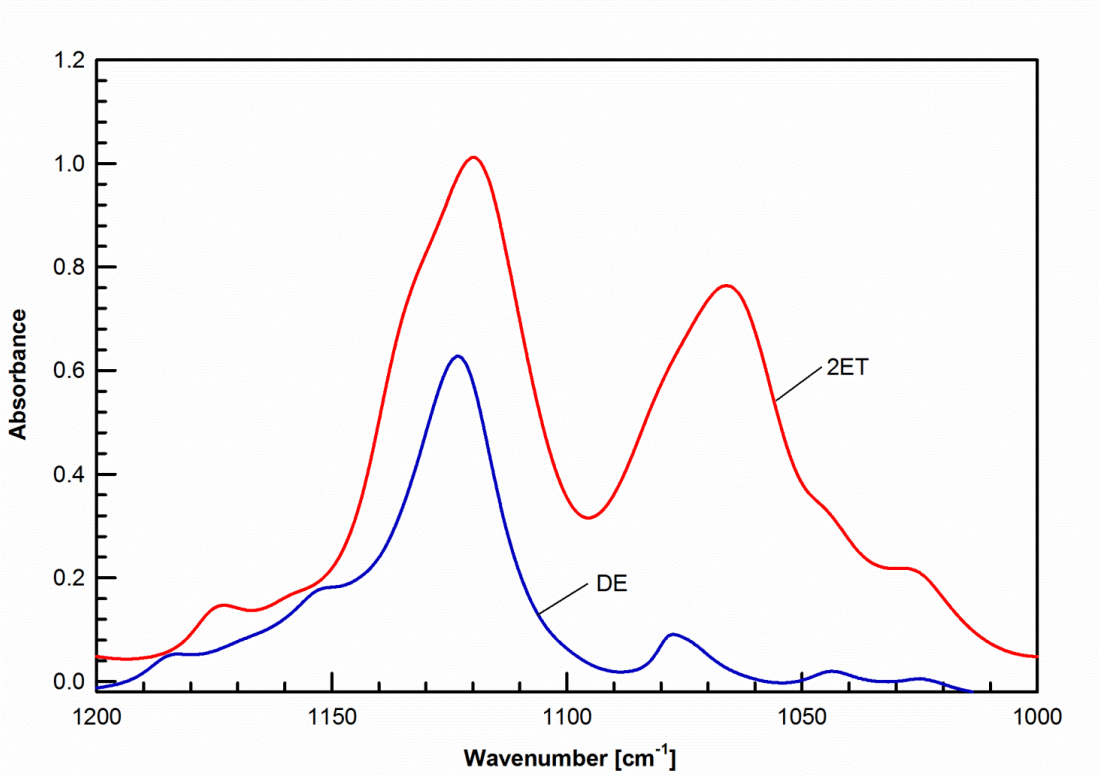

Figure 18. FTIR peaks for C–O bonding of diethyl ether and 2-ethoxyethanol (2ET) (Paper II and Paper III).

For both CW and PEG analogues the response of C–O peak to dilution of self-interaction was highly prominent, however being present in both, it excluded the possibility of determining from which liquid it originates for liquid to liquid dilutions. –OH group in PEG analogues and C=O group in CW analogues were only functional bounding not repeated in each other allowing further analysis.

The investigation of the interactions between CW and AW substitutes (AM-NMA and BV-NMA) using the shift of N–H amino group, suggests that the interactions are negative. The major peak of methylacetamide (NMA) at 3300 cm^{-1} tended to higher wavenumbers for CW analogues amyl butyrate (AM) and butyl valerate (BV), while the peak for hexane and decalin shift to smaller

wavenumbers Figure 19. In contrast the minor peak at 3103 cm^{-1} shifted to lower wavenumbers for all tested liquids, which is an indicator of favourable interactions [84,119].

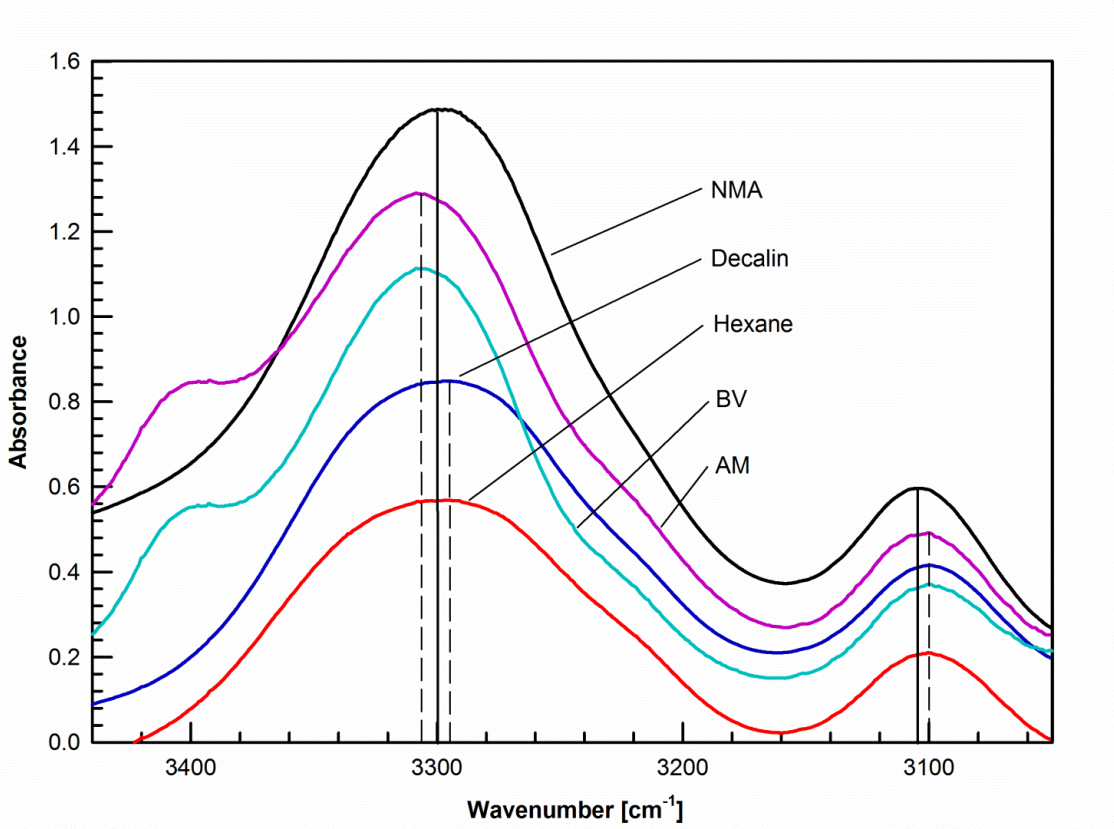

Figure 19. Shift of FTIR peaks for N–H stretch bonding of 1% methylacetamide (NMA) in hexane, decalin, AM and BV (Paper III).

Peak shift correction was applied, to quantitatively analyse the shift. The peak shift in buffer liquids - hexane and decalin together with the low molecular analogues surface tension γ, represents a baseline for the corrected peak shift calculation (schematically showed in Figure 20).
Smallest peak shift 5.2 cm^{-1}, after peak shift correction was observed for C–O stretch bonding of 1 % diethylene glycol monoethyl ether (DGME) dilution in NMA, which can be explained by the length of the chemical structure of DGME, as well as the resulting high value of self-interactions energies (Table 10). This can be also seen in the case of peak shift correction for C=O stretch bonding of 1 % AM diluted in NMA, where the shift was 5.5 cm^{-1}, which can be also interpreted as not all of self-interactions were broken for forming new pairs with diluted liquid.

Average peak shift values were observed for the C=O stretch bonding of 1 % AM diluted in 2-ethoxyethanol (2ET) and C–O stretch bonding of 1 % 2ET diluted in NMA with shift of 7.2 and 9.8 cm^{-1}, respectively.

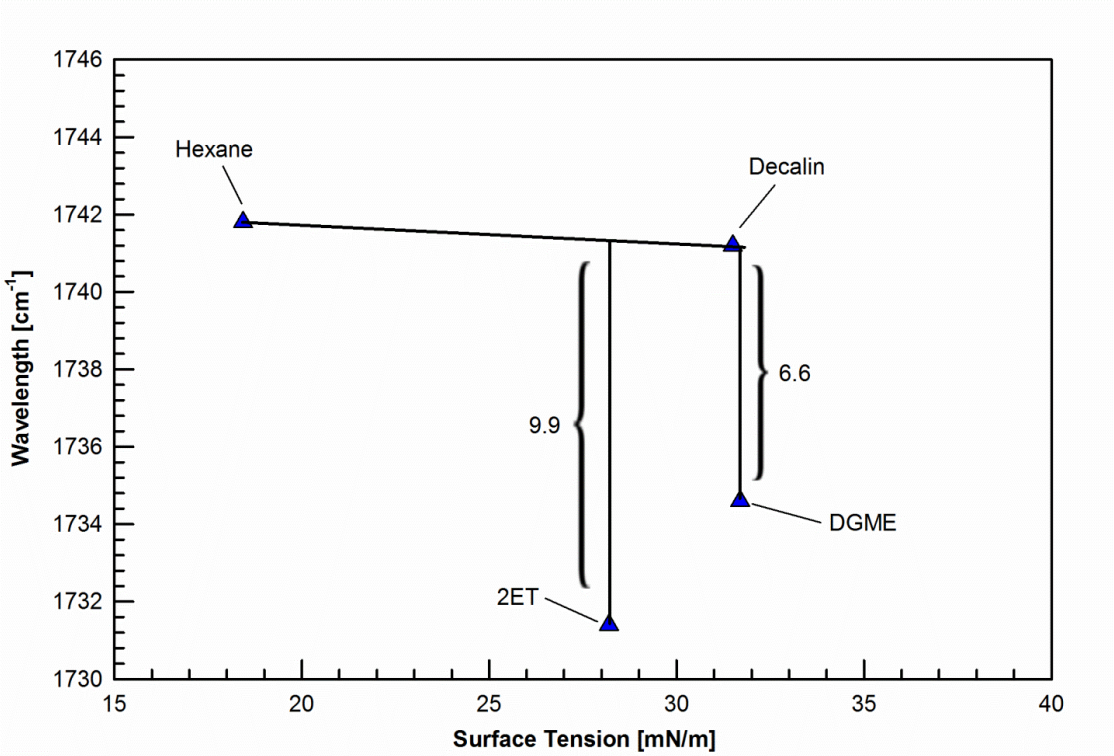

Figure 20. Calculation of a corrected peak shift from the baseline for C=O bonding butyl valerate (1 %) in hexane, decalin, 2-ethoxyethanol and diethylene glycol monoethyl ether (Paper II).

Meanwhile, the results showed that the largest peak shift 14.2 cm^{-1} and 13.0 cm^{-1} were obtained for N–H stretch bounding peak of amino group in range 3280 to 3320 cm^{-1} of 1 % NMA diluted in BV, and O–H stretch bounding in range of 3400 to 3450 cm^{-1} for 1 % 2ET diluted in BV, respectively (Table 10). This may suggest that the chemical structure plays crucial role regardless the concentration, while high dilution rate gives the possibility to observe and quantify the peak shift for the functional bounding.

The obtained results from FTIR suggested presence of specific interactions between tested liquid pairs, by displaying shift of peaks towards lower wavenumbers, which was in agreement with the reports [94-96].

The study of thermodynamics for interactions of two components by calorimetric analysis allowed determining the temperature drop ΔT (Figure 21). The analysis of the liquid pairs showed an exothermic reaction for the dilution of AW-PEG substitutes, while the dilution of CW-PEG and CW-AW substitutes exhibited endothermic reaction. The increase in temperature during mixing is associated with strong, newly formed interactions between blended liquids.

Table 10. Peak position ν, surface tension γ and corrected peak shift $\Delta\nu_{XY}$ for corresponding liquids (Paper II and Paper III).

Name	Peak position ν [cm^{-1}]	Surface tension γ [mN/m]	Corrected peak shift $\Delta\nu_{XY}$ [cm^{-1}]
C=O, 1 % Amyl butyrate			
Hexane	1741.8	18.40	0
Decalin	1741.2	29.40	0
2-ethoxyethanol (2ET)	1733.3	28.20	7.8
Diethylene glycol monoethyl ether (DGME)	1735.7	31.70	5.5
–OH, 1 % 2-ethoxyethanol			
Hexane	3425.2	18.40	0
Decalin	3421.3	29.40	0
Amyl butyrate (AM)	3432.7	25.55	11.4
Butyl valerate (BV)	3434.3	26.36	13.0
C–O, 1 % 2-etoxy ethanol			
Hexane	1122	18.40	-
Decalin	1124	29.40	-
Methylacetamide (NMA)	1115	28.20	9.1
C–O, 1 % Diethylene glycol monoethyl ether			
Hexane	1122	18.40	-
Decalin	1124	29.40	-
Methylacetamide (NMA)	1119	31.70	5.2
N–H, 1 % Methylacetamide			
Hexane	3295	18.40	-
Decalin	3293	29.40	-
Amyl butyrate (AM)	3306	25.55	12.1
Butyl valerate (BV)	3308	26.36	14.2

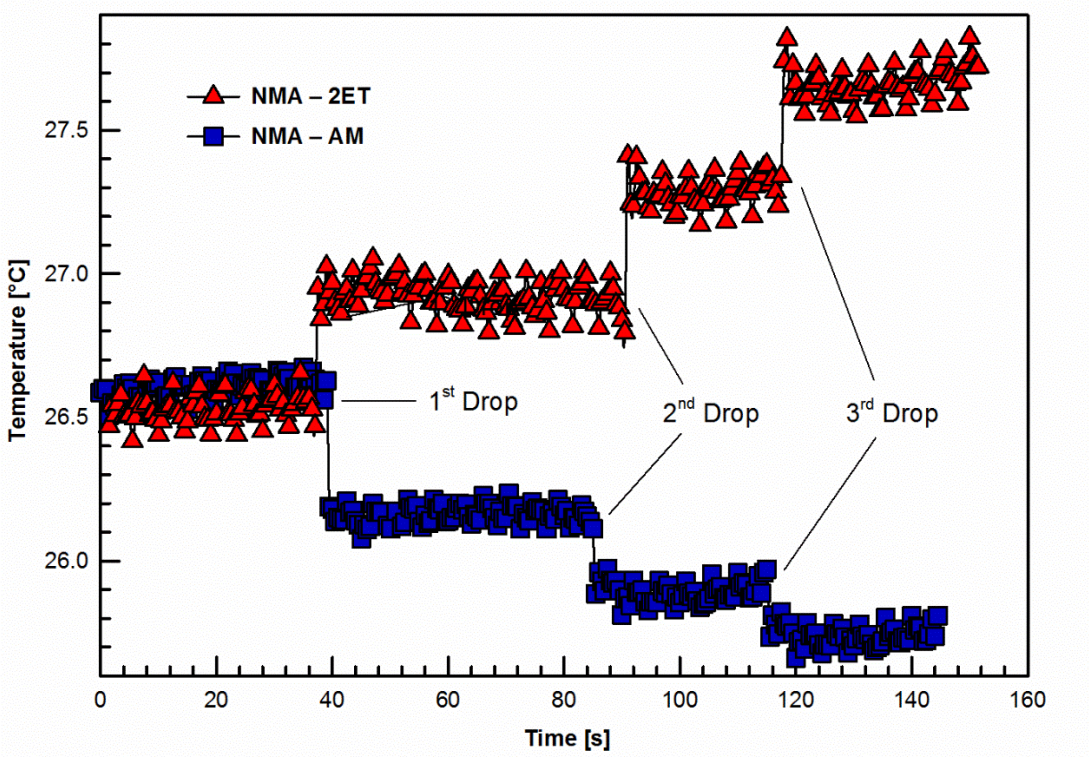

Figure 21. Temperature change for the 0.05 ml drop of NMA diluted in 5 ml 2ET and AM (Paper III).

For the dilution in hexane, as a buffer solvent, the largest temperature drop of 0.81 and 0.80 °C was observed for 2ET and DGME, respectively, while in contrast BV and NMA both showed the smallest negative temperature change of 0.15 °C (Table 11). To define the component fraction of the blend after dilution, the heat of mixing vs. molar fraction and fraction of diluted liquid into solvent were also calculated. As it can be seen from Figure 22, the association of heat of mixing and molar fraction of the dilution are tending to linearity, the less is the bonding of curve, the more linear is ΔT.

The comparison of self-interaction energies together with the molecular weight for the PEG analogues revealed, that for the liquids without –OH bounding, the self-interactions energies are smaller, compared to the ones with –OH, suggesting that presence of –OH surges the self-interactions value of low molecular substitutes (Figure 23) [120]. Moreover, the study revealed that chemicals with –OH may have an optimum value at which the interaction energies are highest and start to decline at some point, however it requires further analysis.

As it can be seen from Figure 23, the self-interaction values are lowest for the diethyl ether which also has the smallest molecular weight. Self-interactions values are the highest for DGME, which can be explained by the fact that it has the highest number of oxygen molecules along its chain, meaning that more self-interactions are likely to occur between two molecules.

The shift of peaks towards lower wavenumbers in FTIR measurements, as well as observed temperature surge for certain blends with help of analogue calorimetry can independently serve as

a proof of the presence of specific interactions [94-96,100-102], while combing both data together allowed to define the relationship of two independent experiments.

Table 11. Temperature drop ΔT, heat of mixing $\Delta H_M/(n_X+n_Z)$ and molar fraction $n_X/(n_X+n_Z)$ (Paper II and Paper III).

Name	Temperature drop ΔT [°C]	$\Delta H_M/(n_X+n_Z)$ [J/mol]	$n_X/(n_X+n_Z)$ [10^{-3} mol]
Amyl butyrate (AM)	0.19	28.35	6.708
Butyl valerate (BV)	0.15	29.38	6.754
Methylacetamide (NMA)	0.15	29.14	16.835
2-ethoxyethanol (2ET)	0.81	157.82	12.633
Diethyl ether (DE)	0.28	54.58	11.672
Diethylene glycol monoethyl ether (DGME)	0.80	156.41	9.146
Diethylene glycol dimethyl ether (DGDE)	0.44	86.05	8.639
Triethylene glycol monoethyl ether (TGME)	0.32	62.69	7.045

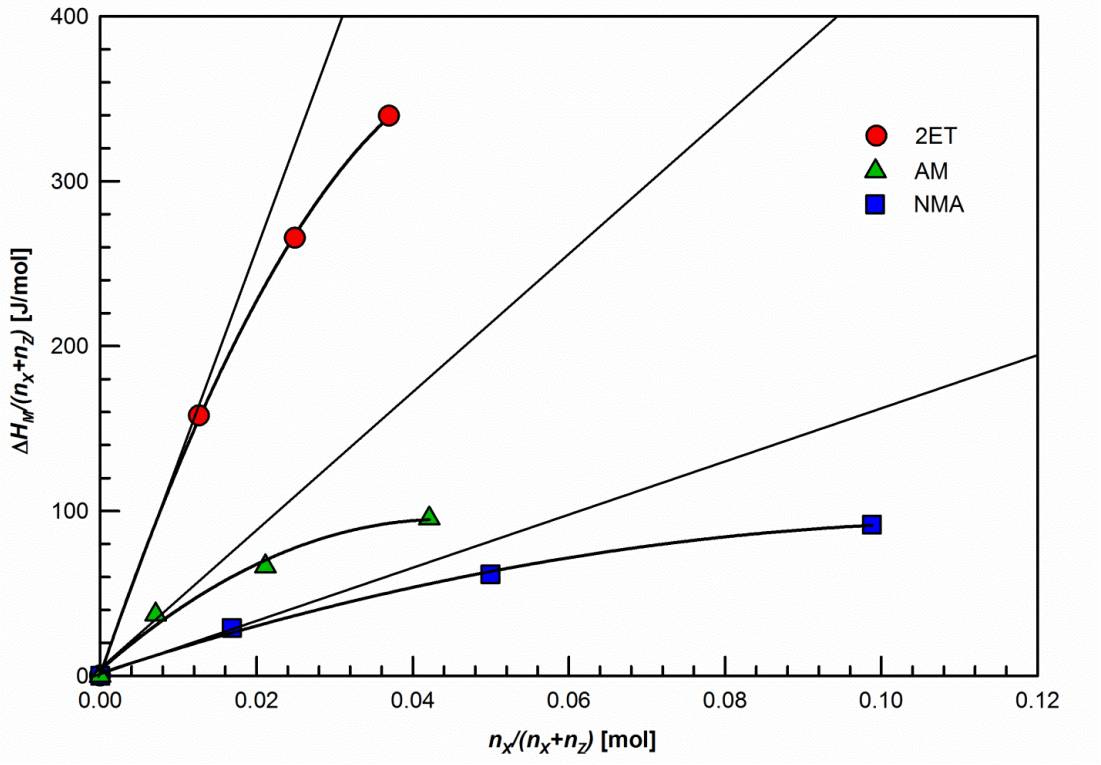

Figure 22. Heat of mixing vs molar fraction of liquid *X* diluted into solvent *Z* (Paper III).

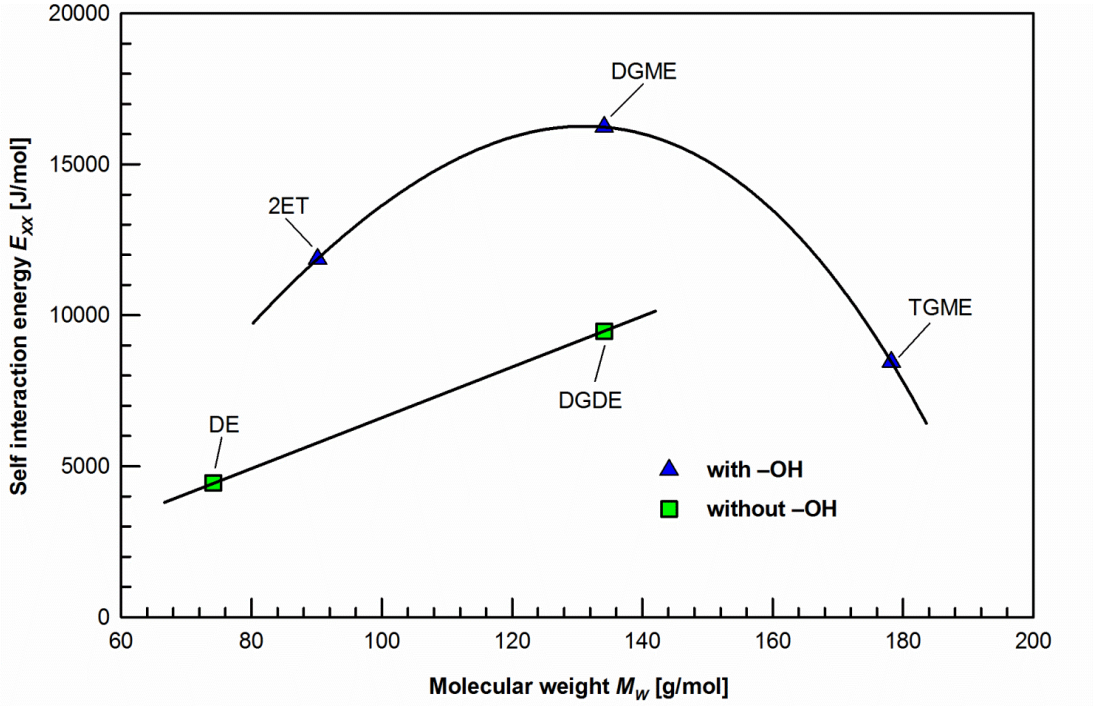

Figure 23. Self-interaction energies E_{XX} vs molecular weight M_W for PEG substitutes (Paper II).

Data from both experiments were used to plot respective association energies (obtained by calorimetry) vs shifts of peaks (measured using FTIR) Figure 24.

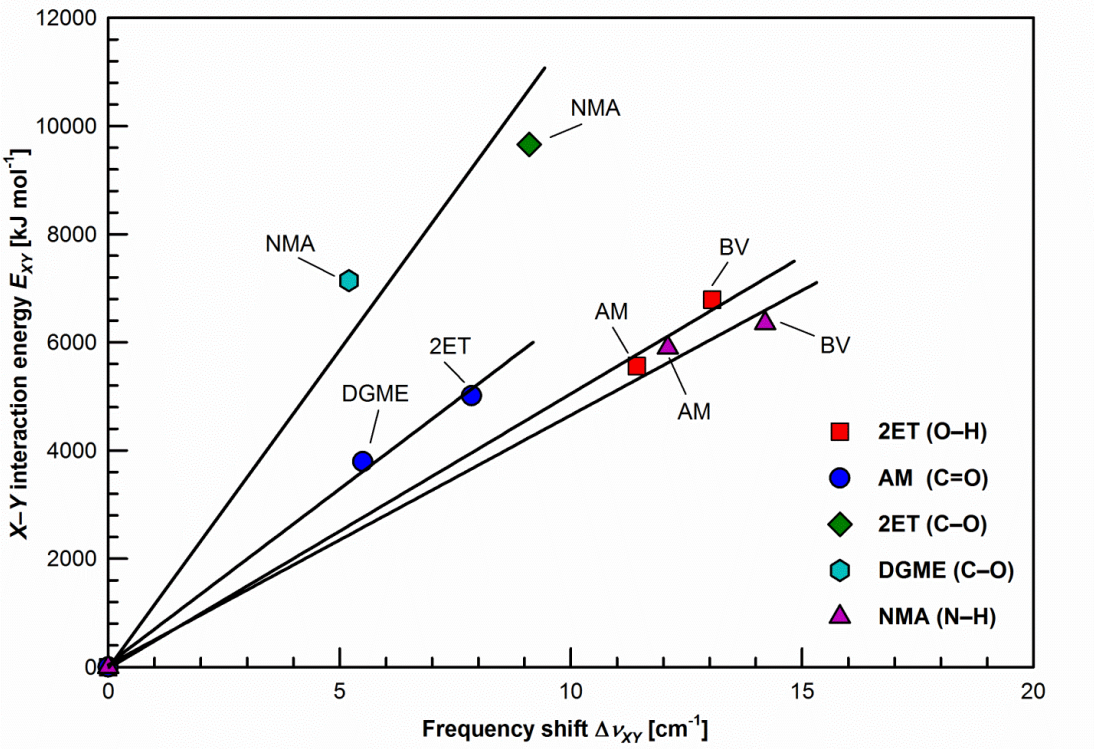

Figure 24. Association energies E_{XY} vs. shift of peaks for low-molecular analogues of acrawax, carnauba wax and polyethylene glycol. (Paper III).

A linear dependence was found for the tested pairs, which is in agreement with the Drago's [121] linear relationship between enthalpy of adduct formation and shift in the frequency of vibration ($\Delta H = k\Delta\nu^{XY}$), confirming the validity of data and calculations from two independent analysis.

4. CONCLUSION

The aim of the doctoral thesis – to study the role of particular binder components in PIM processing and their interactions – was achieved.

The novel binder system was developed by introducing eco-friendly components, which allowed to compose feedstocks with advanced processing properties. The natural waxes were used as a substitute to commonly utilized backbone – low density polyethylene. Furthermore, use of different molecular weights of PEG enhanced the early thermal degradation stage as well as created a network of pores within the sample body, allowing faster and defect free extraction of residual backbone component. Carnauba wax ensured gradual and step by step debinding up to final stages.

Use of low molecular weight analogues of polymers made possible the study of interactions of binder system components (PEG, acrawax, carnauba wax), giving an advantage of eliminating the majority of self-interactions for cross-interaction measurements, which was not available for polymer - polymer interaction evaluation. For FTIR analysis an optimum dilution level was defined at 1 % concentration. The peak shift in a buffer solution served for constructing a baseline and defining the corrected peak shift. The calorimetric measurements allowed to quantitatively analyse the self and cross-interactions. Further, a linear connection of two independent experiments was found, where higher the shift from FTIR, the higher the association energies, which is in agreement with Drago's linear equation.

For PEG substitute liquids, the presence of –OH bounding in chemical structure resulted in higher values of self-interaction energies, reaching its maximum for diethylene glycol monoethyl ether. The highest cross interaction values was calculated between 2-etoxy ethanol and methylacetamide, suggesting strong interactions between corresponding both polar PEG and acrawax binders.

The interactions present between binder components can positively influence the energy efficiency of applications, at the same time noticeably enhancing the mixing and moulding characteristics.

In addition, the nature of adhesion of binder components to powders as well as channel walls of moulding tools has been investigated. Considering the wettability of the channel walls of the mold revealed about ten times higher surface energy of heat-treated steel than nitridized, hardened, and hardened TiN materials. Among the binder components studied it has been found that the role of the surfactant (stearic acid) might be substituted with carnauba wax. Acrawax and especially polyethylene glycol have shown the highest values of polar component of surface energy determining their key role in PIM feedstocks.

CONTRIBUTION TO THE SCIENCE

This PhD study focused on possibility of substituting polyolefin backbones in PIM binder systems by environmentally friendly waxes, as well as on the study of the role of polyethylene glycols (PEG) molecular weight on debinding properties. Further, this research covered an important and scarcely studied topic of interactions of binder system components among each other as well as with powders and mould materials. 22 new feedstocks were composed using three different molecular weight PEGs to study the debinding properties as well as carnauba wax was exploited as a substitute to low molecular weight polyethylene. Due to the complexity of the PIM feedstocks, the interactions among the binder system components were studied together with the interactions of the binders, powders and mould materials. This expands the understanding of the mechanisms occurring within such systems and allows to precisely balancing the compositions of novel feedstocks.

The following topics can be considered as the most important contributions of the PhD work to the science and practice:

1) Role of low molecular weight polyethylene glycols (PEG1000, PEG4000) in early debinding stage. The advancement of gradual binder extraction and avoiding sharp initial weigh loss.

2) The use of combination of various PEGs (PEG1000, PEG4000 and PEG6000) in feedstock serving as a bridge between early debinding stage and backbone extraction. Creating a gradual, step by step debinding profile, excluding sharp weight drops.

3) Study of adhesion among feedstock components and mould materials. Defining that carnauba wax having similar values as stearic acid can take over the role of a processing aid.

4) Study of interactions between both polar polymers by substituting them with their low molecular analogues. Determination of interactions for analogues showing twice stronger bounding for acrawax/PEG substitutes than for carnauba wax/PEG, suggesting strong interactions between former corresponding polymers.

In summary, this work gave an understanding of the role of each binder system component during the debinding stage as well as entered the field of studying the binder systems in detail, which was not done before. Hopefully, it shall serve as an endorsement for further investigations.

ACKNOWLEDGMENTS

First of all, I would like to express my sincere gratitude to my supervisor, Prof. Berenika Hausnerova. This work would not be possible without her enormous support and guidance.

I am thankful Doc. Ivo Kuritka and Prof. Petr Svoboda for their special support and attention to my research.

Also, I would like to acknowledge the financial support of Internal Grant Agency (IGA) UTB and Visegrad Fund, which had been an enormous support for my research.

I would like to thank my family for their unceasing encouragement, support and understanding throughout all years of the study.

Further, I would like to extend my appreciation to one and all, who directly or indirectly, have lent their hand during this research.

LIST OF SYMBOLS

2ET	2-ethoxyethanol
AFM	atomic force microscopy
AM	amyl butyrate
AW	acrawax
BV	butyl valerate
CW	carnauba wax
DE	diethyl ether
DEP	diethyl phthalate
DGDE	diethylene glycol dimethyl ether
DGME	diethylene glycol monoethyl ether
DSC	differential scanning calorimetry
EWC	equilibrium water content
HDPE	high-density polyethylene
HPIM	high pressure injection moulding
LDPE	low-density polyethylene
LLDPE	linear low-density polyethylene
LPIM	low pressure injection moulding
NMA	methylacetamide
PC	polycarbonate
PE	polyethylene
PEG	polyethylene glycol
PIM	powder injection moulding
PMMA	poly(methyl methacrylate)
PP	polypropylene
PVMK	poly(vinyl methyl ketone)
PVPh	poly(4-vinylphenol)
PVT	pressure-volume-temperature
PW	paraffin wax

SA	stearic acid
TGA	thermogravimetric analysis
TGME	tri(ethylene glycol) monoethyl ether

LIST OF FIGURES AND TABLES

Figures

Scheme

Tables

Table 8. Roughness profiles R_z (μm) of the tested powders and mould-die materials (Paper IV).

Table 9. Self-interaction and association energies of low molecular analogues [J/mol] (derived from Paper II and Paper III).

Table 10. Peak position ν, surface tension γ and corrected peak shift $\Delta\nu_{XY}$ for corresponding liquids (Paper II and Paper III).

Table 11. Temperature drop ΔT, heat of mixing $\Delta H_M/(n_X+n_Z)$ and molar fraction $n_X/(n_X+n_Z)$ (Paper II and Paper III).

REFERENCES

1. German, R.M., *Powder injection molding*. Metal Powder Industries Federation: 1990.
2. Danitz, D. In *Scarles surgery*, Proceedings of International Conference on Powder Injection Molding, Princeton, 2009; Metal Powder Industries Federation: Princeton.
3. German, R.M.; Bose, A., *Injection molding of metals and ceramics*. Metal Powder Industries Federation: Princeton, N.J., 1997.
4. Thomas-Vielma, P.; Cervera, A.; Levenfeld, B.; Varez, A., Production of alumina parts by powder injection molding with a binder system based on high density polyethylene. *J Eur Ceram Soc* **2008**, *28*, 763-771.
5. Griffin, E.; McMillin, S.; Griffin, C., Modelling the powder injection moulding process for ceramics and metals. *Powder Metall* **1997**, *40*, 248-249.
6. Hausnerova, B.; Sanetrnik, D.; Ponizil, P., Surface structure analysis of injection molded highly filled polymer melts. *Polym Composite* **2013**, *34*, 1553-1558.
7. Tseng, W.J.; Hsu, C.K., Cracking defect and porosity evolution during thermal debinding in ceramic injection moldings. *Ceram Int* **1999**, *25*, 461-466.
8. Hwang, K.S., Common defects in metal injection molding (MIM). *Woodhead Publ Mater* **2012**, 235-253.
9. Zhang, T.; Blackburn, S.; Bridgwater, J., Debinding and sintering defects from particle orientation in ceramic injection moulding. *J Mater Sci* **1996**, *31*, 5891-5896.
10. Ren, S.B.; He, X.B.; Qu, X.H.; Humail, I.S.; Li, Y., Effects of binder compositions on characteristics of feedstocks of microsized sic ceramic injection moulding. *Powder Metall* **2007**, *50*, 255-259.
11. Chung, C.I.; Rhee, B.O.; Cao, M.Y.; Liu, C.X., Requirements of binder for powder injection-molding. *Adv Pow Met* **1989**, *1-3*, 67-78.
12. Chuankrerkkul, N.; Davies, H.A.; Messer, P.F., Application of peg/pmma binder for powder injection moulding of hardmetals. *Mater Sci Forum* **2007**, *561-565*, 953-956.
13. BASF, Carbonyl iron powder and metal systems. *Powder Injection Moulding International* 2014, 88.
14. Shivashankar, T.S.; Enneti, R.K.; Park, S.J.; German, R.M.; Atre, S.V., The effects of material attributes on powder-binder separation phenomena in powder injection molding. *Powder Technol* **2013**, *243*, 79-84.
15. Li, Y.M.; Liu, X.Q.; Luo, F.H.; Yue, J.L., Effects of surfactant on properties of MIM feedstock. *T Nonferr Metal Soc* **2007**, *17*, 1-8.
16. Chan, T.Y.; Lin, S.T., Effects of stearic-acid on the injection-molding of alumina. *J Am Ceram Soc* **1995**, *78*, 2746-2752.
17. Ren, S.B.; He, X.B.; Qu, X.H.; Humail, I.S.; Wei, Y.P., Influence of binder composition on the rheological behavior of injection-molded microsized sic suspensions. *J Univ Sci Technol B* **2008**, *15*, 297-301.
18. Fan, J.L.; Han, Y.; Liu, T.; Cheng, H.C.; Gao, Y.; Tian, J.M., Influence of surfactant addition on rheological behaviors of injection-molded ultrafine 98W-1Ni-1Fe suspension. *T Nonferr Metal Soc* **2013**, *23*, 1709-1717.
19. Rak, Z.S., New trends in powder injection moulding. *Cfi-Ceram Forum Int* **1998**, *75*, 19-21.

20. Hausnerova, B.; Marcanikova, L.; Filip, P.; Saha, P., Optimization of powder injection molding of feedstock based on aluminum oxide and multicomponent water-soluble polymer binder. *Polym Eng Sci* **2011**, *51*, 1376-1382.
21. Ahn, S.; Park, S.J.; Lee, S.; Atre, S.V.; German, R.M., Effect of powders and binders on material properties and molding parameters in iron and stainless steel powder injection molding process. *Powder Technol* **2009**, *193*, 162-169.
22. German, R.M.; Cornwall, R.G., Summary report on the worldwide market and technology for injection molding of metals and ceramics. *Adv Pm Part* **1997**, 183-185.
23. Li, Y.M.; Jiang, F.; Zhao, L.G.; Huang, B.Y., Critical thickness in binder removal process for injection molded compacts. *Mat Sci Eng a-Struct* **2003**, *362*, 292-299.
24. Shivashankar, T.S.; German, R.M., Effective length scale for predicting solvent-debinding times of components produced by powder injection molding. *J Am Ceram Soc* **1999**, *82*, 1146-1152.
25. Li, S.L.; Huang, B.Y.; Qu, X.H.; Li, Y.M., Solvent de-binding of water-soluble binder in powder injection moulding. *T Nonferr Metal Soc* **1999**, *9*, 578-581.
26. Tsai, D.S.; Chen, W.W., Solvent debinding kinetics of alumina green bodies by powder injection-molding. *Ceram Int* **1995**, *21*, 257-264.
27. Hwang, K.S.; Hsieh, Y.M., Comparative study of pore structure evolution during solvent and thermal debinding of powder injection molded parts. *Metall Mater Trans A* **1996**, *27*, 245-253.
28. Justino, J.G.; de Resende, L.M.; Fredel, M.C.; Wendhausen, P.A.; Neto, J.A.; Ristow, K.W.; Klein, A.N., Powder injection molding: A comparison of two debinding procedures based on solvent extraction. *Adv Powder Technol* **1999**, *299-3*, 448-456.
29. Zhao, L.G.; Li, Y.M., Pore opening and binder flow during initial stage of thermal debinding in MIM. *T Nonferr Metal Soc* **2003**, *13*, 1194-1198.
30. Yang, W.W.; Hon, M.H., In situ evaluation of dimensional variations during water extraction from alumina injection-moulded parts. *J Eur Ceram Soc* **2000**, *20*, 851-858.
31. Lin, H.K.; Hwang, K.S., In situ dimensional changes of powder injection-molded compacts during solvent debinding. *Acta Mater* **1998**, *46*, 4303-4309.
32. Westcot, E.J.; Binet, C.; German, R.M., In situ dimensional change, mass loss and mechanisms for solvent debinding of powder injection moulded components. *Powder Metall* **2003**, *46*, 61-67.
33. Yang, W.W.; Yang, K.Y.; Wang, M.C.; Hon, M.H., Solvent debinding mechanism for alumina injection molded compacts with water-soluble binders. *Ceram Int* **2003**, *29*, 745-756.
34. Clayton, A.B.; Chirila, T.V.; Dalton, P.D., Hydrophilic sponges based on 2-hydroxyethyl methacrylate .3. Effect of incorporating a hydrophilic crosslinking agent on the equilibrium water content and pore structure. *Polym Int* **1997**, *42*, 45-56.
35. Hammond, P.D.; Evans, J.R.G., Thermolytic debinding of ceramic moldings using overpressure. *Chem Eng Sci* **1995**, *50*, 3187-3200.
36. Hwang, K.S.; Tsou, T.H., Thermal debinding of powder injection molded parts - observations and mechanisms. *Metall Trans A* **1992**, *23*, 2775-2782.
37. Liang, S.Q.; Huang, B.Y.; Qu, X.H., Debinding mechanism and kinetics for PW in PW-WC feedstock under air atmosphere. *T Nonferr Metal Soc* **1996**, *6*, 72-75.
38. Wang, J.S.; Lin, S.P.; Hon, M.H.; Wang, M.C., Debinding process of Fe-6Ni-4Cu compact fabricated by metal injection molding. *Jpn J Appl Phys 1* **2000**, *39*, 616-621.

39. Belgacem, M.; Thierry, B.; Jean-Claude, G., Investigations on thermal debinding process for fine 316L stainless steel feedstocks and identification of kinetic parameters from coupling experiments and finite element simulations. *Powder Technol* **2013**, *235*, 192-202.
40. German, R.M., *Sintering theory and practice*. Wiley: New York, 1996, 15, 550.
41. Brandrup, J.; Immergut, E.H.; Grulke, E.A., *Polymer handbook, 4th edition*. 4th ed.; Wiley: New York ; Chichester, 2004.
42. Wen, G.A.; Cao, P.; Gabbitas, B.; Zhang, D.; Edmonds, N., Development and design of binder systems for titanium metal injection molding: An overview. *Metall Mater Trans A* **2013**, *44*, 1530-1547.
43. Ani, S.M.; Muchtar, A.; Muhamad, N.; Ghani, J.A., Characterisation of mixing uniformity and rheological properties of alumina-zirconia powder for ceramic injection moulding. *Sains Malays* **2013**, *42*, 1311-1317.
44. Okada, K.; Nagase, Y., Prediction of shear viscosity for ceramic injection molding mixtures. *J Chem Eng Jpn* **2000**, *33*, 927-929.
45. Bhat, V.V.; Madras, G.; Joshi, P.; Das, R.N.; Umarji, A.M., Determination of viscosities for alumina-polyethylene blends. *J Mater Sci* **2002**, *37*, 1333-1336.
46. Huang, M.S.; Hsu, H.C., Effect of backbone polymer on properties of 316L stainless steel MIM compact. *J Mater Process Tech* **2009**, *209*, 5527-5535.
47. Bakan, H.I.; Jumadi, Y.; Messer, P.F.; Davies, H.A.; Ellis, B., Study of processing parameters for MIM feedstock based on composite peg-pmma binder. *Powder Metall* **1998**, *41*, 289-291.
48. Anwar, M.Y.; Messer, P.F.; Ellis, B.; Davies, H.A., Injection-molding of 316L stainless-steel powder using novel binder system. *Powder Metall* **1995**, *38*, 113-119.
49. Newell, M.A.; Davies, H.A.; Messer, P.F.; Greensmith, D.J., Metal injection moulding of scissors using hardenable stainless steel powders. *Powder Metall* **2005**, *48*, 227-230.
50. Omar, M.A.; Davies, H.A.; Messer, P.F.; Ellis, B., The influence of pmma content on the properties of 316L stainless steel MIM compact. *J Mater Process Tech* **2001**, *113*, 477-481.
51. Singh, A.K.; Mishra, R.K.; Prakash, R.; Maiti, P.; Singh, A.K.; Pandey, D., Specific interactions in partially miscible polycarbonate (PC)/poly (methyl methacrylate) (PMMA) blends. *Chem Phys Lett* **2010**, *486*, 32-36.
52. Moballegh, L.; Morshedian, J.; Esfandeh, M., Copper injection molding using a thermoplastic binder based on paraffin wax. *Mater Lett* **2005**, *59*, 2832-2837.
53. Guo, S.B.; Qu, X.H.; He, X.B.; Zhou, T.; Duan, B.H., Powder injection molding of Ti-6Al-4V alloy. *J Mater Process Tech* **2006**, *173*, 310-314.
54. Krauss, V.A.; Oliveira, A.A.M.; Klein, A.N.; Al-Qureshi, H.A.; Fredel, M.C., A model for PEG removal from alumina injection moulded parts by solvent debinding. *J Mater Process Tech* **2007**, *182*, 268-273.
55. Sharmin, K.; Schoegl, I., Optimization of binder removal for ceramic microfabrication via polymer co-extrusion. *Ceram Int* **2014**, *40*, 3939-3946.
56. Lee, S.H.; Jeung, W.Y., Anisotropic injection molding of strontium ferrite powder using a PP/PEG binder system. *J Magn Magn Mater* **2001**, *226*, 1400-1402.
57. Xie, Z.P.; Luo, H.S.; Wang, X.; Li, H.B.; Huang, Y., The effect of organic vehicle on the injection molding of ultra-fine zirconia powders. *Mater Design* **2005**, *26*, 79-82.
58. Gutierrez, J.A.E.; Fredel, M.C.; Wendhausen, P.P.; Klein, A.N., Preparation of hard metal (WC-10Co) components by powder injection moulding. *Key Eng Mat* **2001**, *189-1*, 579-585.

59. Martyn, M.T.; Issitt, D.A.; Haworth, B.; James, P.J., Injection-molding of powders. *Powder Metall* **1988**, *31*, 106-112.
60. Soykan, H.S.; Karakas, Y., Injection moulding of thin walled zirconia tubes for oxygen sensors. *Adv Appl Ceram* **2005**, *104*, 285-290.
61. Tseng, W.J., Influence of surfactant on rheological behaviors of injection-molded alumina suspensions. *Mat Sci Eng a-Struct* **2000**, *289*, 116-122.
62. Fang, W.; He, X.B.; Zhang, R.J.; Yang, S.D.; Qu, X.H., The effects of filling patterns on the powder-binder separation in powder injection molding. *Powder Technol* **2014**, *256*, 367-376.
63. Mannschatz, A.; Hohn, S.; Moritz, T., Powder-binder separation in injection moulded green parts. *J Eur Ceram Soc* **2010**, *30*, 2827-2832.
64. Rhee, B.O.; Chung, C.I., Effects of the binder characteristics on binder separation in powder injection-molding. *Powder Injection Molding Symposium - 1992* **1992**, 131-153.
65. Hausnerova, B.; Sanetrnik, D.; Paravanova, G., Wall-slip of highly filled powder injection molding compounds: Effect of flow channel geometry and roughness. *Times of Polymers (Top) and Composites 2014* **2014**, *1599*, 518-521.
66. Yang, D.; Xu, Z.; Liu, C.; Wang, L.D., Experimental study on the surface characteristics of polymer melts. *Colloid Surface A* **2010**, *367*, 174-180.
67. Chinnam, J.; Das, D.; Vajjha, R.; Satti, J., Measurements of the contact angle of nanofluids and development of a new correlation. *Int Commun Heat Mass* **2015**, *62*, 1-12.
68. Michalski, M.C.; Hardy, J.; Saramago, B.J.V., On the surface free energy of pvc/eva polymer blends: Comparison of different calculation methods. *J Colloid Interf Sci* **1998**, *208*, 319-328.
69. Ucar, I.O.; Doganci, M.D.; Cansoy, C.E.; Erbil, H.Y.; Avramova, I.; Suzer, S., Combined xps and contact angle studies of ethylene vinyl acetate and polyvinyl acetate blends. *Appl Surf Sci* **2011**, *257*, 9587-9594.
70. Harth, M.; Schubert, D.W., Simple approach for spreading dynamics of polymeric fluids. *Macromol Chem Physic* **2012**, *213*, 654-665.
71. Bruinsma, R., Slow spreading of polymer melts. *Macromolecules* **1990**, *23*, 276-280.
72. Silberzan, P.; Leger, L., Spreading of polymer microdrops on high-energy solid-surfaces. *Cr Acad Sci Ii* **1991**, *312*, 1089-1094.
73. Schonhor.H; Frisch, H.L.; Kwei, T.K., Kinetics of wetting of surfaces by polymer melts. *J Appl Phys* **1966**, *37*, 4967-4970.
74. Lanteri, B.; Burlet, H.; Poitou, A.; Campion, I., Rheological behaviour of a polymer-ceramic blend used for injection moulding. *J Mater Sci* **1996**, *31*, 1751-1760.
75. Kwon, T.H.; Ahn, S.Y., Slip characterization of powder/binder mixtures and its significance in the filling process analysis of powder injection-molding. *Powder Technol* **1995**, *85*, 45-55.
76. Krauss, V.A.; Pires, E.N.; Klein, A.N.; Fredel, M.C., Rheological properties of alumina injection feedstocks. *Materials Research* **2005**, *8*, 187-189.
77. Pearson, J.R.; Petrie C.J., In *On the melt flow instability of extruded polymers*, Polymer systems: deformation and Flow, London, 1968; Wetton, R.E.W., R.W., Ed. Macmillan,: London, 163-168.
78. Jabbarzadeh, A.; Atkinson, J.D.; Tanner, R.I., Wall slip in the molecular dynamics simulation of thin films of hexadecane. *J Chem Phys* **1999**, *110*, 2612-2620.
79. Zheng, R.; Tanner, R.I.; Fan, X.J., *Injection molding: Integration of theory and modeling methods*. Springer Berlin Heidelberg, 2011.

80. Paul, D.R.; Bucknall, C.B., *Polymer blends*. Wiley: New York ; Chichester, 2000.
81. Rajabi, J.; Muhamad, N.; Sulong, A.B.; Aziz, H.; Fayyaz, A.; Zakaria, H., Characterization of fabricated feedstock using nano powders and a water-soluble binder in micro metal injection molding. *J Nano Res-Sw* **2013**, *25*, 174-180.
82. Khudhair, A.M.; Farid, M.M., A review on energy conservation in building applications with thermal storage by latent heat using phase change materials. *Energ Convers Manage* **2004**, *45*, 263-275.
83. Chen, F.; Wolcott, M.P., Miscibility studies of paraffin/polyethylene blends as form-stable phase change materials. *Eur Polym J* **2014**, *52*, 44-52.
84. Sudhakar, Y.N.; Selvakumar, M., Miscibility of chitosan and poly(ethyleneglycol) blends in buffer solution. *E-Polymers* **2012**.
85. Doulabi, A.H.; Mirzadeh, H.; Imani, M., Miscibility study of chitosan/polyethylene glycol fumarate blends in dilute solutions. *J Appl Polym Sci* **2013**, *127*, 3514-3521.
86. Kate, K.H.; Enneti, R.K.; Park, S.J.; German, R.M.; Atre, S.V., Predicting powder-polymer mixture properties for PIM design. *Crit Rev Solid State* **2014**, *39*, 197-214.
87. Zheng, Z.S.; Qu, X.H., Numerical simulation of powder injection moulding filling process for intricate parts. *Powder Metall* **2006**, *49*, 167-172.
88. Suri, P.; German, R.M.; de Souza, J.P.; Park, S.J., Numerical analysis of filling stage during powder injection moulding: Effects of feedstock rheology and mixing conditions. *Powder Metall* **2004**, *47*, 137-143.
89. Panayiotou, C., Polymer-polymer miscibility and partial solvation parameters. *Polymer* **2013**, *54*, 1621-1638.
90. Coleman, M.M.; Graf, J.F.; Painter, P.C., *Specific interactions and the miscibility of polymer blends practical guides for predicting & designing miscible polymer mixtures*. Technomic: Lancaster, PA, 1991, 18, 495.
91. Svoboda, P.; Kressler, J.; Ougizawa, T.; Inoue, T.; Ozutsumi, K., Ftir and calorimetric analyses of the specific interactions in poly(epsilon-caprolactone)/poly(styrene-co-acrylonitrile) blends using low molecular weight analogues. *Macromolecules* **1997**, *30*, 1973-1979.
92. Landry, C.J.T.; Teegarden, D.M., Heats of mixing of strongly interacting model compounds and miscibility of the corresponding polymers. *Macromolecules* **1991**, *24*, 4310-4321.
93. French, R.N.; Machado, J.M.; Linvien, D., Miscible polyacetal poly(vinyl phenol) blends .1. Predictions based on low-molecular-weight analogs. *Polymer* **1992**, *33*, 755-759.
94. Brune, B.J.; Koehler, J.A.; Smith, P.J.; Payne, G.F., Correlation between adsorption and small molecule hydrogen bonding. *Langmuir* **1999**, *15*, 3987-3992.
95. Huang, H.; Hu, Y.; Zhang, J.M.; Sato, H.; Zhang, H.T.; Noda, I.; Ozaki, Y., Miscibility and hydrogen-bonding interactions in biodegradable polymer blends of poly(3-hydroxybutyrate) and a partially hydrolyzed poly(vinyl alcohol). *J Phys Chem B* **2005**, 109, 19175-19183.
96. Qin, C.; Pires, A.T.N.; Belfiore, L.A., Spectroscopic investigations of specific interactions in amorphous polymer polymer blends - poly(vinylphenol) and poly(vinyl methyl ketone). *Macromolecules* **1991**, *24*, 666-670.
97. Cruzramos, C.A.; Paul, D.R., Evaluation of interactions in blends of ethylene vinyl-acetate copolymers with polyvinyl-chloride) using model compounds. *Macromolecules* **1989**, *22*, 1289-1300.

98. Pfennig, J.L.G.; Keskkula, H.; Barlow, J.W.; Paul, D.R., Experimental simulation of the effect of intramolecular repulsion on the heat of mixing for polymer blends. *Macromolecules* **1985**, *18*, 1937-1940.
99. Brannock, G.R.; Barlow, J.W.; Paul, D.R., Blends of styrene acrylic-acid copolymers and acrylic polymers. *J Polym Sci Pol Phys* **1990**, *28*, 871-891.
100. Rana, D.; Mandal, B.M.; Bhattacharyya, S.N., Analogue calorimetry of polymer blends: Poly(styrene-co-acrylonitrile) and poly(phenyl acrylate) or poly(vinyl benzoate). *Polymer* **1996**, *37*, 2439-2443.
101. Bernazzani, L.; Cardelli, C.; Conti, G.; Gianni, P., Analog calorimetry and uniquac group contributions approaches to the miscibility of pvc with eva copolymers. *J Therm Anal Calorim* **2002**, *70*, 927-947.
102. Ziaee, S.; Paul, D.R., Polymer-polymer interactions via analog calorimetry. Blends of polystyrene with poly(2,6-bimethyl-1,4-phenylene oxide). *Abstr Pap Am Chem S* **1996**, *212*, 12-14.
103. Bourara, H.; Hadjout, S.; Benabdelghani, Z.; Etxeberria, A., Miscibility and hydrogen bonding in blends of poly(4-vinylphenol)/poly(vinyl methyl ketone). *Polymers-Basel* **2014**, *6*, 2752-2763.
104. Nogueira, R.E.; Bezerra, A.C.; dos Santos, F.C.; de Sousa, M.R.; Acchar, W., Low-pressure injection molding of alumina ceramics using a carnauba wax binder: Preliminary results. *Key Eng Mat* **2001**, *189-1*, 67-72.
105. Supriadi, S.; Baek, E.R.; Choi, C.J.; Lee, B.T., Binder system for STS 316 nanopowder feedstocks in micro-metal injection molding. *J Mater Process Tech* **2007**, *187*, 270-273.
106. Rei, M.; Souza, J.P.; Schaeffer, L., Debinding properties' study of a 316L stainles steel feedstock. *Key Eng Mat* **2001**, *189-1*, 616-622.
107. Ahmad, M.J.B.; Bin Ahmad, M.A.; Bin Ibrahim, R.; Bin Mohamad, M.; Abu Kasim, N.B.; Kadir, M.R.; Bin Muhamad, S.; Itoh, Y.; Hanada, K.; Shimizu, T., Physical and mechanical properties of sintered titanium alloy produced through metal injection molding (MIM) process for craniofacial application. *Advanced Materials Conference (Amc 2012)* **2014**, *879*, 85-89.
108. Cho, T.S., Solvent extraction of polyethylene glycol by ethanol in powder injection molded compacts. *Polym-Korea* **2001**, *25*, 665-670.
109. Chuankrerkkul, N.; Sooksaen, P.; Pakunthod, P.; Kosalwit, T.; Pinthong, W., Powder injection moulding of alumina using PEG/PVB binder systems. *Key Eng Mater* **2013**, *545*, 173-176.
110. Chen, G.; Cao, P.; Wen, G.A.; Edmonds, N., Debinding behaviour of a water soluble PEG/PMMA binder for ti metal injection moulding. *Mater Chem Phys* **2013**, *139*, 557-565.
111. Yang, W.W.; Yang, K.Y.; Hon, M.H., Effects of PEG molecular weights on rheological behavior of alumina injection molding feedstocks. *Mater Chem Phys* **2003**, *78*, 416-424.
112. Craig, R.G.; Eick, J.D.; Peyton, F.A., Properties of natural waxes used in dentistry. *J Dent Res* **1965**, *44*, 1308-1312.
113. Hsu, K.C.; Lin, C.C.; Lo, G.M., The effect of wax composition on the injection molding of carbonyl iron powder with LDPE. *Can Metall Quart* **1996**, *35*, 181-187.
114. Shafrin, E.G.; Zisman, W.A., Constitutive relations in the wetting of low energy surfaces and the theory of the retraction method of preparing monolayers. *J Phys Chem-Us* **1960**, *64*, 519-524.
115. Chiou, Y.H.; Liu, S.J.; Lin, S.T., Superplastic behaviour of a zirconia powder binder blend. *Ceram Int* **1996**, *22*, 211-217.

116. Lin, S.T.; German, R.M., Interaction between binder and powder in injection-molding of alumina. *J Mater Sci* **1994**, *29*, 5207-5212.
117. Richards, V.L., Adsorption of dispersants on zirconia powder in tape-casting slip compositions. *J Am Ceram Soc* **1989**, *72*, 325-327.
118. Mittal, K.L.; Anderson, H.R.; Fowkes, F.M., *Acid-base interactions : Relevance to adhesion science and technology : In honor of the 75th birthday of professor frederick m. Fowkes*. VSP: Utrecht, 1991.
119. George, W.O.; McIntyre, P.S.; Mowthorpe, D.J., *Infrared spectroscopy*. Published on behalf of ACOL by Wiley: Chichester, 1987.
120. Ma, J.K.H.; Hadzija, B., *Basic physical pharmacy*. Jones & Bartlett Learning, 2013.
121. Drago, R.S.; Vogel, G.C.; Needham, T.E., 4-parameter equation for predicting enthalpies of adduct formation. *J Am Chem Soc* **1971**, *93*, 6014-6018.

PAPER I

Molecules **2014**, *19*, 2748-2760; doi:10.3390/molecules19032748

OPEN ACCESS

molecules

ISSN 1420-3049

www.mdpi.com/journal/molecules

Article

Polyolefin Backbone Substitution in Binders for Low Temperature Powder Injection Moulding Feedstocks

Berenika Hausnerova [1,2,*], Ivo Kuritka [2,3] and Davit Bleyan [1,2]

[1] Department of Production Engineering, Faculty of Technology, Tomas Bata University in Zlin, nam. T.G. Masaryka 5555, Zlin 760 01, Czech Republic; E-Mail: bleyan@ft.utb.cz

[2] Centre of Polymer Systems, University Institute, Tomas Bata University in Zlin, Nad Ovcirnou 3685, Zlin 760 01, Czech Republic; E-Mail: kuritka@ft.utb.cz

[3] Polymer Centre, Faculty of Technology, Tomas Bata University in Zlin, nam. T.G. Masaryka 5555, Zlin 760 01, Czech Republic

* Author to whom correspondence should be addressed; E-Mail: hausnerova@ft.utb.cz; Tel.: +420-576-035-167; Fax: +420-576-031-444.

Received: 3 January 2014; in revised form: 20 February 2014 / Accepted: 21 February 2014 / Published: 27 February 2014

Abstract: This paper reports the substitution of polyolefin backbone binder components with low melting temperature carnauba wax for powder injection moulding applications. The effect of various binder compositions of Al_2O_3 feedstock on thermal degradation parameters is investigated by thermogravimetric analysis. Within the experimental framework 29 original feedstock compositions were prepared and the superiority of carnauba wax over the polyethylene binder backbone was demonstrated in compositions containing polyethylene glycol as the initial opening agent and governing the proper mechanism of the degradation process. Moreover, the replacement of synthetic polymer by the natural wax contributes to an increase of environmental sustainability of modern industrial technologies.

Keywords: binder; polyolefin; carnauba wax; debinding; thermogravimetric analysis; powder injection moulding

---

1. Introduction

Powder Injection Moulding (PIM) has attracted great attention in the production of net-shape, high precision parts for the medical, aerospace and automotive industry in high production volumes due to its low processing cost and time effectiveness. PIM offers clear advantages over other net-shaping techniques, including pressing and casting, for high volume, complex geometry parts of tight dimensional tolerances [1].

During the process, metallic or ceramic powder is mixed with polymeric substances to create a homogeneous feedstock which is moulded into the desired shape after pelletizing. To extract the binder the moulded compacts are treated by chemical (solvent) and thermal routes in the step called debinding. Then, during the final stage the porous products are sintered to a density near the theoretical one.

Such a multi-step processing necessarily evolves often contradictory or inconsistent requirements on the composition of binder system, which must ensure agglomeration-free and uniform distribution of powder particles within feedstock during mixing, and provide the feedstock with moderate viscosity during injection moulding. Then, during debinding it must have steady thermal degradation properties and high yield stress to retain the shape of the product during binder burnout up to early sintering [2].

Furthermore, as the PIM technology expands to reactive powders, an additional requirement on binder appears – the need to mix and mould the feedstock at low temperatures in order to diminish the oxidation reactions at elevated temperatures. Additional benefits are energy and material (with protective inert atmospheres such as argon) savings through mixing and moulding steps of the process.

Lack of any of these requirements may result in cracks, voids, distortions, non-uniform shrinkage and warping in the final products [3,4]. Clearly, in order to provide feedstocks tailored to the process demands, multi-component binder systems must be used. A typical binder system includes a thermoplastic polymer (polyolefin) as a backbone, waxes and processing aids [5,6].

In this paper, low density polyethylene (PE) will be substituted with a carnauba wax (CW) and polyethylene glycols (PEG) of different molecular weights. Thermal and combined solvent-thermal debinding of aluminum oxide feedstocks based on PE and CW will be analysed by themogravimetry.

In a previous paper [7] it has been shown that due to the relatively high hygroscopicity of fine alumina powder it imposes rather sophisticated requirements on binder system. A lot of effort has been done [8–10] to investigate the thermal degradation properties of thermoplastic feedstocks based on aluminum oxide occurring as evaporation, thermal degradation and oxidative degradation (in the case of oxygen presence in the atmosphere). Trunec and Cihlar [8] have shown for 60 vol.% feedstock containing ethylene-vinyl acetate copolymer, paraffin wax and stearic acid (SA) in nitrogen (flow rate 3.3 $cm^3 \cdot s^{-1}$, heating rate 10 $°C \cdot min^{-1}$) that high binder loss rates may not allow uniform binder redistribution, resulting in inhomogeneous saturation of the body with binder with porous surface layers and excess binder in the body center, leading to the formation of cracks.

Krauss *et al.* [9] demonstrated that the solvent (water) extraction of PEG from 55 vol.% alumina feedstock containing polyvinyl butyral as a backbone, PEG and SA is diffusion-controlled, since the weight loss of PEG is square root time dependent. They also developed a mathematical model based on a core-shrinkage mechanism with diffusion in the porous region, and confirmed its good agreement with the experimental data.

Voorhees *et al.* [10] investigated thermal degradation products of PEG in an alumina feedstock and proposed the concept of the major pyrolysis reactions. The thermogravimetric curves showed that alumina has no effect on PEG/alumina feedstock thermal degradation products.

Finally, it should be mentioned that providing conclusions of general relevance is a rather complicated task, since in the majority of cases the debinding mechanism(s) of one component is dependent on the other components of a binder system, and systematic study of the effect of particular binder components and their concentration in the bulk binder is still missing. The complexity of the compositions used requires detailed studies on each component. Here we report on the role of PEG with different molar mass, polyethylene and paraffin and substitution of these two components by CW from natural sources.

2. Results and Discussion

2.1. Design of Binder Composition

The binder components employed in the study were selected with respect to the requirements described in the Introduction. The first group of binder compositions (Table 1) contained low density polyethylene (PE). Huang and Hsu [11] studied the effect of high and low density polyethylenes and their blend (50:50) on the properties of 316 L stainless steel feedstocks containing also paraffin wax (PW) and stearic acid (SA) and found out that low density PE results in more favorable flow behavior, however high density PE provides better dimensional stability of the molded part, and thus the combination of both PEs was recommended to gain the maximum benefits.

Table 1. Polyolefin-based feedstocks.

Name	PE	PW	PEG1000	PEG4000	PEG6000	SA	ϕ_m
	wt.%	wt.%	wt.%	wt.%	wt.%	wt.%	wt.%
F1	20	20	10	39	10	1	84.7
F2	10	30	10	39	10	1	85.2
F3	20	20	10	39	10	1	85.2
F4	40	-	20	39	-	1	85.2
F5	40	-	10	25	20	5	85.2
F6a	40	10	-	20	29	1	85.2
F6b							85.5
F6c							85.9
F6d							86.5
F7a	40	10	-	10	39	1	85.2
F7b							85.5
F7c							85.8
F8a	50	-	-	10	39	1	85.2
F8b							85.5
F8c							85.8
F9	20	30	-	20	29	1	85.5
F10	30	30	-	-	39	1	85.2
F11	35	30	-	15	19	1	85.2
F12	30	40	-	12	13	5	85.6
F13	31	33	-	15	16	5	85.2
F14	20	30	10	15	22	3	85.5
F15	25	36	10	10	16	3	85.2
F16	20	10	20	20	27	3	85.2

Hsu *et al.* [12] compared PW, carnauba (CW), polyethylene wax (PEW) and acrawax (AW) in 56 vol.% 304 L stainless steel feedstocks containing 22 vol.% of low density polyethylene (PE) and demonstrated that usage of PW-PE based binders resulted in the highest tensile strength of the sintered parts, however polar waxes (CW and AW) improved the process-ability of the feedstock due to enhanced interactions with powder. Furthermore, AW containing strong polar amide groups and short hydrocarbon chain ends provides the highest carbon content in brown (debinded) parts, and also is less compatible with PE than CW. In order to prevent possible separation and aggregation of PE molecules from the binder during mixing as well as due to the better mechanical properties of CW based feedstocks than AW ones, the former (CW) has been employed as a backbone of the second feedstocks group in this study (Table 2).

Table 2. Non-polyolefin based feedstocks.

Name	CW wt.%	PW wt.%	PEG1000 wt.%	PEG4000 wt.%	PEG6000 wt.%	SA wt.%	ϕ_m wt.%
F17	-	45	-	-	50	5	84.7
F18	-	40	-	15	40	5	84.2
F19	25	30	-	20	20	5	84.5
F20	35	20	10	10	20	5	84.2
F21	40	10	10	12	25	3	84.2
F22	40	10	10	14	25	1	85.2

Waxes and polyethylene glycol are common components of both feedstocks investigated. With low melting temperatures, waxes can be removed at the early stage of debinding consequently creating a network of pores which will promote the thermal degradation of higher molecular weight polymers. Waxes also increase the wetting characteristics of the powder, ensuring uniform coating of the particles.

In this study, the effect of molecular weight of polyethylene glycols is also considered. Yang and Hon [13] and Yang *et al.* [14] studied the influence of low molecular weight polyethylene glycol (PEG) on rheological and debinding characteristics of aluminum oxide feedstock containing PEG, PE wax and SA. Higher content of low-molecular PEG improved the flow-ability of the bulk feedstock. As a processing aid, stearic acid (SA) lubricating and wetting powder particles [15] is used. As it has been reported [16], it plays a critical role in creating homogenous mixture as well as insuring higher rate of binder extraction throughout the network of pores created in body during early stage of thermal debinding.

2.2. Thermal Analysis of Feedstocks

The TGA results are presented through the peak degradation temperatures and corresponding mass losses depicted in Table 3. The thermal degradation of highly filled systems proceeds evidently in several steps, however, they are relatively poorly resolved due to the influence of transport processes and the data analysis was elaborated with the aid of numerical derivation. The peak degradation temperature on the negative derivative TGA curve corresponds to the inflexion point in the respective thermal degradation step signalizing thus the highest mass loss rate temperature. In several cases of even less resolved peaks, higher derivatives were calculated and the position of the significant points was refined. If needed, the onset temperatures were obtained from common analytical procedure

employing the intersection of the horizontal line at the transition between the distinguishable steps and the tangent in the inflection point [6]. During the debinding stage three main processes are involved: evaporation, thermal degradation and oxidative degradation [17,18]. The low molecular weight compounds or fragments of polymers are mainly evaporated by propagation towards the specimen surface, while high molecular weight components are subjected to thermal degradation [19].

Table 3. Feedstock thermal degradation peaks in percentage of weight loss.

Feedstock	Peak 1		Peak 2		Peak 3		Peak 4	
	[°C]	[wt.%]	[°C]	[wt.%]	[°C]	[wt.%]	[°C]	[wt.%]
F1	185	0.36	223	11.61	-	-	455	4.98
F2	180	0.19	215	11.92	-	-	447	4.8
F3	175	0.51	215	10.09	-	-	465	5.77
F4	171	0.33	223	10.15	348	4.33	469	2.11
F5	175	0.21	238	9.35	349	4.53	473	2.2
F6a	176	0.15	251	8.82	352	4.97	473	2.18
F6b	184	0.15	234	7.77	338	4.9	472	2.21
F6c	192	0.17	243	8.47	348	4.17	470	1.82
F6d	192	0.14	230	7.8	338	4.42	457	1.95
F7a	189	0.11	242	8.11	356	3.92	462	1.94
F7b	197	0.31	240	8.62	341	4.14	471	2.14
F7c	194	0.19	238	8.21	335	4.34	453	2.1
F8a	181	0.15	232	7.67	348	6.38	454	2.67
F8b	185	0.19	237	7.34	349	5.1	446	2.23
F8c	188	0.18	234	6.9	344	5.3	450	2.34
F9	180	0.23	204	7.51	352	4.48	459	1.29
F10	189	0.22	205	7.63	350	4.6	456	1.54
F11	205	0.32	-	-	354	13.9	462	1.95
F12	201	0.29	245	7.62	348	4.62	460	1.85
F13	207	0.35	251	8.29	349	4.88	455	1.96
F14	176	0.36	219	9.52	-	-	448	5.16
F15	203	0.38	248	9.25	348	4.04	455	1.74
F16	171	0.23	200	9.88	-	-	458	5
F17	174	0.18	208	10.03	-	-	442	4.64
F18	172	0.12	209	12.68	-	-	442	4.51
F19	190	0.16	231	9.07	-	-	460	6.42
F20	194	0.17	245	8.89	341	4.56	458	2.16
F21	189	0.16	-	-	346	13.71	460	2.08
F22	195	0.23	247	8.74	345	4.45	459	1.91

For polyolefins, the thermal degradation occurs by random polymer chain scission [20]. The debinding in an air atmosphere involves oxidative degradation, which acts from the surface towards the center of the specimens, while being limited by the diffusion of oxygen into the binder components and their extraction towards the surface [21].

For PE-based feedstocks, the earliest mass loss was exhibited at 171 °C for F4 (40 PE/20 PEG1000/39 PEG4000/1 SA wt.%.) and F16 (20 PE/10 PW/20 PEG1000/20 PEG4000/27 PEG 6000/3

SA wt.%.) compositions by 0.33 and 0.23 wt.% respectively, while the earliest weight drop for CW/PW based compositions took place at 172 °C for feedstock F18 by only 0.12 wt.%.

CW is composed of a mixture of linear chain esters, alcohols, acids and hydrocarbons. It exhibits the smallest linear expansion in temperature range 22–52 °C compared to other waxes [22].

For polyethylene glycol (PEG), the polymer degradation process leads to a reduction in molecular weight and to diminution of chain length, resulting from the bond scission in the backbone of the macromolecules as in the case of linear polymers [23]. The TGA data (Table 3) shows that higher overall content of PEG significantly lowers the starting temperature of thermal degradation.

The role of different molecular weight PEG on gradual thermal debinding can be seen from Figures 1 and 2 comparing two contrasting TG curves for PE based feedstock F10 (30 PE/30 PW/39 PEG6000/1 SA wt.%) and F14 (20 PE/30 PW/10 PEG1000/15 PEG4000/22 PEG6000/3 SA wt.%). For feedstock F10 the first mass loss starts at around 189 °C with a sharp drop which is linked to start of the evaporation or degradation of PW and PEG with the lowest molecular mass. Meanwhile, the higher amount of low molecular PEG1000 in feedstock F14 developed a slight slope by the start point at 176 °C. The second stage for both (F10 and F14) feedstocks starting at 205 and 219 °C, respectively, depicts the evaporation of volatile PE degradation products. The weight loss of 13.79 and 15.08 wt.% indicates of a full extraction of the binder system at 456 and 448 °C, respectively.

Figure 1. TGA weight loss and corresponding derivative curve for F10 (30 PE/30 PW/39 PEG6000/1 SA wt.%).

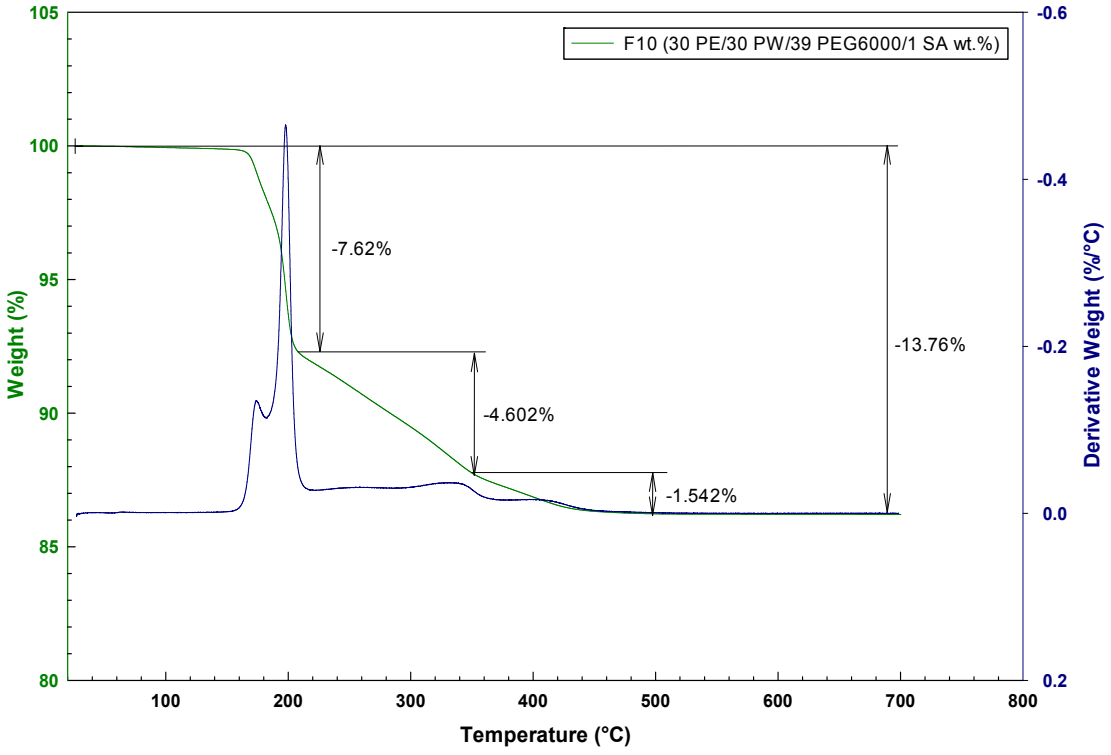

Typical feedstocks developed by using binder systems with PW and CW as a backbone binders are F17 (45 PW/50 PEG6000/5 SA wt.%) and F22 (10 PW/40 CW/10 PEG1000/14 PEG2000/25 PEG6000/1 SA wt.%), respectively. The feedstock F17 with higher amount of PW and high molecular PEG6000 shows a sharp significant drop of 10.21% at 174 °C. This tendency may lead to cracks and

distortions in the sample, and thus must be avoided in further development of binder compositions for the application. The combination of different molecular weight PEG in feedstock F22 developed a slight decrease before the first degradation stage. The first reasonable weight drop starts at 195 °C corresponding to the degradation of PEG blend and passes to a gradual decrease as of the second stage.

Figure 2. TGA weight loss and corresponding derivative curve for F14 (20 PE/30 PW/10 PEG1000/15 PEG4000/22 PEG6000/3 SA wt.%).

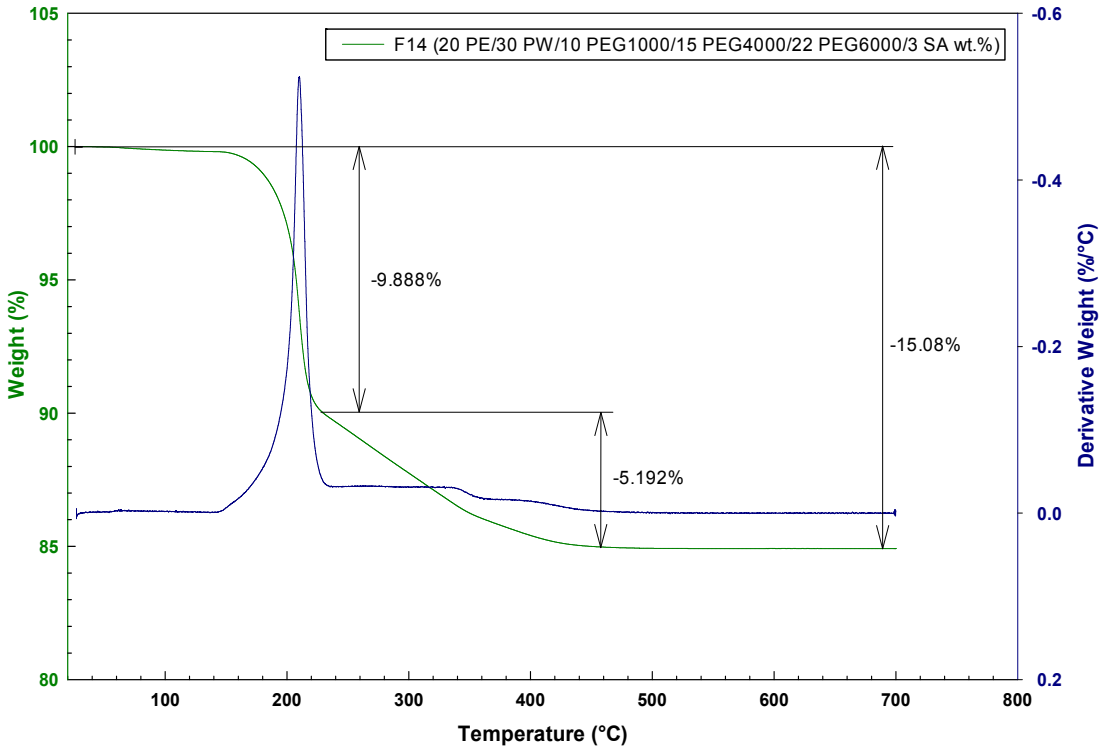

In this respect, the second stage represents the extraction of CW, where the exhibited moderate decline is connected with narrow setting range of CW. It shows that the noticeable unwanted rapid drop at the first stage for feedstock F17 can be superceded by proper choice of component's mass distribution.

The presence of the third peak in –dTGA curves situated in the temperature range 330–360 °C clearly correlates with the presence of reasonable amounts of the high molar mass polymer component in the binder. No peak was observed for compositions having less than 25 wt.% of PE and less than 30 wt.% of CW in the binder. The first step of the thermal decomposition of the binder's polymer component is manifested in this narrow temperature region regardless of the chemical nature of the polymer used which testifies to the importance of the transport phenomena in the fired body.

The highest activation energy is needed for decomposition and volatilisation of residual binder mass inside the fired body at the end of the thermal debinding process which is manifested by a decomposition step above 400 °C corresponding to the second decomposition step known for PE and CW. The scatter range of the peak maxima from 440–475 °C is narrow and most likely not influenced by the aluminium oxide filler level regardless of the use of PE or CW, like in the previous step. According to the total mass loss, full binder extraction was achieved for all examined materials.

2.3. Thermal Analysis of Water Debinded Feedstocks

The study of TGA results for previously water debinded feedstocks is summarized in Table 4.

Table 4. Water debinded feedstock thermal degradation peaks in percentage of weight loss.

Feedstock	Peak 1		Peak 2		Peak 3	
	[°C]	[wt.%]	[°C]	[wt.%]	[°C]	[wt.%]
F2	210	0.93	225	5.75	487	4.86
F6a	200	2.43	364	11.4	475	1.91
F7a	170	2.48	-	-	477	13.52
F9	170	1.33	250	6.1	480	3.56
F10	220	0.16	229	5.77	490	4.44
F14	199	0.89	220	6.57	494	4.64
F16	175	1.17	252	10.1	449	4.19
F22	208	1.8	230	6.37	467	5.35

The water debinding stage imparts the water-soluble binder components and can be used for two purposes, *i.e.*, as the technological debinding step opening pores serving as channels for volatiles generated during firing. and as the analytical tool for clarification of the role of the aforesaid extractables in the feedstock. A remarkable weight drop was obviously observed for the samples with high vol.% of low molecular PEG binders. The samples with high content of PEG and low content of PW showed the highest water debinding results, and *vice versa* for the samples with high vol.% of PW. PW and PE have the same hydrophobic behaviour but the correlation of debinding efficiency with PW rather than with PE points towards the role of PW as the key blocking agent in the investigated composition framework which may be due a better miscibility of the low molecular compounds with other component of the material system. The same tendency was observed for binders containing the CW although the CW can be considered as less hydrophobic than PE.

At first sight, the thermal decomposition of the feedstocks was influenced by the water debinding simply by removal of the low molecular PEG component and only three decomposition steps are manifested in the TGA curves. Indeed, the diminishing or disappearance of the low temperature peaks from –dTGA curves as well as depreciation of the observed mass loss steps correlates with the efficiency of the water debinding procedure discussed in the above paragraph. The changes in the mass loss proportions can be explained by the selectivity of the water debinding which removes water-soluble components. Moreover, the peaks seem to be slightly shifted towards lower temperatures indicating thus easier mass removal from the fired body in this temperature region. It can be assumed that the water debinding opened pores into the specimen body by removal of the extractable part of the binder [22].

Thorough analysis of the data in Table 4 in comparison with Table 3 showed that the thermal degradation process appearing in the range between 300 and 400 °C virtually vanishes. As shown in the section above, this decomposition step may be ascribed to the insoluble polymer component of the binder, hence it was not expected that it can be affected by water debinding. One of the effects of the water bath treatment can be not only easier removal of low molecular fractions, but also a faster and

better densification of the fired body which can increase the barrier against high molecular binder components decomposition and shift the respective mass loss step to higher temperature.

The high temperature decomposition step between 400 and 500 °C was shifted slightly to higher temperatures (467–485 °C). Such a shift corresponds to an increase of activation energy of the respective process which supports the explanation given in the previous paragraph. The high temperature final step corresponds to the decomposition of residuals entrapped strongly inside the fired body thus requiring a higher activation energy to be removed from the specimen. The mass loss connected with this decomposition step remained unchanged in samples which contained higher amounts of low or moderate molar mass PEG and lower amount of high molecular PEG. The proportion between PE and PW plays important role too. Water debinded specimen F7a which has the highest content of high molecular weight components, *i.e.*, both PE and PEG, showed an enormous increase of mass degraded in this step. A similar correlation was found for the proportion of CW and high molecular PEG. It can be summarized that a balanced proportion of PEG components results into the low high temperature mass loss. According to that the use of PEG with broad molecular mass distribution can be suggested for future experiments. However, it must be pointed out that the aforesaid rule of thumb only works for compounds with balanced proportions between PE and PW or compositions with higher amounts of CW and small additions of PW. The latter conclusion supports the effort to replace synthetic materials by renewable natural stocks. As in the simple thermal debinding, full binder extraction was achieved for all examined water debinded materials.

3. Experimental

3.1. Materials

High compressible superground aluminum oxide powder (MARTOXID MR70, Albemarle Corp, Barton Rouge, LA, USA) with tap density 2.2–2.4 g/cm³, sintered density 3.74–3.95 g/cm³ and specific surface 6–10 m²/g was used. The the particle size distribution (Figure 3) was measured on a Laser Diffraction Particle Sizing Instrument (Mastersizer 3000, Malvern Instruments Ltd, Malvern, UK).

Figure 3. Al_2O_3 powder particle size distribution curve (Mastersizer 3000).

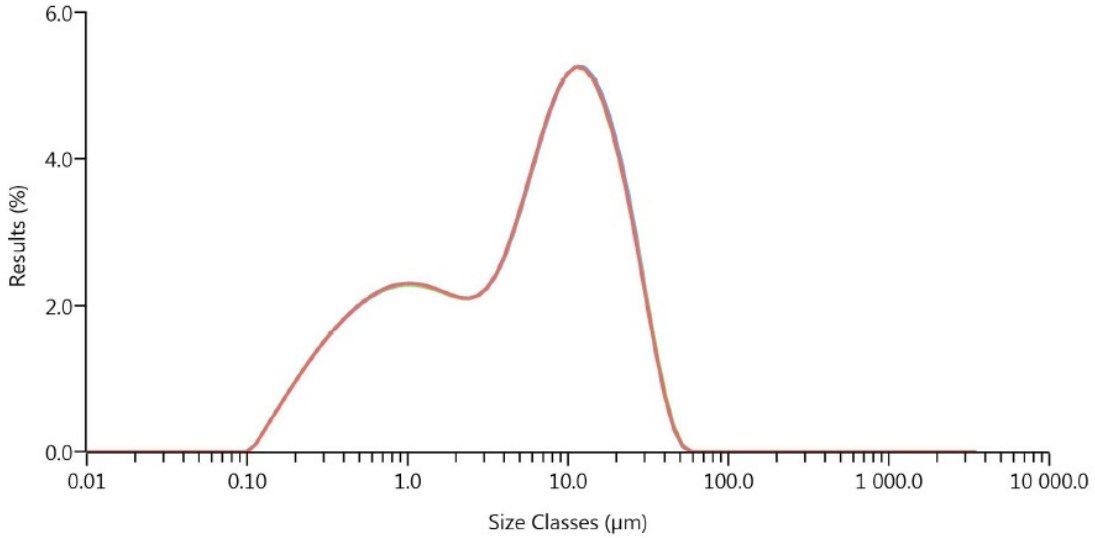

The properties of polymers serving as a binder components - low density polyethylene (PE), paraffin wax (PW), carnauba wax 2442 (CW), polyethylene glycols differing in their molecular weights (PEG1000, PEG4000, PEG6000) and stearic acid (SA) – are summarized in Table 5. Peak melting temperature was obtained from differential scanning calorimetry (Mettler Toledo DSC1, Greifensee, Switzerland) with heating-cooling rate of 10 °C/min on aluminium pan in nitrogen atmosphere with (60 mL/min) flow. Apparent shear viscosity was determinated with a rotational rheometer Bohlin Gemini CVOR 150 CE/WIN (Malvern Instruments) using a cone-plate geometry (cone angle 2.5°, plate diameter 40 mm) in an air atmosphere. Measurements were carried out at 140 °C and shear rate of 80 rad/s. Other properties were taken from the material data sheets provided by suppliers.

Table 5. Characteristic properties of the binder components.

Name	PE	PW	CW	PEG1000	PEG4000	PEG6000	SA
Density [g/cm³] ISO 1133	0.918	0.9	0.97	1.09	1.41	1.21	0.85
Melting Temperature [°C]	108	58	84	32	62	62	70
Molecular Weight [g/mol]	250,000	400	1000	1000	4000	6000	284
Viscosity [kPa.s]	20	2	12	10	72	147	3

3.2. Preparation of Feedstocks

A Brabender plasticorder with a mixing chamber of 50 cm³ volume was used for mixing the components. Mixing temperature varied between 100 and 160 °C depending on the composition of mixed feedstock, with the mixing time of 30 min at a speed 20 rpm. In sum 29 feedstock compositions were prepared, with powder loadings (ϕ_m) varying between 84.2 and 86.5 wt.%.

3.3. Methods

The thermal degradation properties were studied using a thermogravimetric analyzer TA TGA Q500 (TA Instruments, New Castle, DE, USA) with a platinum pan in an air atmosphere with a constant heating rate of 10 °C/min in temperature range between 30 and 700 °C. Purge gas flow on the balance and sample were 40 mL/min and 60 mL/min, respectively. Feedstock specimens of irregular form were tested. The mass varied between 45 to 58 mg which assured minimization of the specimen weight on the thermogravimetric analysis. In the case of the combined debinding route testing the debinding of water soluble components of binder system components was performed at 60 °C for one hour prior to the thermal debinding.

4. Conclusions

From the results it may be concluded that low molecular PEG enhances the early thermal degradation and opens a network of pores in the sample which allows defect free debinding of residual backbone binder. A well balanced ratio between different PEG fractions is required for best

performance of the debinding procedure, both for single thermal or two step debinding involving a water bath prior the thermal step. It suggests future use of polydispersive PEG.

The CW as a backbone ensures gradual and stage followed debinding process, while retaining the shape of the component up to late debinding – early sintering stage due to its very narrow setting range. In next, the application of CW allows one to decrease the amount of PW in the composition.

The thermal debinding process at temperatures above 300 °C is not influenced by the choice of PE or CW but depends exclusively on transport phenomena in the highly filled system. It can be advantageously influenced by the water debinding step application. Besides it may successfully replace the polyethylene as a backbone binder and lower the consumption of PW, so carnauba wax would be the most appropriate choice since it serves as a renewable natural resource which is an outstanding property from an environmental perspective.

Acknowledgments

This article was written with the support of Operational Program Research and Development for Innovations co-funded by the ERDF and national budget of Czech Republic, within the framework of project Centre of Polymer Systems (reg. number: CZ.1.05/2.1.00/03.0111) and of Operational Program Education for Competitiveness co-funded by the European Social Fund (ESF) and national budget of Czech Republic, within the framework of project Advanced Theoretical and Experimental Studies of Polymer Systems (reg. number: CZ.1.07/2.3.00/20.0104). The author D.B. would like to acknowledge the support of the internal grant of Tomas Bata University in Zlin No. IGA/FT/2014/ and support of Visegrad Fund.

Author Contributions

Berenika Hausnerova – state of art, idea and concept of the paper, compositions of feedstocks; Ivo Kuritka – discussion of the TGA results and conclusions; Davit Bleyan – experimental.

Conflicts of Interest

The authors declare no conflict of interest.

References

1. Onbattuvelli, V.P.; Vallury, S.; McCabe, T.; Park, S.J.; Atre, S.V. Properties of SiC and AlN feedstocks for the powder injection moulding of thermal management devices. *PIM Int.* **2010**, *4*, 64–70.
2. Chung, C.; Rhee, B.; Cao, M.; Liu, C. Requirements of binder for powder injection molding. In *Advances in Powder Metallurgy*; In Proceedings of Powder Metallurgy Conference and Exhibition, San Diego, USA, 11–14 June 1989; Gasbarre, T.G., Jandesca, W.F., Eds.; Metal Powder Industries Federation: Princeton, NJ, USA, 1989; pp. 67–78.
3. Tseng, W.J.; Hsu, C.K. Cracking defect and porosity evolution during thermal debinding in ceramic injection moldings. *Ceram. Int.* **1999**, *25*, 461–466.

4. Zhang, J.; Edirisinghe, M.; Evans, J. A catalogue of ceramic injection moulding defects and their causes. *Ind. Ceram.* **1989**, *9*, 72–82.
5. Hausnerova, B.; Vltavska, P.; Sedlacek, T. Pressure-Affected Flow Properties of Powder Injection Moulding Compounds. *Powder Technol.* **2009**, *194*, 192–196.
6. Onbattuvelli, V.P.; Enneti, R.K.; Park, S.; Atre, S.V. The effects of nanoparticle addition on binder removal from injection molded aluminum nitride. *Int. J. Refract. Metals Hard Mater.* **2013**, *36*, 77–84.
7. Hausnerova, B.; Marcanikova, L.; Filip, P.; Saha, P. Optimization of powder injection molding of feedstock based on aluminum oxide and multicomponent water-soluble polymer binder. *Polym. Eng. Sci.* **2011**, *51*, 1376–1382.
8. Trunec, M.; Cihlar, J. Thermal removal of multicomponent binder from ceramic injection mouldings. *J. Eur. Ceram. Soc.* **2002**, *22*, 2231–2241.
9. Krauss, V.A.; Oliveira, A.A.M.; Klein, A.N.; Al-Qureshi, H.A.; Fredel, M.C. A model for PEG removal from alumina injection moulded parts by solvent debinding. *J. Mater. Process. Technol.* **2007**, *182*, 268–273.
10. Voorhees, K.J.; Baugh, S.F.; Stevenson, D.N. The thermal degradation of poly(ethylene glycol)/poly(vinyl alcohol) binder in alumina ceramics. *Thermochim. Acta* **1996**, *274*, 187–207.
11. Huang, M.S.; Hsu, H.C. Effect of backbone polymer on properties of 316L stainless steel MIM compact. *J. Mater. Process. Technol.* **2009**, *209*, 5527–5535.
12. Hsu, K.C.; Lin, C.C.; Lo, G.M. Effect of wax composition on injection moulding of 304L stainless steel powder. *Powder Metall.***1994**, *37*, 272–276.
13. Yang, W.W.; Hon, M.H. *In situ* evaluation of dimensional variations during water extraction from alumina injection-moulded parts. *J. Eur. Ceram. Soc.* **2000**, *20*, 851–858.
14. Yang, W.W.; Yang, K.Y.; Hon, M.H. Effects of PEG molecular weights on rheological behavior of alumina injection molding feedstocks. *Mater. Chem. Phys.* **2003**, *78*, 416–424.
15. Ren, S.B.; He, X.B.; Qu, X.H.; Humail, I.S.; Li, Y. Effects of binder compositions on characteristics of feedstocks of microsizedSiC ceramic injection moulding. *Powder Metall.* **2007**, *50*, 255–259.
16. Persson, H.; Hausnerova, B.; Nyborg, L.; Rigdahl, M. Rheological and thermal properties of a model system for PIM. *Int. Polym. Proc.* **2009**, *24*, 206–212.
17. Knapp, A.M.; Halloran, J.W. Binder removal from ceramic-filled thermoplastic blends. *J. Am. Ceram. Soc.* **2006**, *89*, 2776–2781.
18. Chartier, T.; Delhomme, E.; Baumard, J.F. Mechanisms of binder removal involved in supercritical debinding of injection moulded ceramics. *J. Phys. III* **1997**, *7*, 291–302.
19. Maximenko, A.; Biest, O. Finite element modelling of binder removal from ceramic mouldings. *J. Eur. Ceram. Soc.* **1998**, *18*, 1001–1009.
20. Seeger, M.; Gritter, R.J. Thermal decomposition and volatilization of poly(α-olefins). *J. Polym. Sci.: Polym. Chem.* **1977**, *15*, 1393–1402.
21. Wright, J.K.; Evans, J.R.G. Kinetics of the oxidative degradation of ceramic injection-moulding vehicle. *J. Mater. Sci.* **1991**, *26*, 4897–4904.
22. Craig, R.G.; Eick, J.D.; Peyton, F.A. Properties of natural waxes used in dentistry. *J. Dent. Res.* **1965**, *44*, 1308–1316.

23. Han, S.; Kim, C.; Kwon, D. Thermal/oxidative degradation and stabilization of polyethylene glycol. *Polymer* **1997**, *38*, 317–323.

Appendix

Figure A1. TGA weight loss curves for binders used.

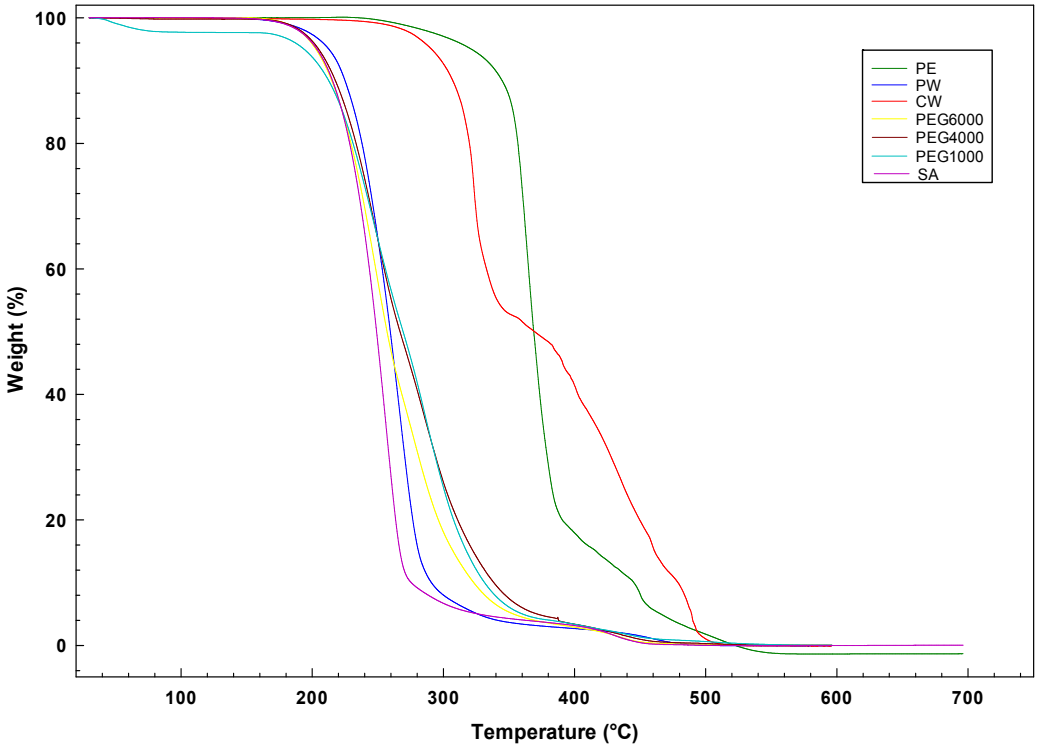

Sample Availability: Samples of all compounds F1–F22 are available from the authors.

PAPER II

Available online at www.sciencedirect.com

ScienceDirect

Ceramics International 41 (2015) 3975–3982

CERAMICS INTERNATIONAL

www.elsevier.com/locate/ceramint

Specific interactions of low molecular weight analogues of carnauba wax and polyethylene glycol binders of ceramic injection moulding feedstocks

D. Bleyan[a,b], P. Svoboda[b,c], B. Hausnerova[a,b,*]

[a]Department of Production Engineering, Faculty of Technology, Tomas Bata University in Zlin, nam. T.G. Masaryka 5555, 760 01 Zlin, Czech Republic
[b]Centre of Polymer Systems, University Institute, Tomas Bata University in Zlin, Nad Ovcirnou 3685, 760 01 Zlin, Czech Republic
[c]Department of Polymer Engineering, Faculty of Technology, Tomas Bata University in Zlin, nam. T.G. Masaryka 275, 762 72 Zlin, Czech Republic

Received 17 October 2014; received in revised form 13 November 2014; accepted 16 November 2014
Available online 26 November 2014

Abstract

This paper is devoted to understanding of the molecular interactions between components of Ceramic Injection Moulding (CIM) binders – carnauba wax (CW) and polyethylene glycol (PEG). Due to the complexity of interactions mechanisms the binders were substituted by their basic low-molecular analogues, which were then investigated using the combination of FTIR and calorimetry. Calorimetric analysis derived the self-interaction energies and association energies for the respective pairs. FTIR spectra were collected in the range of 400 to 4000 cm^{-1} for the analogue blends, where the shift of C=O and O–H stretch bounding peaks were assumed as the evidence of the presence of the partial interactions between the components. Combining obtained data a linear relation of these two independent analyses was found. The results proved reliable quantification of interactions between CW and PEG low molecular substitutes implying the partial miscibility of the respective polar polymers.

Keywords: Ceramic injection moulding; Binder; Polyethylene glycol; Carnauba wax; Low molecular weight analogue

1. Introduction

In Ceramic Injection Moulding (CIM) the binder system serves important role by granting ceramic powder with suitable viscoelastic properties [1]. For the meeting of the processing requirements (especially debinding) and simultaneous exploitation of the attractive features of each component, the typical binder system is usually composed of 3 to 5 polymers, making the systems complex, where understanding of complete and individual reaction pathways or chemical mechanisms still remains a challenge [2,3].

In majority cases, polymers serving as components of binder systems include polyolefins, waxes (mainly paraffin) and polyethylene glycols. In the papers devoted to the development of the binders system [e.g. [4,5]], the interactions of a binder with a powder and among specific binder components are often deduced from their rheological performance during mixing and injection moulding.

Though a combination of polyethylene (PE) and paraffin wax (PW) is widely used in CIM industry, it creates many issues, including insufficient initial pore formation resulting in weak internal transport mechanisms within the specimens and highly affecting debinding rates. Binder system solely composed of PE/PW may also limit the control of viscoelastic properties. A role of plasticizer in such systems is often granted to polyethylene glycol (PEG), which also serves as an endorsement for enabling initial gradual debinding process [3,6]. Furthermore, a binder system based on paraffin wax requires usage of various chemicals (heptane, hexane, or kerosene) for a solvent debinding step [7,8], which not only raises the cost of the overall process, but also – in a large scale – have a negative ecological impact. On the opposite, PEG can be easily debound in water.

The substitution of PE or PW with acrylic polymers such as poly(methyl methacrylate) (PMMA) has also been reported

*Corresponding author at: Department of Production Engineering, Faculty of Technology, Tomas Bata University in Zlin, nam. T.G. Masaryka 5555, 760 01 Zlin, Czech Republic.
E-mail address: hausnerova@ft.utb.cz (B. Hausnerova).

http://dx.doi.org/10.1016/j.ceramint.2014.11.082
0272-8842/

[9], however they still require a range of additional components to make the feedstock applicable. In addition, in CIM the feedstock processing temperature, being one of the key factors, highly influences the success of the overall process [10], and thus elevates the need of novel backbone binders such as carnauba wax (CW). As we have shown in the previous work [2,3], in contrast to PE, the CW (having lower melting temperature) significantly advances processing characteristics of CIM feedstocks.

There have been tries devoted to simplification of the process and reducing the conventional steps by implementing sophisticated techniques and by merging of two consequent stages [11], but the development of an advanced binder system may eliminate such needs by making the feedstock more robust, and significantly shortening the processing time. In addition to processing advantages, feedstocks based on CW/PEG are environmentally benign.

An understanding of molecular interactions between the particular components of CIM binders is complicated due to the complexity of interactions mechanisms. Chen et al. [12] investigated the miscibility of both nonpolar PW and polyethylenes (HDPE, LDPE and LLDPE) using differential scanning calorimetry (DSC) and atomic force microscopy. By evaluating the morphology, crystallisation and crystallinity, combined together with equilibrium melting temperature and melting point depression, the interaction parameters for polymer-diluent systems were defined. This data served as an evidence of a partial miscibility of paraffin in polyethylenes with LLDPE/PW being favourable over the PW/HDPE.

Sudhakar et al. [13] reported on miscibility of chitosan and PEG blend using a buffer solution. From collected Fourier transform infrared spectroscopy (FTIR) spectra for polyblend films and polymers it was observed that by increasing the amount of PEG the O–H stretch peak tends to lower peak wavenumbers, serving as an evidence of blend components miscibility.

Hsu et al. [4] studied the effect of PW and CW on carbonyl iron based feedstock, where LDPE served as a backbone. The rheological measurements using capillary viscometer and a statistical analysis based on the McLean-Anderson design method showed that polar CW has stronger interactions or adsorptions with iron powder than nonpolar PW, exhibiting higher viscosity, greater pseudoplasticity and lower flow activation energy than PW/LDPE. The carbon contents in sintered specimens were also in favour of CW/LDPE composition.

Studying the interactions of both polar polymers (such as in the case of CW/PEG) might be a challenging task. For polymer blends, the interactions measured will mainly present their self-interactions, even there are polymer (*X*) to polymer (*Y*) interactions they are significantly weaker than the self-interactions. Due to this fact, the polymers need to be substituted with low molecular weight analogues, which bring an advantage of eliminating the majority of self-interactions and their replacing by newly formed *XY* interactions. The component *X* can be fully surrounded by component *Y*, therefore, the interactions can be measured precisely. Such an approach representing advanced understanding of compatibility of blend components has been reported scarcely [14,15].

Using low molecular weight analogues also gives the opportunity to measure the interactions by calorimetry, which cannot be applied to polymer blends. Consequently, combining two techniques – FTIR and calorimetry – provides the possibility to evaluate the interactions quantitatively. Only few studies reported on achieving results by using analogue calorimetry as a tool for extending and scaling the results of interactions present [16–18], while FTIR combined with other techniques is commonly used as for investigating miscibility where the shift of peaks is assumed as an evidence of a partial miscibility [19–21]. Meanwhile, to our best knowledge there has been no investigation of the miscibility between CW and PEG.

2. Experimental

2.1. Materials

Several low molecular weight analogues of PEG and CW were used in this study (Table 1). As buffer solutions (solvents) hexane and decahydronaphthalene (decalin) were chosen. The properties of used analogues and solvents, including molar mass M_w, density ρ, and the specific heat capacity c_p are shown in Table 2.

2.2. FTIR analysis

The FTIR measurements were carried out in order to study the peak shift for both *X–X* and *X–Y* interactions. FTIR reflection spectroscope (Nicolet 6700, Fisher Scientific, USA) equipped with KBr glasses holder accessory was used. A drop of each mixture was measured between two KBr glasses in a transmission mode. The spectra in the range 400–4000 cm^{-1} with 32 scans were averaged and recorded at a resolution of 1 cm^{-1}. The procedure was repeated three times and the data was averaged.

2.3. Calorimetry

Calorimetric measurements were performed in order to study the thermodynamics of interactions of two components. The data

Table 1
Chemical structure of polymers, their low molecular weight analogues and solvents.

Name	Chemical formulas
Carnauba wax (CW)	$H_3C(CH_2)_{30}COO(CH_2)_{33}CH_3$
Analogues	
Amyl butyrate (AM)	$C_9H_{18}O_2$
Butyl valerate (BV)	$CH_3(CH_2)_3CO_2(CH_2)_3CH_3$
Polyethylene glycol (PEG)	$C_{2n}H_{4n+2}O_{n+1}$
Analogues	
2-ethoxyethanol (2ET)	$C_2H_5OCH_2CH_2OH$
Diethyl ether (DE)	$(CH_3CH_2)_2O$
Diethylene glycol monoethyl ether (DGME)	$C_2H_5OCH_2CH_2OCH_2CH_2OH$
Diethylene glycol dimethyl ether (DGDE)	$(CH_3OCH_2CH_2)_2O$
Triethylene glycol monoethyl ether (TGME)	$CH_3CH_2(OCH_2CH_2)_3OH$
Solvents	
Hexane	C_6H_{14}
Decalin	$C_{10}H_{18}$

Table 2
Properties of low molecular liquid substitutes and solvents.

Name	Molar mass, M_w [g/mL]	Density, ρ [g/cm³]	Heat capacity, c_p [J/Kg K]
Amyl butyrate	158.24	0.863	1927
Butyl valerate	158.24	0.868	1927
2-ethoxyethanol	90.12	0.930	2414
Diethyl ether	74.12	0.706	2320
Diethylene glycol monoethyl ether	134.17	0.999	2193
Diethylene glycol dimethyl ether	134.17	0.943	2083
Tri(ethylene glycol) monoethyl ether	178.23	1.020	2210
Hexane	86.18	0.659	2293
Decahydronaphthalene	138.25	0.896	1677

acquisition of temperature change during mixing was obtained by the help of a thermocouple (type copper-constantan) that was connected to National Instruments data acquisition equipment (NI USB-9211 A, Data Acquisition for Thermocouples). LabVIEW Signal Express 2.5 software was used for temperature data acquisition. The ratio between solvent/liquid was defined at 1%, e.g. 0.05 ml drop was blended in 5 ml solvent each time. Sampling period was set at 0.5 s. Thermocouple was dipped into the liquid which was placed on a hot plate in the insulated flask with a magnetic stir, set at 250 rpm. The temperature change during each liquid drop was acquired and the time-temperature curve was evaluated.

3. Results and discussion

In order to carry out the quantitative analysis of interactions the following assumptions were employed [22]:

(1) A change of van der Waals intermolecular interactions accompanying mixing is negligible (e.g. mixing of hexane and heptane);
(2) All contributions to heat of mixing are due to specific acid-base interactions;
(3) All organic liquids (except for saturated hydrocarbons) make the specific self-association based on electron donor (basic) and electron acceptor (acid) sites of one molecule. Namely, molecules are self-associated in *X–X* pairs consisting of two molecules by the acid-base interaction;
(4) All *X–X* interactions are broken in the case of high dilution;
(5) All dissociated *X* molecules form new *X–Y* interactions;
(6) Molecules *Z* (saturated hydrocarbons) do not have any acid-base self-associations, neither and they do not form acid-base interactions with another molecule (*X* or *Y*).

4. Fourier transform infrared spectroscopy

The contrast between symmetric and asymmetric C–O bonding of FTIR peaks for diethyl ether (DE) and 2-ethoxyethanol (2ET) are shown in Fig. 1. This occurs due to intramolecular vibrations created by presence of additional –OH in chemical structure of 2ET (see Table 1) [23]. Regardless of two C–O couples present in DE, only one major peak at 1123 cm^{-1} is observed. This can be explained by the fact that for 2ET, one C–O couple is influenced by a close presence of –OH group, resulting in an asymmetric peak at 1120 and 1066 cm^{-1}, respectively. Fig. 2 shows the influence of gradual dilution and shift of carbonyl C–O stretching peak for 2ET diluted in hexane at different concentrations. As it can be seen, initially at 40% only the shoulder is be observed. Minor shoulder becomes more prominent at 20 and 12% concentrations, while at 6% concentration the peaks at 1119 and 1131 cm^{-1} are having the same magnitude. It can be assumed that half of 2ET molecules are still associated in *X–X* pair, while half of the molecules are already isolated by the hexane. At 1% concentration the curve suggests that the majority of the 2ET molecules are separated (or surrounded by the hexane molecules), even though the small peak at 1119 cm^{-1} is a hint of a presence of negligible amount of *X–X* pairs. It is also important to observe the second peak at 1065 cm^{-1}, where at 12 and 6% a minor shoulder appears, and finally at 1% clearly another peak arises at 1056 cm^{-1}. What is important to notice in this case is the fact that dilution caused the shift of the peak towards lower wavenumber.

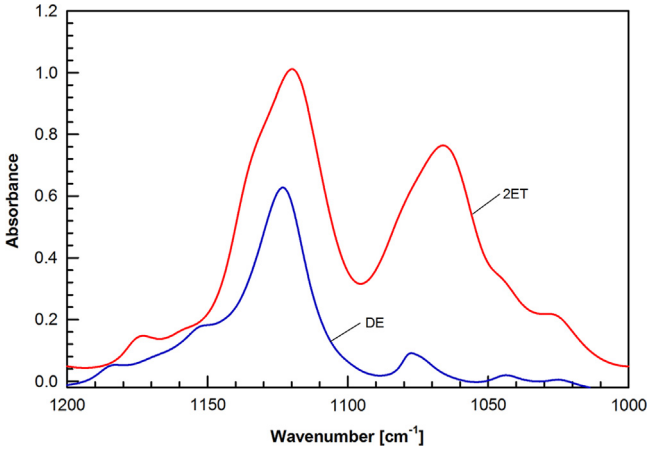

Fig. 1. FTIR peaks for C–O bonding of diethyl ether (DE) and 2-ethoxyethanol (2ET).

This analysis allowed defining the percentage of optimal dilution for observing the peak shift. At concentration of 1% the major peak shift is observed and it is assumed that this occurs when molecules of liquid break the self-interactions and each molecule of liquid is fully surrounded by molecules of hexane (or decalin). It can be noticed that the response of C–O peak to dilution of self-interaction is highly dominant. Meanwhile, it is not possible to use this strong C–O peak in future study of *X–Y* interactions, since C–O group is present in both – carnauba wax (and in its analogues) and also in PEG (and in its analogues), which eliminates the possibility to determine from which particular liquid the peak originates. The choice of a strong peak that can be visible even at 1% dilution in other chemical is required, and thus –OH group in PEG analogues and C=O group in CW analogues were further considered.

The results have shown that O–H stretch bonding peak shift from hydroxyl functional group is larger in hexane for PEG low

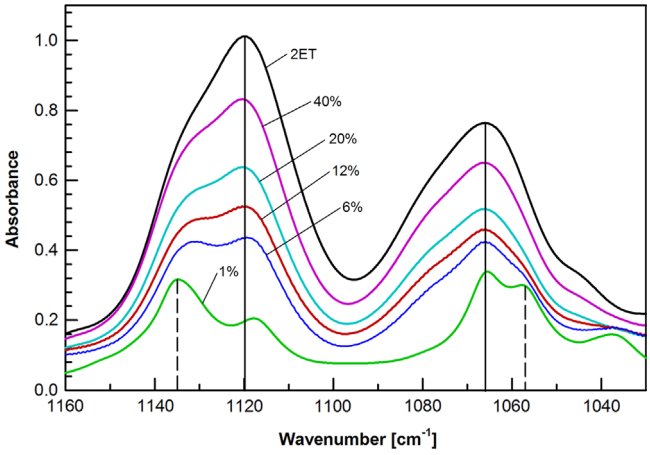

Fig. 2. Shift of FTIR peaks for C–O bonding of 40, 20, 12, 6 and 1% of 2-ethoxyethanol (2ET) in hexane.

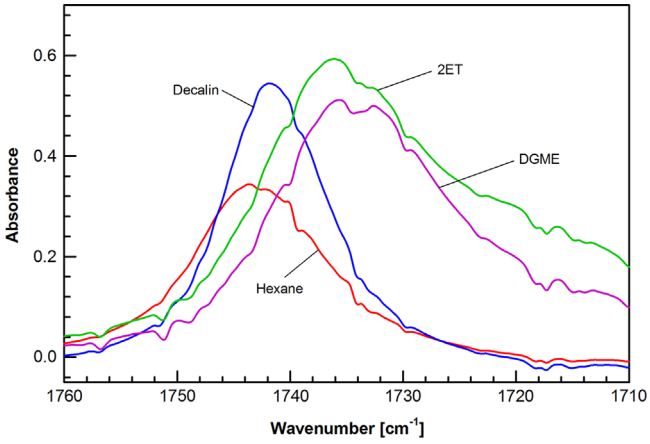

Fig. 3. FTIR peaks of the carbonyl group C=O stretch of butyl valerate (1% solution) in hexane, decalin, 2-ethoxyethanol (2ET) and diethylene glycol monoethyl ether (DGME).

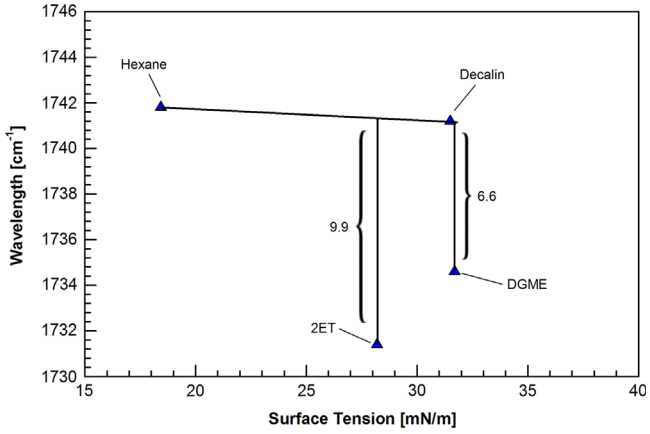

Fig. 4. Calculation of a corrected peak shift from the baseline for C=O bonding butyl valerate (1% solution) in hexane, decalin, 2-ethoxyethanol (2ET) and diethylene glycol monoethyl ether (DGME).

Table 3
Peak position v, surface tension γ and shift of peaks for corresponding liquids Δv_{XY}.

Name	Peak position v [cm^{-1}]	Surface tension γ [mN/m]	Corrected peak shift Δv_{XY} [cm^{-1}]
C=O, 1% Amyl butyrate			
Hexane	1741.8	18.40	0
Decalin	1741.2	29.40	0
2-ethoxyethanol	1733.3	28.20	7.8
Diethylene glycol monoethyl ether	1735.7	31.70	5.5
–OH, 1% 2-ethoxyethanol			
Hexane	3425.2	18.40	0
Decalin	3421.3	29.40	0
Amyl butyrate	3432.7	25.55	11.4
Butyl valerate	3434.3	26.36	13.0

molecular analogues, vice versa to CW low molecular analogues, where a shift is higher in decalin. The shift of the peaks gave a qualitative evidence of the presence of specific interactions, however for a quantitative analysis of the magnitude of respective interactions, calorimetric measurements still needs to be applied. As it is shown in Fig. 2, the peak of the original liquid shifts when it is diluted at low concentration. The magnitude of a peak shift (Δv_{XY}) varies according to a solvent or liquid it is diluted in. Fig. 3 shows the peak shifts of the carbonyl group C=O stretch for 1% butyl valerate (BV) solution in hexane, decalin, 2ET and diethylene glycol monoethyl ether (DGME). The values of shifted peaks in hexane or decalin together with surface tension γ of the liquids are combined to plot a baseline (Fig. 4), in order to calculate Δv_{XY}. The obtained parameters are shown in Table 3. It was observed, that diluting the liquid in hexane or decalin results in the peak shift to a higher wavenumber, while the difference between shifts is related to the surface tension value. In contrast diluting BV in 2ET and DGME the peaks shift to a lower peak wavenumber, due to newly formed XY interactions [23]. Peak shifting to lower peak wavenumber is often observed in blends where high level of interactions takes place [13].

The peak shift for BV (at 1% concentration) in hexane and decalin represents a baseline for the corrected peak shift calculations. The peak position in hexane and decalin are slightly different due to different surface tensions. The correction to surface tensions has to be accounted for in the peak shift evolution (schematically shown in Fig. 4).

For DGME the self-interactions are higher, since it has higher number of oxygen molecules along the chain, therefore more self-interactions are likely to happen between two molecules. As it is shown in Fig. 5, for liquids without –OH, the self-interactions values are smaller, which confirms that presence of –OH is increasing the value. Also it was observed that chemicals with –OH may have an optimum value at which the interaction energies are highest and start to decline at some point, meanwhile it requires more detailed study.

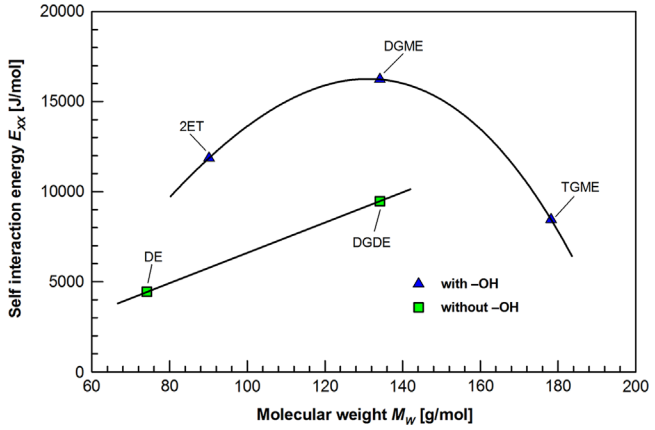

Fig. 5. Self-interaction energies E_{XX} vs. molecular weight for PEG substitutes M_w.

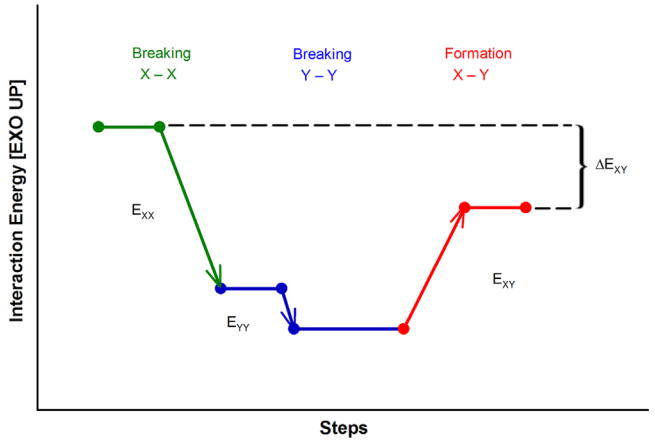

Fig. 6. Simplified schema of breaking self-interactions (X–X and Y–Y) followed by formation of new X–Y interactions when liquid X is mixed with liquid Y.

4.1. Calorimetric analysis – neat liquid X (low molecular weight liquid)

The total self-interaction energy E_{XX} (J mol^{-1}) is expressed as

$$E_{XX} = \tfrac{1}{2} N_{Avo} \varepsilon_{XX} \tag{1}$$

where N_{Avo} is Avogadro's number (6.022×10^{23} (particles/mol)) and ε_{XX} is the contact energy of two molecules (or one pair) (J). E_{XX} can be experimentally obtained, when liquid X is diluted into a non-self-interacting liquid Z, such as hexane. This mixing can be described with a semichemical equation

$$N_X(X-X) + N_Z(Z) \overset{\Delta H_M}{\rightarrow} N_X'(X-X) + N_X''(X) + N_Z(Z) \tag{2}$$

where (X–X) means liquid X self-associated in X–X pairs, while (X) means liquid X in which molecules are isolated (or dissociated). N_X and N_X' are numbers of X molecules (that are associated in X–X pairs) before and after mixing, respectively. N_X'' means the number of X molecules which are isolated after mixing ($N_X = N_X' + N_X''$). ΔH_M means the heat of mixing. The number of X–X pairs before and after mixing NP_{XX} and NP_{XX}', respectively, can be easily obtained ($NP_{XX} = 1/2N_X$; $NP_{XX}' = 1/2N_X'$). Dividing Eq. (2) by N_{Avo} we get

$$n_X(X-X) + n_Z(Z) \overset{\Delta H_M}{\rightarrow} n_X'(X-X) + n_X''(X) + n_Z(Z) \tag{3}$$

where n_X means the number of moles of liquid X. Under condition that $n_X \ll n_Z$, $n_X' \rightarrow 0$ *and* $n_X'' = n_X$. For $n_X = 1$, ΔH_M becomes E_{XX}. Eq. (3) becomes simpler

$$1(X-X) + n_Z(Z) \overset{E_{XX}}{\rightarrow} 1(X) + n_Z(Z) \tag{4}$$

Experimental data for the dilution of liquid into hexane can be seen in Fig. 7a. In order to describe the shape of the curve it is convenient to set the names of axes

$$x = \frac{n_X}{n_X + n_Z} \qquad y = \frac{\Delta H_M}{n_X + n_Z} \tag{5}$$

The shape of the curve can be described as a polynomial by ($y = k_1 x + k_2 x^2 + \ldots$). For $x \rightarrow 0$ higher terms are much smaller than the first term ($k_2 x^2 \ll k_1 x$), and the equation becomes linear ($y = k_1 x$). The meaning of the initial slope can be expressed as

$$k_1 = \frac{\Delta y}{\Delta x} = \frac{\Delta H_M / n_X + n_Z}{n_X / n_X + n_Z} = \frac{\Delta H_M}{n_X} \tag{6}$$

Then the slope is equal to E_{XX} which is the self-interacting energy of 1 mol of liquid X (J mol^{-1}). The contact energy of

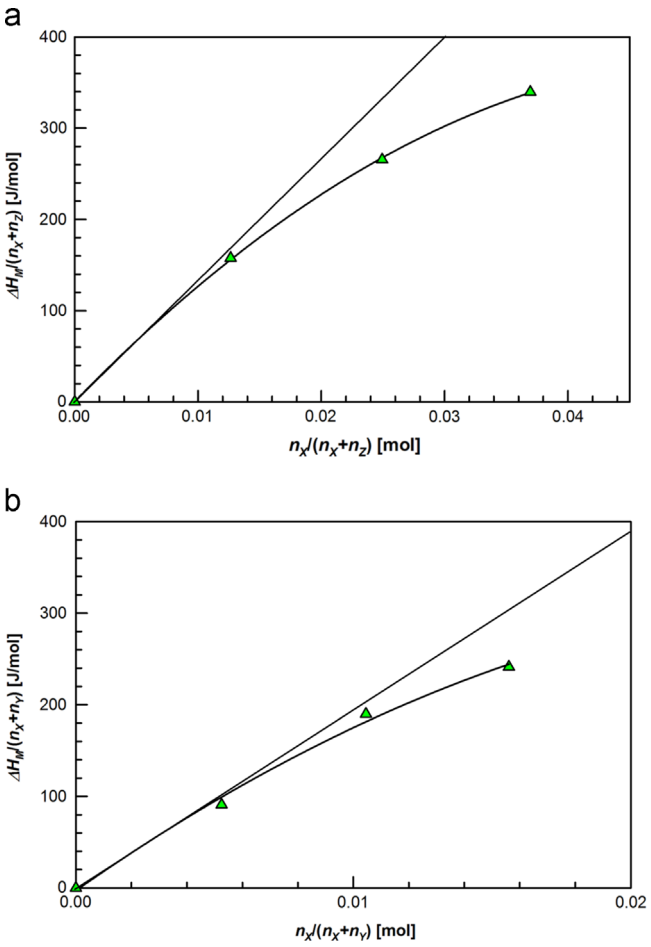

Fig. 7. (a) Heat of mixing $H_M/(n_X+n_Z)$, vs. molar fraction of liquid X diluted into solvent Z $n_X/(n_X+n_Z)$; (b) Heat of mixing $H_M/(n_X+n_Y)$ vs. molar fraction of liquid X diluted into liquid Y $n_X/(n_X+n_Y)$.

two molecules (one pair) of ε_{XX} can be obtained from Eq. (1). Measured temperature drop ΔT, heat of mixing $\Delta H_M/(n_X+n_Z)$, molar fraction $n_X/(n_X+n_Z)$ and self-interaction energies E_{XX} are depicted in Table 4.

4.2. Calorimetric analysis – liquid X mixed with liquid Y

Both X and Y have some degree of acid-base self-interaction, E_{XX} and E_{YY}. The semichemical equation in this case is

$$N_X(X-X)+N_Y(Y-Y)\overset{\Delta H_M}{\rightarrow}N_{XY}(X-Y)+N_X'(X-X)+N_Y'(Y-Y) \quad (7)$$

where N_{XX} is the number of X and Y molecules that are associated in X–Y pairs. The total number of molecules is equal before and after mixing ($N_X+N_Y=N_{XY}+N_X'+N_Y'$). The number of X–Y pairs is given by ($NP_{XY}=1/2N_{XY}$) and the total number of pairs before and after mixing is given by($NP_{XX}+NP_{YY}=NP_{XY}+NP_{XX}'+NP_{YY}''$). By dividing Eq. (7) by N_{Avo}, we get

$$n_X(X-X)+n_Y(Y-Y)\overset{\Delta H_M}{\rightarrow}n_{XY}(X-Y)+n_X'(X-X)+n_Y'(Y-Y) \quad (8)$$

If $n_X \ll n_Y$, than $n_X'\rightarrow 0$. Setting $n_X = 1$ mol, then

$$1(X-X)+n_Y(Y-Y)\overset{\Delta H_M}{\rightarrow}2(X-Y)+(n_Y-1)(Y-Y) \quad (9)$$

ΔH_M becomes ΔE_{XY} and the only changing quantities are

$$1(X-X)+1(Y-Y)\overset{\Delta E_{XY}}{\rightarrow}2(X-Y) \quad (10)$$

Description by self-interacting (E_{XX}) and by association (E_{XY}) energies gives

$$E_{XX}+E_{YY}+\Delta E_{XY}=2E_{XY} \quad (11)$$

Self-interaction energies (E_{XX}) were obtained by diluting liquid X into hexane. The value ΔE_{XY} can be obtained from slope analysis similar to the case of diluting of liquid X into hexane, but in this case liquid X is diluted into liquid Y. Continuing mathematical analysis, the respective interaction energy of 1 mol of X–Y pairs can be expressed as

$$E_{XY}=1/2(E_{XX}+E_{YY}-\Delta E_{XY}) \quad (12)$$

and the respective contact energy of one pair is

$$\varepsilon_{XY}=\frac{2E_{XY}}{N_{Avo}} \quad (13)$$

A simplified schema (Fig. 6) explains the calculations of E_{XY} based on the measurements of ΔE_{XY} according to Eq. (12). Four liquids were chosen for further analysis (Table 5). Calculations of E_{XY} for respective pairs showed that XY interaction values are asymmetric. The value for liquid X diluted in liquid Y showed slightly different value than liquid Y diluted in liquid X, which can be a result of a difference in heat capacity values c_p of those liquids.

An example of evaluation of heat of mixing and molar fraction for the dilution of liquid into solvent and dilution of liquid into liquid is shown in Figs. 7a and b, respectively. The curve represents the linearity of the temperature drop ΔT; the less is the bonding of curve, the more linear is ΔT.

4.3. Combined FTIR and calorimetry

Both FTIR and calorimetry lead to information about specific interactions. For example the shift of the carbonyl (C=O) stretch to lower frequencies is generally accepted as a result of specific interactions such as hydrogen bonding. For the quantitative analysis of the shift of the peaks it is necessary to use the following approach. The vibrating frequency of a

Table 4
Temperature drop ΔT, heat of mixing $\Delta H_M/(n_X+n_Z)$, molar fraction $n_X/(n_X+n_Z)$ and self-interaction energies E_{XX}.

Name	Temperature drop ΔT[°C]	$\Delta H_M/(n_X+n_Z)$ [J/mol]	$n_X/(n_X+n_Z)$ [10^{-3} mol]	Self-interaction energy E_{XX} [J/mol]
Amyl butyrate	0.19	28.35	6.708	5264
Butyl valerate	0.15	29.38	6.754	4132
2-ethoxyethanol	0.81	157.82	12.633	11861
Diethyl ether	0.28	54.58	11.672	4442
Diethylene glycol monoethyl ether	0.80	156.41	9.146	16236
Diethylene glycol dimethyl ether	0.44	86.05	8.639	9464
Triethylene glycol monoethyl ether	0.32	62.69	7.045	8449

Table 5
Association energies E_{XY} of the respective pairs X–Y.

Pairs	2ET-AM	2ET-BV	AM-2ET	AM-DGME
Interaction energy of $X-Y$ pair E_{XY} [J/mol]	5560	6780	5008	3793

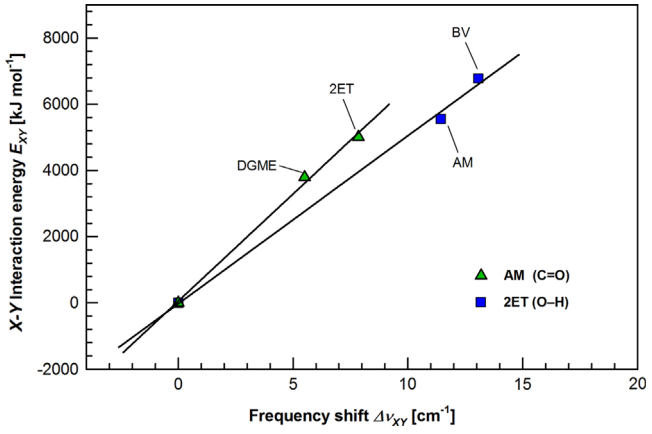

Fig. 8. Association energies E_{XY} vs. shift of peaks for amyl butyrate (AM) and 2-ethoxyethanol (2ET).

certain group (such as C=O) is given by

$$\nu = \nu^{v} + \Delta\nu^{d} + \Delta\nu^{XY} \quad (14)$$

where ν^{v} means the frequency in the vapour phase, $\Delta\nu^{d}$ is the frequency shift caused by dispersion force interactions between a certain group and its local environment (non-acid-base interacting liquid such as hexane), and $\Delta\nu^{XY}$ means a frequency shift due to acid-base interactions.

When the tested liquid was diluted in non-interacting liquids (as cyclohexane, heptane, octane, etc.), a linear relationship of $\Delta\nu^{d}$ with the dispersion force contribution to the surface tension γ^{d} was found ($\Delta\nu^{XY}=0$). In our case the tested liquids were diluted in two non-interacting liquids (hexane and decalin) with an appreciably different surface tension in order to obtain the linear relationship ($\nu=\nu^{v}+X\gamma^{d}$). For the acid-base interacting liquids the exact values of $\Delta\nu^{XY}$ were calculated by the deviation from the linear relationship satisfied in non-interacting liquids [24]. On the basis of quantum mechanics, Drago [21] explained the linear relationship between enthalpy of adduct formation and shift in the frequency of vibration:

$$H = k\ \Delta\nu^{ab} \quad (15)$$

This simple relation offers a possibility of the confirmation of data obtained by two independent experiments. The E_{XY} association energies obtained by calorimetry and shifts of peaks $\Delta\nu^{XY}$ measured using FTIR are shown in Fig. 8. For both groups of liquids a linear dependence was found that confirms the validity of data and calculations from two independent experiments.

5. Conclusion

Detailed analysis of specific interactions between binder components often used in Ceramic Injection Moulding - carnauba wax (CW) and polyethylene glycol (PEG) - was performed using their low molecular weight analogues. The calorimetric measurements allowed to quantitatively analyse the *X–X* and *X–Y* interactions. For PEG substitute liquids the presence of –OH in chemical structure resulted in higher self-interaction energies, reaching its maximum for diethylene glycol monoethyl ether. An optimum dilution level was defined at 1% concentration. The FTIR results of peak shift in solvent were used to construct a baseline and calculate the correction of peak shift. A linear connexion of two independent experiments was found. Higher the shift from FTIR, the higher the association energies, which is in accordance with Drago's linear equation. Observed endothermic reaction from calorimetric analysis combined with the shift of the spectral peaks in FTIR suggests a presence of specific interactions between substitutes, predicting a partial miscibility of respective polymers.

In contrast to the studies of miscibility of polymer/polymer blends where self-interactions are significantly higher than polymer *X* to polymer *Y* interactions, this paper showed the analysis of low molecular substitutes where the majority of self-interactions were eliminated, and thus the values of *X–Y* interactions were precisely calculated.

CW/PEG binders attract attention not only by its eco-friendly nature, but also due to the fact that interactions present between two polymers can positively influence the energy efficiency of applications, at the same time noticeably enhancing the debinding and sintering characteristics.

Acknowledgements

This article was written with the support of Operational Programme Research and Development for Innovations co-funded by the ERDF and national budget of Czech Republic, within the framework of project Centre of Polymer Systems (reg. number: CZ.1.05/2.1.00/03.0111). The author D.B. would like to acknowledge the support of the internal grant of Tomas Bata University in Zlin No. IGA/FT/2014/003 and support of Visegrad Fund.

References

[1] R.M. German, A. Bose, Injection molding of metals and ceramics, Metal Powder Industries Federation, Princeton, N.J., 1997.
[2] D.R. Paul, C.B. Bucknall, in: Polymer blends, Wiley, New York; Chichester, 2000.
[3] B. Hausnerova, I. Kuritka, D. Bleyan, Polyolefin backbone substitution in binders for low temperature powder injection moulding feedstocks, Molecules 19 (2014) 2748–2760.
[4] K.C. Hsu, C.C. Lin, G.M. Lo, The effect of wax composition on the injection molding of carbonyl iron powder with ldpe, Can. Metall. Q. 35 (1996) 181–187.
[5] M. Sahli, G. Larsen, T. Barriere, J.C. Gelin, G. Michel, Analysis and characterisation for 3161 stainless metal micro-structure replication of micro-components produced by micro-powder injection moulding, Steel Res. Int. 81 (2010) 1292–1295.
[6] K. Sharmin, I. Schoegl, Optimization of binder removal for ceramic microfabrication via polymer co-extrusion, Ceram. Int. 40 (2014) 3939–3946.
[7] S.M. Ani, A. Muchtar, N. Muhamad, J.A. Ghani, Binder removal via a two-stage debinding process for ceramic injection molding parts, Ceram. Int. 40 (2014) 2819–2824.
[8] S.M. Ani, A. Muchtar, N. Muhamad, J.A. Ghani, Fabrication of zirconia-toughened alumina parts by powder injection molding process: Optimized processing parameters, Ceram. Int. 40 (2014) 273–280.
[9] T. Hanemann, O. Weber, Polymethylmethacrylate/polyethyleneglycol-based partially water soluble binder system for micro ceramic injection moulding, Microsyst. Technol.-Micro- Nanosyst.-Inf. Storage Process. Syst. 20 (2014) 51–58.
[10] J. Lenz, R.K. Enneti, S.J. Park, S.V. Atre, Powder injection molding process design for uav engine components using nanoscale silicon nitride powders, Ceram. Int. 40 (2014) 893–900.
[11] L. Gorjan, T. Kosmac, A. Dakskobler, Single-step wick-debinding and sintering for powder injection molding, Ceram. Int. 40 (2014) 887–891.
[12] F. Chen, M.P. Wolcott, Miscibility studies of paraffin/polyethylene blends as form-stable phase change materials, Eur. Polym. J. 52 (2014) 44–52.
[13] Y.N. Sudhakar, M. Selvakumar, Miscibility of chitosan and poly (ethyleneglycol) blends in buffer solution, E-Polymers (2012).
[14] R.N. French, J.M. Machado, D. Linvien, Miscible polyacetal poly(vinyl phenol) blends.1. Predictions based on low-molecular-weight analogs, Polymer 33 (1992) 755–759.
[15] P. Svoboda, J. Kressler, T. Ougizawa, T. Inoue, K. Ozutsumi, Ftir and calorimetric analyses of the specific interactions in poly(epsilon-caprolactone)/poly(styrene-co-acrylonitrile) blends using low molecular weight analogues, Macromolecules 30 (1997) 1973–1979.
[16] D. Rana, B.M. Mandal, S.N. Bhattacharyya, Analogue calorimetry of polymer blends: Poly(styrene-co-acrylonitrile) and poly(phenyl acrylate) or poly(vinyl benzoate), Polymer 37 (1996) 2439–2443.
[17] L. Bernazzani, C. Cardelli, G. Conti, P. Gianni, Analog calorimetry and uniquac group contributions approaches to the miscibility of pvc with eva copolymers, J. Therm. Anal. Calorim. 70 (2002) 927–947.

[18] S. Ziaee, D.R. Paul, Polymer–polymer interactions via analog calorimetry. Blends of polystyrene with poly(2,6-bimethyl-1,4-phenylene oxide). Abstr Pap Am Chem S, 1996, 212, 12-Pmse.

[19] B.J. Brune, J.A. Koehler, P.J. Smith, G.F. Payne, Correlation between adsorption and small molecule hydrogen bonding, Langmuir 15 (1999) 3987–3992.

[20] H. Huang, Y. Hu, J.M. Zhang, H. Sato, H.T. Zhang, I. Noda, Y. Ozaki, Miscibility and hydrogen-bonding interactions in biodegradable polymer blends of poly(3-hydroxybutyrate) and a partially hydrolyzed poly(vinyl alcohol), J. Phys. Chem. B 109 (2005) 19175–19183.

[21] C. Qin, A.T.N. Pires, L.A. Belfiore, Spectroscopic investigations of specific interactions in amorphous polymer polymer blends – poly(vinylphenol) and poly(vinyl methyl ketone), Macromolecules 24 (1991) 666–670.

[22] K.L. Mittal, H.R. Anderson, F.M. Fowkes, Acid-base Interactions: Relevance to Adhesion Science and Technology: In Honor of the 75th Birthday of Professor Frederick M, Fowkes. VSP, Utrecht, 1991.

[23] W.O. George, P.S. McIntyre, D.J. Mowthorpe, Infrared Spectroscopy, Published on behalf of ACOL by Wiley: Chichester, 1987.

[24] F.M. Fowkes, D.O. Tischler, J.A. Wolfe, L.A. Lannigan, C.M. Ademujohn, M.J. Halliwell, Acid-base complexes of polymers, J. Polym. Sci. Pol. Chem. 22 (1984) 547–566.

PAPER III

Powder Technology 286 (2015) 84–89

Contents lists available at ScienceDirect

Powder Technology

journal homepage: www.elsevier.com/locate/powtec

The development of powder injection moulding binders: A quantification of individual components' interactions

D. Bleyan [a,b], B. Hausnerova [a,b,*], P. Svoboda [b,c]

[a] Department of Production Engineering, Faculty of Technology, Tomas Bata University in Zlin, nam. T.G. Masaryka 5555, 760 01 Zlin, Czech Republic
[b] Centre of Polymer Systems, University Institute, Tomas Bata University in Zlin, Nad Ovcirnou 3685, 760 01 Zlin, Czech Republic
[c] Department of Polymer Engineering, Faculty of Technology, Tomas Bata University in Zlin, nam. T.G. Masaryka 275, 762 72 Zlin, Czech Republic

ARTICLE INFO

Article history:
Received 10 April 2015
Received in revised form 17 July 2015
Accepted 22 July 2015
Available online 8 August 2015

Keywords:
Powder injection moulding
Binder
Low molecular weight analogue
Specific interactions
FTIR
Calorimetry

ABSTRACT

The study of interactions between binder system components is critical for improving the processing properties of powder injection moulding (PIM) feedstocks. In this paper the interactions between acrawax (AW) and polyethylene glycol (PEG) were analysed and compared with those obtained for carnauba wax (CW). Due to the complexity of interaction mechanisms, the polymers were substituted with their basic low molecular weight analogues and analysed by FTIR and calorimetry. Self-interaction energies and association energies were determined using calorimetric analysis. Shifts of FTIR absorption peaks (C–O stretch and N–H stretch) served as evidence of the presence of interactions between the components. The calorimetric study of AW/PEG analogues showed a temperature increase during mixing, indicating the presence of strong interactions. The combined data from FTIR and calorimetry allowed a quantitative evaluation, which indicated about two times stronger interactions between AW (with C═O and N–H groups) and PEG (with C–O and –OH groups), as compared to CW (with C═O and C–O groups) and PEG analogues.

1. Introduction

In recent years, powder injection moulding (PIM) has established itself as a cost-effective production technique derived from plastic injection moulding, allowing large scale production of complex parts. The binder system in PIM plays an important role, bestowing on the feedstock the required processing properties and ensuring defect-free processing throughout each production stage [1].

Suitable processing properties of a powder feedstock are usually achieved by using a binder system consisting of up to 5 different polymers and waxes, which complicates the investigation of the complete and individual reaction pathways and the chemical mechanisms occurring within such a system. The majority of binder systems is based on polyolefin backbones such as polyethylene (PE) or polypropylene (PP), and includes also polyethylene glycols (PEGs) with various molecular weights and waxes such as paraffin wax (PW).

Despite the substantial effort made in studying PE and PP binders [e.g. 2], their usage often leads to processing issues such as insufficient initial pore formation and weak internal transport mechanisms within the green parts, resulting in lower debinding rates. PEG's main role is as plasticiser [3]; besides improving the viscoelastic properties its use is endorsed by water solubility allowing an environmentally safe debinding process [4] (in contrast to PW, which dissolves in heptane, hexane, or kerosene [5]).

At present, the binder's properties are assessed by rheological measurements and thermogravimetry [6–11]. There is a noticeable lack of research effort in the area of specific interactions among the particular binder system components. In order to improve the feedstock properties, mathematical models for predicting the feedstock properties or substituting conventional processing stages by implementing sophisticated techniques requiring the merging of two consequent stages are employed. However, even the latter approach can be justified if an outsourced and intensive study of the adhesion of binder to powder, and the interactions between binder components are performed prior to it.

Various techniques were exploited for studying the interactions in polymer blends. Chen and Wolcott [12] reported on a study of interaction parameters for polymer-diluent systems of PW and PE (HDPE, LDPE and LLDPE). The morphology, crystallization and crystallinity together with equilibrium melting temperature and melting point depression were analysed using differential scanning calorimetry and atomic force microscopy. The results showed evidence of partial miscibility of blends, with LLDPE having an advantage over HDPE and LDPE.

Doulabi et al. [13] studied the miscibility of PEG and chitosan by using an acetate buffer solution for different blend compositions. Viscosity, density, and refractive index were measured in order to quantify the interaction parameters. The results showed that the components at

* Corresponding author at: Department of Production Engineering, Faculty of Technology, Tomas Bata University in Zlin, nam. T.G. Masaryka 5555, 760 01 Zlin, Czech Republic.
E-mail address: hausnerova@ft.utb.cz (B. Hausnerova).

http://dx.doi.org/10.1016/j.powtec.2015.07.046
0032-5910/

80% or higher chitosan concentration were miscible by means of the intermolecular hydrogen-bonding interaction between hydroxyl groups of polyethylene glycol fumarate with amino and hydroxyl groups of chitosan.

In our previous research, polar waxes were exploited as binder system components applicable to the PIM process [14] to substitute nonpolar PE and PW with the aim of eliminating the necessity to use processing aid, e.g., stearic acid (SA), in order to achieve the adhesion of the binder to the powder required to withstand high shear forces during injection moulding. Similarly to the most recent work by Liu et al. [15], who substituted paraffin wax with bee wax for the production of micro-injection moulding gears from zirconia, better feedstock stability has been achieved. However, with such novel binders, an understanding of core mechanisms of interactions between the individual system components would allow a precisely-balanced composition, bringing the feedstock properties to their higher limits (e.g., substantially lowering the processing temperatures in the case of substitution of PE by carnauba wax (CW) or acrawax(AW)) [14].

While quantification of the interactions of two polymers is a difficult task, in the case where both polymers are polar it becomes even more challenging. This is because the interactions between polymer (*X*) and polymer (*Y*) are significantly weaker than the self-interactions *X*–*X* and *Y*–*Y* in each polymer. To bypass this issue, polymers might be substituted with low molecular weight analogues to have an advantage of eliminating the majority of self-interactions, and replacing them with newly formed *X*–*Y* interactions. This rarely used [16,17] approach allows the substitute liquid for the *X* polymer to be fully surrounded by the substitute liquid for the *Y* polymer, resulting in precise measurements of the present interactions. Furthermore, the calorimetric analysis combined together with Fourier transform infrared spectroscopy (FTIR) measurements can provide a quantitative evaluation of specific interactions.

Some researchers have reported on the successful use of FTIR or calorimetry techniques for quantifying and evaluating interactions [18–20]. To our best knowledge, no research has yet been performed on the miscibility of PEG and polar waxes.

In our previous paper [21], we tested this approach to verify the presence of interactions between CW and PEG low molecular substitutes. Motivated by the work of Hsu et al. [22] who compared CW and AW in 56 vol.% 304L stainless steel feedstocks containing 22 vol.% of low density polyethylene (LDPE), and from the separation and aggregation of LDPE molecules from the binder during mixing, it was speculated that AW, containing strong polar amide groups and short hydrocarbon chain ends, was less compatible with LDPE than CW. The aim to quantify the interaction potential of both waxes increased.

Thus, in this work, the interactions between AW and PEG are examined and compared to those employed in our novel powder feedstock [14] based on CW/PEG in order to investigate whether the approach of low molecular weight analogues treated with combined FTIR/calorimetry is able to intercept the slight differences in behaviour viewed by other techniques currently used (rheometry and thermogravimetry).

2. Experimental

2.1. Materials

Table 1 shows the low molecular weight analogues of AW, CW and PEG used in this study. The molar mass M_w, density ρ, and the specific heat capacity c_p of analogues are shown in Table 2. As buffer solutions (solvents), hexane and decahydronaphthalene (decalin) were used. The chemicals were obtained from Sigma-Aldrich.

2.2. Methodology

The quantitative analysis of interactions is based on the assumption that the change of Van der Waals intermolecular interactions accompanying mixing is negligible (e.g., the mixing of hexane and heptane) and all contributions to the heat of mixing are due to specific acid–base interactions, as well as that all organic liquids (except for saturated hydrocarbons) make the specific self-association based on electron donor (basic) and electron acceptor (acid) sites of one molecule, all *X*–*X* interactions are broken in the case of high dilution, all dissociated *X* molecules form new *X*–*Y* interactions, and finally, molecules *Z* (saturated hydrocarbons) do not have any acid–base self-associations, nor do they form acid–base interactions with another molecule (*X* or *Y*) [23].

Table 1
Low molecular analogues of corresponding polymers.

Name	Abbreviation	Chemical structure
Acrawax	AW	$CH_3(CH_2)_{16}CNHCH_2CH_2NHC(CH_2)_{16}CH_3$ (O, O)
Analogue		
Methylacetamide	NMA	CH_3CNHCH_3 (O)
Carnauba wax	CW	$H_3C-(CH_2)_{30}-C-O-(CH_2)_{33}CH_3$ (O)
Analogues		
Amyl butyrate	AM	$CH_3\text{-}CH_2\text{-}CH_2\text{-}C\text{-}O\text{-}CH_2\text{-}CH_2\text{-}CH_2\text{-}CH_2\text{-}CH_3$ (O)
Butyl valerate	BV	$CH_3\text{-}CH_2\text{-}CH_2CH_2\text{-}C\text{-}O\text{-}CH_2\text{-}CH_2\text{-}CH_2\text{-}CH_3$ (O)
Polyethylene glycol	PEG	$H-\left[O-CH_2-CH_2\right]_n-OH$
Analogues		
2-Ethoxyethanol	2ET	$C_2H_5OCH_2CH_2OH$
Diethylene glycol monoethyl ether	DGME	$C_2H_5OCH_2CH_2OCH_2CH_2OH$

2.2.1. FTIR analysis

The *X*–*X* self-interactions and *X*–*Y* interactions between two liquids were studied using FTIR analysis. An FTIR reflection spectroscope (Nicolet 6700, Fisher Scientific, USA) equipped with a KBr glass holder accessory was used. A drop of each mixture was placed between two KBr glasses and measured in a transmission mode. The spectra with 32 scans were collected in the range of 400–4000 cm^{-1} at the resolution of 1 cm^{-1}. The procedure was repeated three times, and the results were averaged.

2.2.2. Calorimetry

A thermocouple (type copper–constantan) was connected to National Instruments data acquisition equipment (NI USB-9211A, Data Acquisition for Thermocouples) and used for measuring the temperature change during the mixing. LabVIEW Signal Express 2.5 software was used for collecting the temperature with a precision of 0.0001 °C. A 0.5 s sampling period was applied. The thermocouple was dipped in the blend, which was placed on a hot plate in the insulated flask with

Table 2
Physical properties of low molecular liquid substitutes.

Name	Molar mass M_w [g/mol]	Density ρ [g/cm^3]	Heat capacity c_p [J/kg K]
AW	593.02	0.97	2910
Analogue			
NMA	73.09	0.957	3748
CW	1000	0.97	3373
Analogues			
AM	158.24	0.863	1927
BV	158.24	0.868	1927
PEG	1000–20,000	1.09–1.41	2200–2460
Analogues			
2ET	90.12	0.930	2414
DGME	134.17	0.999	2193

a magnetic stir rotating at 250 rpm. To achieve a 1% concentration of the blend, 0.05 ml of liquid *X* was diluted in 5 ml of liquid *Y*. The temperature change during mixing was measured, and the time–temperature curve was evaluated.

3. Results and discussion

Low molecular weight liquids were diluted at various concentrations in order to define the optimal dilution ratio. The results demonstrated that a 1% dilution was optimal for both *X*–*X* and *X*–*Y* combinations. The shift of the N–H stretch peak was considered for AM-NMA and BV-NMA substitute liquid blends. Previously collected data [21] for CW and PEG substitute peak shifts of –OH and C═O stretch peaks were used for comparison. The obtained data showed that the NMA peak shift for the N–H amino group in the range of 3050 to 3440 cm^{-1} was higher in decalin (see Table 3), similar to CW low molecular analogues, while being significantly smaller in hexane, vice versa to the peak shift of PEG analogues. It is also noticeable that the peak shift was more significant for the second minor peak (Fig. 1). Both major and minor N–H peaks of NMA in hexane and decalin tended to a lower wavenumber, which is often referred to as proof of the presence of interactions [24]. However, when blended with AM and BV, the major peak tended to a higher wavenumber, which can be explained as repulsive interactions between components. The C–O stretch absorption peak at 1125 cm^{-1} for NMA expressed a similar trend to shift to lower wavenumbers for both 2ET and DGME, indicating that new *X*–*Y* interactions were formed [25]. The following data suggests that the interaction between the corresponding polymers AW/PEG is most likely to occur via the C–O group. Liquid surface tension γ together with a shift peak in buffer liquids – hexane and decalin – was used to build a baseline for calculating the magnitude of the corrected peak shift $\Delta\nu_{XY}$. An example of a calculation of the peak shift correction is shown in Fig. 2. The difference of the peak shift in hexane and decalin can be caused by a difference in their chemical structure.

For the calorimetric analysis of a neat liquid *X*, the self-interaction energies were evaluated using the following equations. The total self-interaction energy E_{XX} (J mol^{-1}) is expressed as

$$E_{XX} = \frac{1}{2} N_{Avo} \varepsilon_{XX} \tag{1}$$

where N_{Avo} is Avogadro's number (6.022×10^{23} (particles/mol)) and ε_{XX} is the contact energy of two molecules (or one pair) (J). E_{XX} can be experimentally obtained, when liquid *X* is diluted into a non-self-interacting liquid *Z*, such as hexane. This mixing can be described as

$$N_X(X{-}X) + N_Z(Z) \xrightarrow{\ddot{A}H_M} N'_X(X{-}X) + N''_X(X) + N_Z(Z) \tag{2}$$

Table 3
Surface tension γ, peak position *ν* and corrected peak shift $\Delta\nu_{XY}$ of low molecular liquid substitutes and solvents.

Name	Surface tension γ [mN/m]	Peak position *ν* [cm^{-1}]	Corrected peak shift $\Delta\nu_{XY}$ [cm^{-1}]
C–O, 1% 2-ethoxyethanol			
Hexane	18.40	1122	–
Decalin	29.40	1124	–
Methylacetamide	28.20	1115	9.1
C–O, 1% Diethylene glycol monoethyl ether			
Hexane	18.40	1122	–
Decalin	29.40	1124	–
Methylacetamide	31.70	1119	5.2
N–H, 1% methylacetamide			
Hexane	18.40	3295	–
Decalin	29.40	3293	–
Amyl butyrate	25.55	3306	12.1
Butyl valerate	26.36	3308	14.2

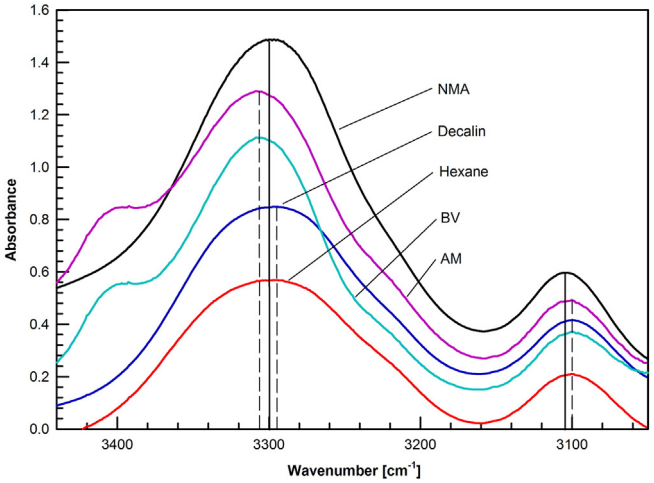

Fig. 1. Shift of FTIR peaks for N–H stretch bonding of 1% methylacetamide (NMA) in hexane, decalin, butyl valerate (BV) and amyl butyrate (AM).

where (*X*–*X*) means liquid *X* self-associated in *X*–*X* pairs, while (*X*) means liquid *X* in which molecules are isolated (or dissociated). N_X and N_X' are numbers of *X* molecules (that are associated in *X*–*X* pairs) before and after mixing, respectively, N_X' stands for the number of *X* molecules which are isolated after mixing ($N_X = N_X' + N_X''$), ΔH_M represents the heat of mixing. The number of *X*–*X* pairs before and after mixing NP_{XX} and NP_{XX}', respectively, can be easily obtained ($NP_{XX} = 1/2N_X$; $NP_{XX}' = 1/2N_X'$). Dividing Eq. (2) by N_{Avo} we get

$$n_X(X{-}X) + n_Z(Z) \xrightarrow{\ddot{A}H_M} n'_X(X{-}X) + n''_X(X) + n_Z(Z) \tag{3}$$

where n_X means the number of moles of liquid *X*, under the condition that $n_X \ll n_Z$, $n_X' \to 0$ and $n_X'' = n_X$. For $n_X = 1$, ΔH_M becomes E_{XX}. Eq. (3) becomes simpler

$$1(X{-}X) + n_Z(Z) \xrightarrow{E_{XX}} 1(X) + n_Z(Z). \tag{4}$$

Experimental data for the dilution of liquid into hexane can be seen in Fig. 3. Trying to describe the shape of the curve, it is convenient to set the axes:

$$x = \frac{n_X}{n_X + n_Z} \qquad y = \frac{\Delta H_M}{n_X + n_Z} \tag{5}$$

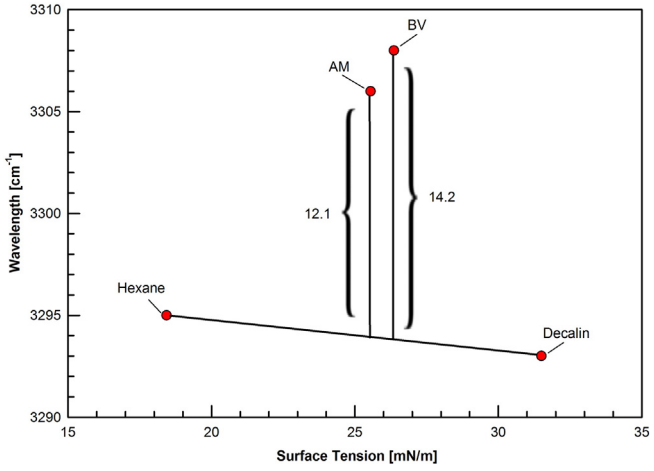

Fig. 2. Calculation of corrected peak shift from the baseline for N–H stretch bonding of 1% methylacetamide (NMA) in hexane, decalin, butyl valerate (BV) and amyl butyrate (AM).

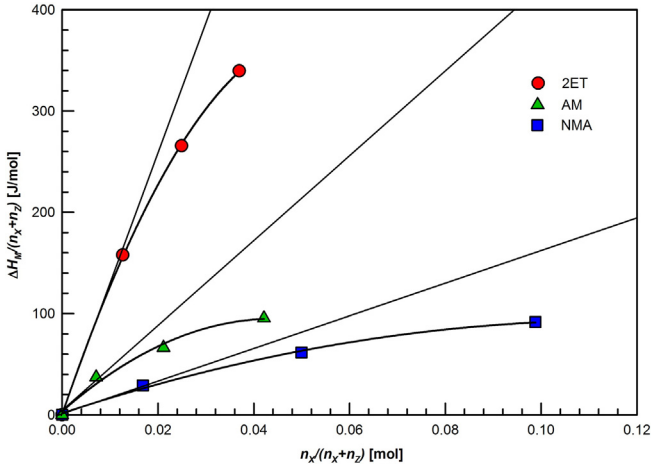

Fig. 3. Heat of mixing $H_M/(n_X + n_Z)$ vs. molar fraction of liquid X diluted into solvent Z $n_X/(n_X + n_Z)$.

The shape of the curve can be described as a polynomial by ($y = k_1x + k_2x^2 + \ldots$). For $x \to 0$, higher terms are much smaller than the first term ($k_2x^2 \ll k_1x$), and the equation becomes linear ($y = k_1x$). The meaning of the initial slope can be expressed as

$$k_1 = \frac{\Delta y}{\Delta x} = \frac{\frac{\Delta H_M}{n_X + n_Z}}{\frac{n_X}{n_X + n_Z}} = \frac{\Delta H_M}{n_X}. \quad (6)$$

Then the slope is equal to E_{XX} that is the self-interacting energy of 1 mol of liquid X (J mol^{-1}). The contact energy of two molecules (one pair) of ε_{XX} can be obtained from Eq. (1).

As can be seen from Fig. 3, the association of the heat of mixing and the molar fraction of the dilution are tending to linearity. The less the bending of the curve, the more linear is ΔT. Fig. 4 shows the self-interaction energies of the studied liquids. As can be seen, regardless of their high molecular weight, the self-interaction energies E_{XX} for both AM and BV are significantly smaller than those for 2ET and DGME. This can be explained by the additional –OH in the chemical structure, but it requires a more detailed study. The NMA having the lowest molecular weight among all investigated liquids and shortest chemical chain showed the smallest value of self-interaction energies. It is also possible that particular self-interactions are rather high, and they cannot be broken in the non-polar buffer solution.

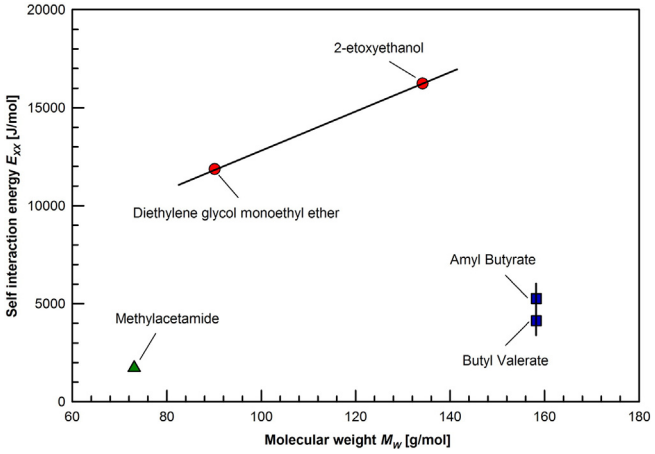

Fig. 4. Self-interaction energies E_{XX} vs. molecular weight M_W for low molecular liquid substitutes.

Similarly, the calorimetric analysis of liquid X mixed with liquid Y can be described as follows (both X and Y have some degree of acid–base self-interactions E_{XX} and E_{YY}). The semichemical equation in this case is

$$N_X(X{-}X) + N_Y(Y{-}Y) \xrightarrow{\ddot{A}H_M} N_{XY}(X{-}Y) + N'_X(X{-}X) + N'_Y(Y{-}Y) \quad (7)$$

where N_{XY} is the number of X and Y molecules that are associated in X–Y pairs. The total number of molecules is equal before and after mixing ($N_X + N_Y = N_{XY} + N_{X'} + N_{Y'}$). The number of X–Y pairs is given by ($NP_{XY} = 1/2N_{XY}$), and the total number of pairs before and after mixing is given by ($NP_{XX} + NP_{YY} = NP_{XY} + NP'_{XX} + NP''_{YY}$). By dividing Eq. (7) by N_{Avo}, we get

$$n_X(X{-}X) + n_Y(Y{-}Y) \xrightarrow{\ddot{A}H_M} n_{XY}(X{-}Y) + n'_X(X{-}X) + n'_Y(Y{-}Y). \quad (8)$$

If $n_X \ll n_Y$, then $n_{X'} \to 0$. Setting $n_X = 1$ mol, then

$$1(X{-}X) + n_Y(Y{-}Y) \xrightarrow{\ddot{A}H_M} 2(X{-}Y) + (n_Y{-}1)(Y{-}Y) \quad (9)$$

ΔH_M becomes ΔE_{XY}, and the only changing quantities are

$$1(X{-}X) + 1(Y{-}Y) \xrightarrow{\ddot{A}E_{XY}} 2(X{-}Y). \quad (10)$$

A description by self-interaction (E_{XX}) and by association (E_{XY}) energies gives

$$E_{XX} + E_{YY} + \Delta E_{XY} = 2E_{XY} \quad (11)$$

Self-interaction energies (E_{XX}) were obtained by diluting liquid X into hexane. The value ΔE_{XY} can be obtained from the slope analysis, similar to the case of diluting of liquid X into hexane, but in this case liquid X is diluted into liquid Y. Continuing the mathematical analysis, the respective interaction energy of 1 mol of X–Y pairs can be expressed as

$$E_{XY} = 1/2(E_{XX} + E_{YY} - \Delta E_{XY}) \quad (12)$$

and the respective contact energy of one pair is

$$\varepsilon_{XY} = \frac{2E_{XY}}{N_{Avo}}. \quad (13)$$

The comparison of the temperature change for NMA diluted in 2ET and AM is shown in Fig. 5. Each temperature change is generated by placing a 0.05 ml droplet into a 5 ml liquid. A constant increase of temperature during dilution was observed only between NMA-2ET and NMA-DGME. For the dilution of all other compositions, the temperature change was negative. An increase in temperature during mixing can be associated with a strong, newly formed X–Y interaction. The background is described in the following two equations.

According to Gibbs free energy, if the change of the ΔG is negative, the reaction can proceed spontaneously. Basically, in the case of mixing it is given by

$$\Delta G_M = \Delta H_M - T\Delta S_M \quad (14)$$

where ΔH_M and ΔS_M are the enthalpy and entropy of mixing, respectively. In binary polymer mixtures, it is convenient to use the Flory and Huggins expression for the Gibbs free energy of mixing per mole of lattice sites

$$\frac{\Delta G_M}{RT(V/V_r)} = \frac{\phi_X}{r_X}\ln\phi_X + \frac{\phi_Y}{r_Y}\ln\phi_Y + \chi\phi_X\phi_Y \quad (15)$$

where V is the total volume, V_r is the molar volume of a segment, and r_X and ϕ_X denote the number of segments per chain and the volume

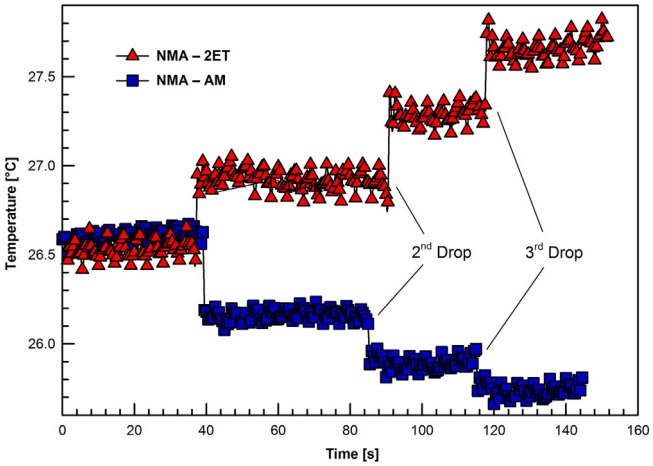

Fig. 5. Temperature change for the 0.05 ml drop of methylacetamide (NMA) diluted in 5 ml 2-ethoxyethanol (2ET) and amyl butyrate (AM).

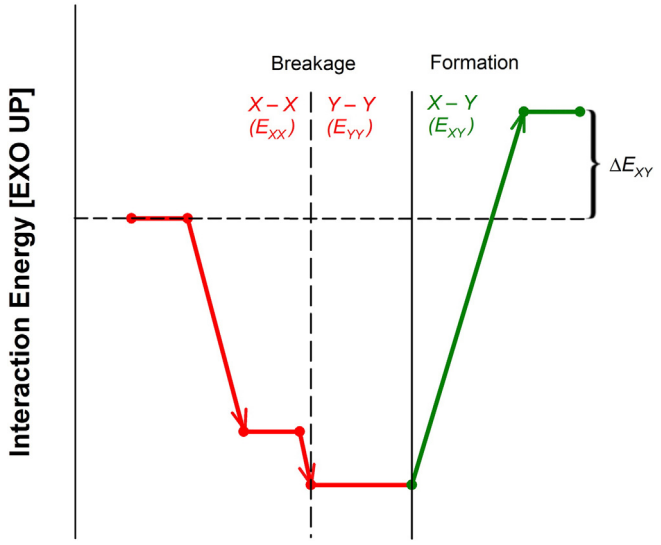

Fig. 6. Simplified schematic of breaking self-interactions (*X*–*X* and *Y*–*Y*) followed by the formation of new *X*–*Y* interactions during dilution of liquid *X* in liquid *Y* for low molecular substitutes.

fraction of component *X*, respectively. On the right side of Eq. (15), the first two terms refer to combinatorial entropy, while all noncombinatorial effects are represented by the χ parameter. The combinatorial entropy of mixing is related to the positional disorder in the system. As the mixture is more disordered than the pure components, the combinatorial entropy of mixing leads to a negative contribution to ΔG_M, i.e., stabilisation of the mixture. However, the combinatorial entropy for the polymer mixture consisting of high molecular weight components (large r_X and r_Y) is virtually zero, and the negative contribution to ΔG_M is comparatively negligibly small due to the mixtures of small molecules [26].

The temperature drops in a buffer solution and the self-interaction energies (E_{XX}) are shown in Table 4. In order to understand the component fraction of the blend after dilution, the heat of mixing vs. molar fraction and the fraction of liquid *X* diluted into solvent *Z* were calculated. A schematic plot (see Fig. 6) shows the principle of calculation of the E_{XY} based on the measurements of ΔE_{XY} according to Eq. (12). An evaluation of E_{XY} for the respective pairs showed that *X*–*Y* interaction values are asymmetric. The value for liquid *X* diluted in liquid *Y* was slightly different than the value of liquid *Y* diluted in liquid *X*. The error was neglected. This could be caused by a difference in the heat capacity c_p of each liquid.

The respective association energies E_{XY} for each *X*–*Y* pair evaluated using Eq. (13) are shown in Table 5. The highest values are observed for 2ET-NMA and DGME-NMA blends, 9659 and 7139 [J/mol], respectively, while the smallest interaction energies were observed between DGME and BV with only 3011 [J/mol].

Together, FTIR and calorimetry provide the necessary information for the evaluation of the specific interactions. The shift of peaks in FTIR measurements as well as the observed temperature surge for certain blends with the sole help of analogue calorimetry can serve as proof of the presence of specific interactions, while combing both data together allows the establishment of the relationship of the two independent experiments.

The vibrating frequency of a certain group (such as C–O) is given by

$$\nu = \nu^{v} + \Delta\nu^{d} + \Delta\nu^{ab} \tag{16}$$

where ν^{v} means the frequency in the vapour phase, $\Delta\nu^{d}$ is the frequency shift caused by dispersion force interactions between a certain group and its local environment (non-acid–base interacting liquid such as hexane), and $\Delta\nu^{ab}$ means the frequency shift due to acid–base interactions.

When the tested liquid was diluted in non-interacting liquids (such as cyclohexane, heptane, octane, etc.), a linear relationship of $\Delta\nu^{d}$ with the dispersion force contribution to the surface tension γ^{d} was found ($\Delta\nu^{ab} = 0$). In our case, the tested liquids were diluted in two non-interacting liquids (hexane and decalin) with an appreciably different surface tension in order to obtain the linear relationship ($\nu = \nu^{v} + a\gamma^{d}$). For the acid–base interacting liquids, the exact values of $\Delta\nu^{ab}$ were calculated by the deviation from the linear relationship satisfied in non-interacting liquids [27]. On the basis of quantum mechanics, Drago [28] explained the linear relationship between enthalpy of adduct formation and the shift in the frequency of vibration:

$$\Delta H = k\,\Delta\nu^{ab} \tag{17}$$

The obtained data from two independent experiments can be verified by this relation. The E_{XY} association energies obtained by

Table 4
Temperature drop ΔT, heat of mixing $\Delta H_M/(n_X + n_Z)$, molar fraction $n_X/(n_X + n_Z)$ and self-interaction energies E_{XX}.

Name	Temperature change ΔT [°C]	$\Delta H_M/(n_X + n_Z)$ [J/mol]	$n_X/(n_X + n_Z)$ [10^{-3}]	Self-interaction energy E_{XX} [J/mol]
AM	0.19	28.35	6.708	5264
BV	0.15	29.38	6.754	4132
2ET	0.81	157.82	12.633	11,861
DGME	0.80	156.41	9.146	16,236
NMA	0.15	29.14	16.835	2308

Table 5
Association energies E_{XY} of respective pairs *X*–*Y*.

Liquid, [1%]	2ET	DGME	AM	BV	NMA
2ET	–	–	5008	6471	9659
DGME	–	–	3793	3011	7139
AM	5560	4162	–	–	5899
BV	6784	3294	–	–	6353
NMA	10,624	7846	5382	5810	–

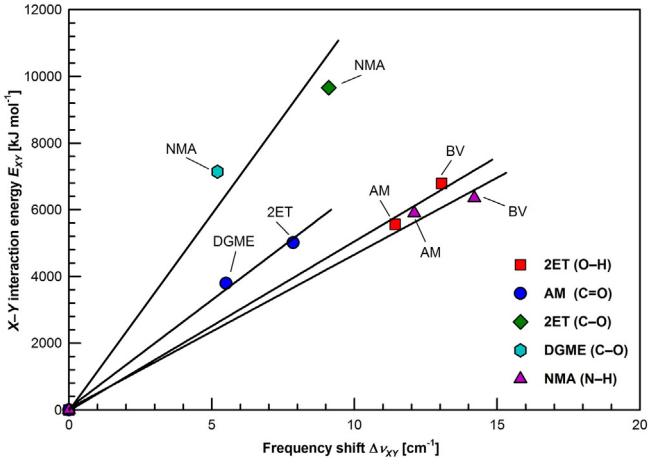

Fig. 7. Association energies E_{XY} vs. shift of peaks for low molecular weight substitutes of acrawax, carnauba wax and polyethylene glycol.

calorimetry and shifts of peaks $\Delta\nu^{ab}$ measured using FTIR are shown in Fig. 7. A linear dependence was found for the tested pairs, confirming the validity of data and calculations from two independent experiments.

4. Conclusion

Understanding the role of particular binder components is key for the development of novel binder systems with advanced processing properties. Interactions of low molecular weight analogues of polyethyleneglycol (PEG) with acrawax (AW) have been compared with those of carnauba wax (CW) in order to quantify the difference between these two polar waxes. FTIR spectra for substitute liquids of AW and PEG showed a shift of the C–O stretch absorption peak to a lower wave number in a range between 5.2–9.1 cm^{-1}, solely referring to the presence of the interactions between the components. Further, the analogue calorimetric analysis showed a temperature drop for all low molecular compositions (AW/CW, CW/PEG) except for AW/PEG substitutes, which attracted each other more than themselves, expressing an up to 0.52 °C temperature increase during the mixing. The E_{XY} association energies for AW/PEG were on average 2.1 times higher than for CW/PEG substitutes. This can be explained by the presence of a C═O group plus an N–H group for each molecule of the AW analogue in comparison with one C═O group plus one C–O group per molecule of the CW analogue. It is conceivable that a strong type of interactions (such as hydrogen bonding) is formed during AW and PEG mixing. The combination of FTIR and calorimetry data in conjunction with Drago's equation allowed for the defining of the linear relationship of two independent experiments. The final results of the analyses for blends of low-molecular weight analogues suggest that the corresponding AW/PEG polymer blend with higher interactions is more favourable than CW/PEG for powder injection moulding.

Acknowledgments

This article was written with the support of the Operational Program Research and Development for Innovations co-funded by the ERDF and the National Budget of Czech Republic, within the framework of the project Centre of Polymer Systems (reg. number: CZ.1.05/2.1.00/03.0111). The author D.B. acknowledges the support of an internal grant from TBU in Zlín, IGA/FT/2015/001.

References

[1] R.M. German, A. Bose, Injection Molding of Metals and Ceramics, Metal Powder Industries Federation, Princeton, N.J., 1997
[2] S.B. Ren, X.B. He, X.H. Qu, I.S. Humail, Y. Li, Effects of binder compositions on characteristics of feedstocks of microsized sic ceramic injection moulding, Powder Metall. 50 (2007) 255–259.
[3] J. Hidalgo, C. Abajo, A. Jimenez-Morales, J.M. Torralba, Effect of a binder system on the low-pressure powder injection moulding of water-soluble zircon feedstocks, J. Eur. Ceram. Soc. 33 (2013) 3185–3194.
[4] R.K. Enneti, T.S. Shivashankar, S.J. Park, R.M. German, S.V. Atre, Master debinding curves for solvent extraction of binders in powder injection molding, Powder Technol. 228 (2012) 14–17.
[5] S.M. Ani, A. Muchtar, N. Muhamad, J.A. Ghani, Fabrication of zirconia-toughened alumina parts by powder injection molding process: optimized processing parameters, Ceram. Int. 40 (2014) 273–280.
[6] B. Hausnerova, L. Marcanikova, P. Filip, P. Saha, Optimization of powder injection molding of feedstock based on aluminium oxide and multicomponent water-soluble polymer binder, Polym. Eng. Sci. 119 (2011) 2925–2932.
[7] J. Hidalgo, A. Jimenez-Morales, J.M. Torralba, Torque rheology of zircon feedstocks for powder injection moulding, J. Eur. Ceram. Soc. 32 (2012) 4063–4072.
[8] F. Sommer, H. Walcher, F. Kern, M. Maetzig, R. Gadow, Influence of feedstock preparation on ceramic injection molding and microstructural features of zirconia toughened alumina, J. Eur. Ceram. Soc. 34 (2014) 745–751.
[9] S. Ahn, S.J. Park, S. Lee, S.V. Atre, R.M. German, Effect of powders and binders on material properties and molding parameters in iron and stainless steel powder injection molding process, Powder Technol. 193 (2009) 162–169.
[10] S.M. Ani, A. Muchtar, N. Muhamad, J.A. Ghani, Binder removal via a two-stage debinding process for ceramic injection molding parts, Ceram. Int. 40 (2014) 2819–2824.
[11] C. Quinard, T. Barriere, J.C. Gelin, Development and property identification of 316L stainless steel feedstock for PIM and μPIM, Powder Technol. 190 (2009) 123–128.
[12] F. Chen, M.P. Wolcott, Miscibility studies of paraffin/polyethylene blends as form-stable phase change materials, Eur. Polym. J. 52 (2014) 44–52.
[13] A.H. Doulabi, H. Mirzadeh, M. Imani, Miscibility study of chitosan/polyethylene glycol fumarate blends in dilute solutions, J. Appl. Polym. Sci. 127 (2013) 3514–3521.
[14] B. Hausnerova, I. Kuritka, D. Bleyan, Polyolefin backbone substitution in binders for low temperature powder injection moulding feedstocks, Molecules 19 (2014) 2748–2760.
[15] L. Liu, X.L. Ni, H.Q. Yin, X.H. Qu, Moldability of various zirconia micro gears in micro powder injection moulding, J. Eur. Ceram. Soc. 35 (2015) 171–177.
[16] R.N. French, J.M. Machado, D. Linvien, Miscible polyacetal poly(vinyl phenol) blends. 1. Predictions based on low-molecular-weight analogs, Polymer 33 (1992) 755–759.
[17] P. Svoboda, J. Kressler, T. Ougizawa, T. Inoue, K. Ozutsumi, FTIR and calorimetric analyses of the specific interactions in poly(epsilon-caprolactone)/poly(styrene-co-acrylonitrile) blends using low molecular weight analogues, Macromolecules 30 (1997) 1973–1979.
[18] D. Rana, B.M. Mandal, S.N. Bhattacharyya, Analogue calorimetry of polymer blends: poly(styrene-co-acrylonitrile) and poly(phenyl acrylate) or poly(vinyl benzoate), Polymer 37 (1996) 2439–2443.
[19] L. Bernazzani, C. Cardelli, G. Conti, P. Gianni, Analog calorimetry and uniquac group contributions approaches to the miscibility of PVC with EVA copolymers, J. Therm. Anal. Calorim. 70 (2002) 927–947.
[20] C. Qin, A.T.N. Pires, L.A. Belfiore, Spectroscopic investigations of specific interactions in amorphous polymer–polymer blends — poly(vinylphenol) and poly(vinyl methyl ketone), Macromolecules 24 (1991) 666–670.
[21] D. Bleyan, P. Svoboda, B. Hausnerova, Specific interactions of low molecular weight analogues of carnauba wax and polyethylene glycol binders of ceramic injection moulding feedstocks, Ceram. Int. 41 (2015) 3975–3982.
[22] K.C. Hsu, C.C. Lin, G.M. Lo, Effect of wax composition on injection moulding of 304L stainless steel powder, Powder Metall. 37 (1994) 272–276.
[23] K.L. Mittal, H.R. Anderson, F.M. Fowkes, Acid–Base Interactions: Relevance to Adhesion Science and Technology: In Honor of the 75th Birthday of Professor Frederick M. Fowkes, VSP, Utrecht, 1991.
[24] Y.N. Sudhakar, M. Selvakumar, Miscibility of chitosan and poly(ethyleneglycol) blends in buffer solution, E-Polymers 12 (2012) 1037–1050.
[25] W.O. George, P.S. McIntyre, D.J. Mowthorpe, Infrared Spectroscopy, Published on behalf of ACOL by Wiley, Chichester, 1987.
[26] H.W. Kammer, Thermodynamics of polymer miscibility, Acta Polym. 37 (1986) 1–6.
[27] F.M. Fowkes, D.O. Tischler, J.A. Wolfe, L.A. Lannigan, C.M. Ademujohn, M.J. Halliwell, Acid–base complexes of polymers, J. Polym. Sci. Polym. Chem. 22 (1984) 547–566.
[28] R.S. Drago, G.C. Vogel, T.E. Needham, 4-Parameter equation for predicting enthalpies of adduct formation, J. Am. Chem. Soc. 93 (1971) 6014–6026.

PAPER IV

Surface Adhesion between Ceramic Injection Molding Feedstocks and Processing Tools

Davit Bleyan[1,2], Berenika Hausnerova[1,2], Vera Kasparkova[1,3], Vladimir Pata[2]

[1] Centre of Polymer Systems, University Institute, Tomas Bata University in Zlin, Trida Tomase Bati 5678, 760 01 Zlin, Czech Republic

[2] Department of Production Engineering, Faculty of Technology, Tomas Bata University in Zlin, nam. T.G. Masaryka 5555, 760 01 Zlin, Czech Republic

[3] Department of Fat, Surfactant and Cosmetics Technology, Faculty of Technology, Tomas Bata University in Zlin, nam. T.G. Masaryka 5555, 760 01 Zlin, Czech Republic

Corresponding author: hausnerova@ft.utb.cz

Keywords: ceramic injection molding; adhesion; aluminum oxide; zirconium oxide; binder; contact angle; surface energy

Abstract

Interfacial adhesion between highly filled aluminium and zirconium oxides ceramic compounds and CIM (Ceramic Injection Molding) processing tools was investigated from contact angle measurement. Polymers considered as binder components were low density polyethylene, paraffin wax, polyethylene glycol, carnauba wax, acrawax, and stearic acid. Channel walls of the mold were constructed from hardened, TiN hardened, nitridized and heat-treated steels. From the calculated surface energies, the superiority of heat-treated steel as well as acrawax and especially polyethylene glycol as binders is derived. Carnauba wax shows similar wettability as stearic acid, thus becoming promising substitute for the role of processing aid. Concerning tested ceramic powders, Al_2O_3 revealed somewhat higher polar component of the surface energy than ZrO_2. The differences in total surface energies of powders and binders are all about 3 J/m^2 lower (PEG) or higher (PW, LDPE, AW, CW, SA) for Al_2O_3 powder than for ZrO_2.

1. Introduction

Ceramic injection molding (CIM) serves as a highly effective technique for manufacturing complex shape parts with high dimension accuracy. This technique also gains superior attention for its ability to reduce production waste and cost by allowing manufacturing parts close to their theoretical net weight. CIM process includes four major stages: (1) mixing; (2) injection molding; (3) debinding; (4) sintering.

The initial stages such as mixing and molding are considered to be of the critical importance, complicated by the necessity of using large number of different materials often with contradicting properties in order to fulfil the processing requirements. Currently, the most efficiency limiting factor of CIM is the separation of powder and binder components during injection molding stage. Thornagel [1] demonstrated that local shear rate gradients are the driving forces initiating phase separation. Assuming no slip condition, i.e. good adhesion of the feedstock to the wall of the channel, a significant shear rate peak occurs close to the wall, while a plateau at much lower shear rate level is observed in the middle of the flow domain. Then, particles flowing in the peak area experience a non-uniform shear rate resulting in their rotation, which becomes severe as the shear stress gradients increase. Such rotating particles try to leave areas of high shear gradients. As a

consequence, high shear rate area is characterized by high binder content, while the plateau region of the lower shear rate accommodates a powder rich material.

Recently, we have proposed a method to quantify the separation *via* SEM/EDX combined with the analytical tool [2] as well as the rheological model suitable for ceramic feedstocks [3]. Further, we have pointed out that wall slip could be considered as a rheological parameter indicating powder-binder separation absence/occurrence [4,5]. Nevertheless, the conditions, at which the highly filled materials slip at the wall resulting in a plug flow (and thus no separation), are not only feedstock characteristics and processing parameters, but the most important is an interfacial adhesion between the channel walls and CIM feedstock (binder and powder), depending on the surface treatment of the mold channels.

Therefore, the aim of the paper is to evaluate the adhesion properties of CIM powders and binder components as well as materials most often employed in construction of channel walls of CIM processing tools. In the recent paper [6] the possibility to substitute the polyolefin backbone in alumina feedstocks with polar waxes has been investigated with the regard to debinding and early stage of sintering process. Over 20 feedstocks differing in the aluminum oxide powder loading as well as binder composition containing low density polyethylene or carnauba wax, paraffin wax, polyethylene glycols varying in their molecular weight, and stearic acid as a plasticizer were studied. Adhesion of these components is now considered for four most often used materials for construction of channels and mold-die walls. Contact angle measurement is provided as it has proved itself a method widely employed as a characterization tool in ceramic processing (e.g. [7-9]).

2. Experimental

2.1. Materials

Commonly used CIM binder components - Low Density Polyethylene (LDPE, Laqtene 1200 MN 8, Atochem), Paraffin wax (PW, Paraffinum Solidum, Tamda), Polyethylene glycol (PEG6000, Sinopol, Sino-Japan Chemical), Stearic acid (SA, 95%, Sigma Aldrich), Carnauba Wax (CW, 2442, Kahl), and Acrawax (AW, ACRAWAX C Atomized, Lonza) were studied. Tested materials properties are shown in Table 1. Ceramic powders employed in the study were highly compressive super-ground aluminium oxide and zirconium oxide powders.

Pure binder components were examined from the flat 1 mm thick samples prepared by a unidirectional pressing at temperatures 20 °C above particular binders' melting points. The contact angles of ceramic powders were studied from the sintered samples prepared as follows: feedstocks (55 vol.%) were mixed in a twin screw extruder Brabender (KETSE 20/40) at mixing rate of 150 RPM at temperature of 150 °C, and then molded into a rectangular shapes in an injection molding machine (Allrounder 370S, Arburg). The optimized injection molding parameters are summarized in Table 2. After molding the polymer binder was removed by combined solvent and thermal debinding, and brown parts were sintered to the final densities at maximum sintering temperatures of 1500 °C (ZrO_2) and 1600 °C (Al_2O_3) at a heating ramp of 50 °C/h with 2 hours temperature holding followed by cooling down spontaneously.

Four most often used treatments of steel were considered for the discs samples (20 mm in diameter, 2 mm thick) of channel walls of an injection mold: hardened, hardened TiN, nitridized and heat-treated.

2.2 Surface properties determination

Surface properties of the samples prepared from ceramic powders, as well as samples of channel wall materials, were examined with contactless 3D Chromatic Length Aberration (CLA) scanner (Talysurf 300, Taylor and Hobson, UK) equipped with Talymap ver.5.0.2 software. Tested surfaces were subjected to a height measurement over a rectangular area (500 x 500) μm. The data supplied is of the form $z = f(x,y)$, where z is the height of the profile, x stands for the position over the scanning direction, and y corresponds to the number of traces. First Interface Detection (FID) was selected as a measurement mode. The software takes into account the height of the first interference (i.e. the upper border of the transparent interference represented by the first peak in the spectrum).

2.3. Contact angle measurements

The surface energy was determined by measurements of contact angles of three test liquids set (deionized water, ethylene glycol and diiodomethane) using the SEE (Surface Energy Evaluation) system (Advex Instruments, Czech Republic) with the contact angle measurement error ±2°. A drop of the test liquid ($V = 3$ μL) was placed with a micropipette on the material surface, the sessile drop was imaged by a color camera, and the contact angle of the test liquid was measured. For a

sessile drop of tested liquid, this is defined as the angle between surface of material under investigation and the tangent of the droplet's oval shape at the edge of the droplet.

Contact angle measurements were taken over 6 different areas for each sample and readings were averaged to obtain one representative value. Using the above data, the total surface energy $\gamma^{(tot)}$ including its components, disperse part $\gamma^{(LW)}$ and polar part $\gamma^{(ab)}$, were obtained. Finally, the γ^{dif} denoting the absolute value of the difference between the surface energy of powder/mold material and the binder was calculated.

3. Theoretical Background

Surface tension γ is defined as the free energy G required to increase an interface of area A

$$\gamma = (\partial G/\partial A)_{T,P} \quad (1)$$

where the constant temperature and pressure, which are frequently encountered, would made the Gibbs free energy the suitable choice for G. It is inherent to refer to γ as a surface tension, if the increase of area is reversible, while otherwise as a surface energy [10].

Generally, work needs to be done to create an interface; it has higher free energy than the bulk. The work of cohesion (*coh*) of solid can be expressed by eq. (2)

$$W^{(coh)} = 2\gamma_1 A = -\Delta G^{(coh)} \quad (2)$$

where ΔG is regarded as per unit area.

Meanwhile, the work of adhesion (*adh*), needed to separate two different substances 1 and 2, can be expressed by eq. (3), which is a known formalism introduced by Dupre [e.g. in 11]

$$W_{12}^{(\mathrm{adh})} = (\gamma_1 + \gamma_2 - \gamma_{12})A = -\Delta G^{(adh)} \quad (3)$$

In eq. (3), γ_1 and γ_2 represent the lost interfaces, while γ_{12} stands for the new gained interface. The theoretical calculations and predictions of terms involving two (or more) substances such as γ_{12}, are the well-known challenges experienced in the field of interfacial interactions.

Fowkes [12] proposed the assumption that the tension at the interface of the substance 1 against the substance 2 is reduced by the presence of an amount equal to the geometric means of the tensions of the two individual substances, hence equal to $\gamma_1 - (\gamma_1\,\gamma_2)^{1/2}$, and similarly the tension at the interface of the substance 2 against the substance 1 is reduced by $\gamma_2 - (\gamma_1\,\gamma_2)^{1/2}$ giving eq. (4)

$$\gamma_{12} = \gamma_1 + \gamma_2 - (\gamma_1\gamma_2)^{1/2} = (\sqrt{\gamma_1^{(\mathrm{LW})}} - \sqrt{\gamma_2^{(\mathrm{LW})}})^2 \quad (4)$$

known as Grifalco-Good-Fowkes equation, which works very well for a polar liquids and solid surfaces. This can be also referred as a work of adhesion being geometric mean of the works of cohesion, i.e. $W_{12} = (W_{11}W_{22})^{1/2}$. The Dupre equation can be expressed as

$$W_{12}^{(\mathrm{adh})} = 2(\gamma_1\gamma_2)^{1/2} \quad (5)$$

Fowkes [13] and van Oss et al. [14] proposed that the total interfacial energy can be linear separated into the dispersive (London-van der Waals), dipole-induced dipole (Debye), dipole-dipole (Debye) and electron donor-acceptor terms. Furthermore, Lifshitz [15] stated that the London-van der Waals, Debye and Keesom interactions are of an identical type, with equal dependence of magnitude on separation between the two interacting substances, and thus

$$\gamma^{(\mathrm{total})} = \gamma^{(\mathrm{LW})} + \gamma^{(\mathrm{ab})} \quad (6)$$

where (LW) denotes Lifshitz-van der Waals and (ab) indicates the Lewis acid-base terms, respectively; and hence

$$\gamma_{12}^{(\mathrm{total})} = \gamma_{12}^{(\mathrm{LW})} + \gamma_{12}^{(\mathrm{ab})}. \quad (7)$$

The ratio between Lewis acids and Lewis bases constituting the two interacting substances dictate the sign of the Lewis acid-base interaction. The Lifshitz-van der Waals interaction is always attractive. Whereas van Oss et al. [14] has suggested that it can be expressed by the geometric mean

$$\gamma^{(\mathrm{ab})} = 2\left(\gamma^{(+)}\gamma^{(-)}\right)^{1/2} \quad (8)$$

where superscript (+) indicates electron-accepting (Lewis acid) moieties and superscript (−) the electron-donating (Lewis base).

From eq. 6 and eq. 8 the $\gamma^{(\mathrm{total})}$ can be expressed as

$$\gamma^{(\mathrm{total})} = \gamma^{(\mathrm{LW})} + 2\left(\gamma^{(+)}\gamma^{(-)}\right)^{1/2} \quad (9)$$

Combining the Dupre equation with the Young equation [e.g. in 16] we have

$$(1+\cos\theta)\gamma_L = 2\left(\gamma_1^{\mathrm{LW}}\gamma_2^{\mathrm{LW}}\right)^{\frac{1}{2}} + 2\left(\gamma_1^{(+)}\gamma_2^{(-)}\right)^{\frac{1}{2}} + 2\left(\gamma_2^{(+)}\gamma_1^{(-)}\right)^{\frac{1}{2}} = W_A \qquad (10)$$

where W_A stands for thermodynamic work of adhesion (expanded to the non-polar plus the polar form) [17].

4. Results and Discussion

The values of contact angle as the basic parameter for a binder wetting the powder as well as mold-die were measured using the standard liquids (water, ethylene glycol and diiodomethane) and are reported in Table 3.

As to chemical nature, the used binders can be roughly divided into three groups. The first group comprises of paraffin wax and LDPE. Paraffin is a soft solid consisting of a mixture of hydrocarbons commonly with twenty to forty carbon atoms in chain and its melting temperature is lying between 45–65 °C. LDPE is of similar hydrocarbon nature being composed of long chains formed during polymerization of the monomer, ethylene. The melting point in average is 105 to 115 °C. The second group covers stearic acid, carnauba wax and acrawax. Stearic acid is a saturated fatty acid with 18 carbons in molecule and well known lubricating agent with melting point of about 70 °C. Esters of stearic acid with high fatty alcohols are present also in carnauba wax, which contains mainly of wax esters (85%), accompanied by small amounts of free fatty acids and alcohols, hydrocarbons and resins. The wax esters constitute C16 to C20 fatty acids linked to C30 to C34 long-chain fatty alcohols. Melting point of the wax is of 82–86 °C. The last mentioned acrawax (N, N'-Ethylene Bis-stearamide) belongs to group of amidic waxes with melting point of 145 °C, and in the present study it has been considered as a possible alternative of carnauba wax because of its stronger interactions to other binder components evaluated in the recent work [18]. All components belonging to this group are more or less derivatives of fatty acids. The last group consists solely of PEG 6000, oligomer of ethylene oxide with molar mass of 6000 g/mol and melting point in the range of 55 – 60 °C. This is the only water-soluble, hydrophilic substance used as a binder in the study.

From the Table 3 it is obvious that for given substance, the contact angles are highest with water and lowest with diiodomethane. Exceptions here are both ceramic powders with the lowest contact angles observed for ethyleneglycol. The low contact angles measured on PEG 6000 surface

with all testing liquids whether hydrophilic or hydrophobic indicates exceptional behaviour of this surface which can be explained by its hydrophilicity.

In general, as the contact angle decreases, the tendency of the binder to spread over the powder particle increases which is natural consequence of better wettability [19]. According to Chiou et al. [20] the role of surface active agent in the feedstock can play low molecular weight substances as stearic acid (SA) as well as high molecular weight polar waxes, such as carnauba wax.

As can be seen from Table 3, SA and carnauba wax reach very similar values of contact angles in water, and for the remaining testing liquids they are similar crosswise. The low molecular weight surface active agents are usually more effective in reducing the feedstock viscosity than the high molecular weight ones due to their lower intrinsic viscosities and higher polarities. In publication [20] it is suggested that SA consists of a functional group adhering to the powder surface and an oriented molecular chain extending into the binder to prevent aggregation of powder, and stabilize particles during high shearing mixing. This effect can be also attributed to the known amphiphilic character of this fatty acid functioning as a surface active agent.

However, interlinking strength among binder components is weak, due to the relatively short chain lengths of the low molecular weight surface active agents (SA), and necking during plastic forming occurs easily [20]. Thus, a polymer having suitable functional groups in each repeating unit can enhance the interlinking strength among binder components, in addition to improving the adhesion force with the powder surface. In our case this applies the best for PEG showing the lowest contact angles and the highest total surface energy (including its polar part) from the tested materials. This is natural as PEG is the only hydrophilic binder tested and this also predestines its role in the feedstock. Polar organic substances are capable of forming hydrogen bonds with powders easier, which is due to acid-base interactions. Interestingly, acrawax, which low molecular weight analogue has been recently found to have strong interactions to the analogues of PEG [18], itself exhibits the values of contact angle comparable with those obtained for paraffin wax (PW), where no adhesion is expected.

Table 4 shows the calculated free surface energy for acid-base model with unpolar Lifshitz-van der Waals component $\gamma^{(LW)}$, electron-donor $\gamma^{(-)}$, electron-acceptor $\gamma^{(+)}$, polar component $\gamma^{(ab)}$ as well as $\gamma^{(total)}$ representing the sum of unpolar and polar components. Changes of surface free energy upon material and its treatment can be seen from data presented in this table.

Enhanced adhesion of binder components onto the powder surface is primarily realized by hydrogen bonding between the powder surface and the surface active agent through a Lewis acid-base reactions [21]. The adsorption of the binder components onto the powder surface is competitive such that patterns similar to the Langmuir adsorption and desorption isotherms usually take place [22]. The lowest total surface energy was obtained for nitridized and hardened TiN surfaces. Here also dispersion and polar components are similar. Significantly different behavior showed, however, heat-treated surface with the highest value of surface energy of 55.4 J/m^2 and significantly higher polar component 23 J/m^2, compared to those measured for both former mentioned surfaces (0.4 J/m^2). Dispersion part of surface energy did not notably differ from other tested surface modifications. The exceptional behavior of heat-treated sample can be seen also from Figure 1, where the differences in $\gamma^{(total)}$ are considered.

It should be noted that the surface properties might substantially influence the adhesion analysis as liquid penetrating the porous surface may result in an artificially lower contact angle. Thus, the tested surfaces have been quantified with the contactless scanner (Table 5) in order to distinguish the effect of surface structure from the adhesion characteristic. From the statistical analyses of the scanned surfaces – namely homoskedasticity F-test (H_0: $\sigma^2_{Rz\_Heat} = \sigma^2_{Rz\_Hardened\_TiN}$, H_a: NON ($\sigma^2_{Rz\_Heat} \neq \sigma^2_{Rz\_Hardened\_TiN}$), $1 - \alpha = 0.95$) as well as T-test (H_0: $\mu_{Rz\_Heat} = \mu_{Rz\_Hardened\_TiN}$, H_a: NON ($\mu_{Rz\_ZrO2} \neq \mu_{Rz\_Hardened\_TiN}$), $1 - \alpha = 0.95$) arises that the heat-treated and e.g. hardened TiN samples surfaces are both homogenous and statistically they have the same surface structure. Thus, the effect of a surface profile can be disregarded, and resulting heat-treated surface can be considered as the mold material with the strongest adhesion to the feedstock components.

Regarding ceramic powders, their surface characteristics were fairly similar, $\gamma^{(total)}$ was 44 and 47 J/m^2 for ZrO_2 and Al_2O_3, respectively, and aluminum oxide showed somewhat higher polar component of the surface energy as well. Figure 2 shows differences of calculated for respective powders and binder components. The differences γ^{dif} are all about 3 J/m^2 lower (PEG) or higher (PW, LDPE, AW, CW, SA) for Al_2O_3 powder than for ZrO_2 sample. At this point it should be noted that both ceramic powders were examined as sintered, while during molding they are in a powder form, where particle shape, size and its distribution play a role too.

By comparison of surface characteristics determined on binders it can be concluded that almost all materials show surprisingly similar values of $\gamma^{(total)}$ ranging from 34 to 38 J/m^2 . Also the polar components measured were similar and low as to absolute values (all below 1 J/m^2), only acrawax

displayed polar component higher $\gamma^{(ab)}$ of 3.7 J/m^2. Hence, AW in principle should demonstrate stronger interactions to powders and other feedstock components. This is consistent with our recent findings obtained for The exception from this rule was PEG 6000 exhibiting the highest surface energy (64.7 J/m^2) of all tested binders, with polar component of 17.6 J/m^2. This is a natural reason of the chemical composition of this polymer. Nonpolar surfaces show only $\gamma^{(LW)}$ with absence of (or very small) polar component and their total surface energy is usually lower compared to polar surfaces with both polar and unpolar components of γ (metals and powders).

4. Conclusion

The adhesion among the binder components, ceramic powders and mold materials was investigated with regard to ceramic injection molding technology. Considering the wettability of the channel walls of the mold revealed about ten times higher surface energy of heat-treated steel than nitridized, hardened, and hardened TiN materials. Among the binder components studied it has been found that the role of the surfactant (stearic acid) might be substituted with carnauba wax, however the surface characteristic is not the only parameter which has to be considered when preparing feedstock with optimum properties. Acrawax and especially polyethylene glycol have shown the highest values of polar component of surface energy determining their key role in CIM feedstocks.

Acknowledgments

Assoc. prof. Marian Lehocky and Daniel Sanetrnik are gratefully acknowledged for the assistance with performing the contact angle measurements and injection molding of powders, respectively. This work was supported by the Ministry of Education, Youth and Sports of the Czech Republic – Program NPU I (LO1504). The author D.B. acknowledges the support of an internal grant from TBU in Zlín, IGA/FT/2015/001.

References

1. Thornagel, M., MIM-Simulation: A virtual study on phase separation. *Proceedings of EURO PM2009 Congress.* Shrewsbury: European Powder Metallurgy Association, 2009, 2, 135-140.
2. Hausnerova, B.; Sanetrnik, D.; Ponizil, P., Surface structure analysis of injection molded highly filled polymer melts. *Polym Compos* **2013**, 34, 1553-1558.
3. Hausnerova, B.; Marcanikova, L.; Filip, P.; Saha, P., Optimization of powder injection molding of feedstock based on aluminum oxide and multicomponent water-soluble polymer binder. *Polym Eng Sci* **2011**, *51*, 1376-1382.
4. Hausnerova, B.; Filip, P.; Saha, P., Wall-slip velocity as a quantitative measure of powder-binder separation during powder injection molding. *World PM2010 Congress*. Firenze, 2010.
5. Hausnerova, B.; Sanetrnik, D.; Paravanova, G. Wall-slip of highly filled powder injection molding compounds: Effect of flow channel geometry and roughness. *AIP Conf. Proc., 2014.* American Institute of Physics (AIP).
6. Hausnerova, B.; Kuritka, I.; Bleyan, D., Polyolefin backbone substitution in binders for low temperature powder injection molding feedstocks. *Molecules* **2014**, 19, 2748-2760.
7. Kuscer, D.; Kosec, M.; Holc, J., Correlation between sintering conditions and water contact angles for Ti-O thick films screen printed on an alumina substrate. *Ceram Int* **2009**, 35, 1063-1069.
8. Isobe, T.; Nakanome, M.; Nakazono, K.; Matsushita, S.; Nakajima, A., Adsorption and adhesion of poly(vinyl alcohol) and poly(ammonium acrylate) as organic additives for wet mold processing of Al2O3. *Ceram Int* **2013**, *39*, 3857-3864.
9. Cui, X.M.; He, Y.; Liang, Z.Y.; Zhang, H.; Zhou, J., Different microstructure $BaO–B_2O_3–SiO_2$ glass/ceramic composites depending on high-temperature wetting affinity. *Ceram Int* **2010**, *36*, 1473-1478.
10. Woodruff, D.P., *The solid-liquid interface*. Cambridge University Press, 1973.
11. van Oss, C.J.; Giese, R.F., *Colloid and surface properties of clay and related minerals.* Marcel Dekker. New York, 2002.

12. Fowkes, F.M., Determination of interfacial tensions, contact angles, and dispersion forces in surfaces by assuming additivity of intermolecular interactions in surfaces. *J Phys Chem-Us* **1962**, *66*, 382.
13. Fowkes, F.M., Attractive forces at interfaces. *Ind Eng Chem* **1964**, *56*, 40.
14. van Oss, C.J.; Chaudhury M.K.; Good, R.J., Interfacial Lifshitz-van der Waals and polar interactions in macroscopic systems. *Chem. Rev.* **1988**, 88, 927-941.
15. Lifshitz, E. M., *J. Exp. Theor. Phys.*, 1955, 29, 94.
16. Schrader, M.E., Young-Dupre revisited. *Langmuir* **1995**, *11*, 3585-3589.
17. Pugh, R.J.; Bergstrom, L., *Surface and colloid chemistry in advanced ceramics processing*. Taylor & Francis, 1993, 319-320.
18. Bleyan, D.; Hausnerova, B.; Svoboda, P., The development of powder injection moulding binders: a quantification of individual components' interactions. *Powder Technol* **2015**, accepted.
19. Li, Y.M.; Liu, X.Q.; Luo, F.H.; Yue, J.L., Effects of surfactant on properties of MIM feedstock. *T Nonferr Metal Soc* **2007**, 17, 1-8.
20. Chiou, Y.H.; Liu, S.J.; Lin, S.T., Superplastic behaviour of a zirconia powder binder blend. *Ceram Int* **1996**, *22*, 211-217.
21. Lin, S.T.; German, R.M., Interaction between binder and powder in injection-molding of alumina. *J Mater Sci* **1994**, *29*, 5207-5212.
22. Richards, V.L., Adsorption of dispersants on zirconia powder in tape-casting slip compositions. *J Am Ceram Soc* **1989**, *72*, 325-327.

List of Tables and Figures

Table 1 Properties of tested binder components.

Binder	Abbreviation	Density ISO 1133 [g/cm³]	Melting Temperature [°C]	Molecular Weight [g/mol]
Low Density Polyethylene	LDPE	0.918	108	250000
Polyethylene glycol 6000	PEG6000	1.21	62	6000
Paraffin wax	PW	0.9	58	400
Carnauba wax	CW	0.97	86	1000
Acrawax	AW	0.99	145	560
Stearic acid	SA	0.85	70	284

Table 2 Injection molding parameters.

Parameter	Value Al_2O_3/ ZrO_2
Zone 1 temperature (°C)	130
Zone 2 temperature (°C)	135
Zone 3 temperature (°C)	140
Zone 4 temperature (°C)	150
Nozzle temperature (°C)	145
Mold temperature (°C)	30
Injection speed (mm/s)	15
Injection pressure (bar)	1800
Hold pressure (bar)	1500/500
Hold pressure time (s)	2/0.5

Table 3 Contact angles of tested mold materials, powers and binders.

Name	Ethylene glycol [°]	Diiodomethane [°]	Water [°]
Mold material			
Hardened	60.9	50.2	72.7
Hardened TiN	57.5	51.7	77.3
Nitridized	71.3	59.8	96.6
Heat-treated	79.9	57.0	78.1
Ceramic powder			
Al_2O_3	23.0	40.6	60.5
ZrO_2	35.6	39.1	67.7
Binder			
LDPE	56.0	44.5	85.8
PW	76.3	52.8	114.1
PEG6000	23.7	22.2	24.0
CW	51.9	64.1	94.6
AW	90.7	57.8	108.8
SA	64.9	52.4	94.9

Table 4 Calculated free surface energy components (J/m^2) for tested mold materials, binder components and ceramic powders.

Material	$\gamma^{(total)}$ [a]	$\gamma^{(LW)}$ [b]	$\gamma^{(ab)}$ [c]	$\gamma^{(+)}$ [d]	$\gamma^{(-)}$ [e]
Mold material					
Hardened	40.7	34.1	6.5	0.5	21.6
Hardened TiN	33.7	33.3	0.4	0	12.3
Nitridized	28.9	28.7	0.3	0	1.8
Heat-treated	53.4	30.3	23.1	4.2	31.9
Ceramic powder					
Al_2O_3	47.2	39.3	7.9	1	15.7
ZrO_2	44.4	40.1	4.4	0.4	12
Binder					
LDPE	38.2	37.3	0.9	0.1	3.4
PW	33.1	32.7	0.4	0	1.4
PEG 6000	64.7	47.1	17.6	1.1	72
CW	33.8	33.2	0.6	0.1	1
AW	33.6	29.8	3.7	2.1	1.7
SA	33.5	32.9	0.6	0.1	1

[a] Sum of unpolar and polar components, [b] Lifshitz-van der Waals component, [c] Polar component, [d] Electron-donor, [e] Electron-acceptor.

Table 5 Roughness profiles R_z (μm) of the tested powders and mold materials.

Material	Mean	Std dev	Min	Max
Ceramic powder				
Al_2O_3	2.90	0.451	1.89	4.15
ZrO_2	2.68	0.387	1.90	4.00
Mold die material				
Heat-treated	3.24	0.371	2.44	4.68
Hardened	4.00	1.060	2.09	8.02
Hardened TiN	3.22	0.445	2.23	4.50
Nitridized	3.72	0.675	2.68	5.97

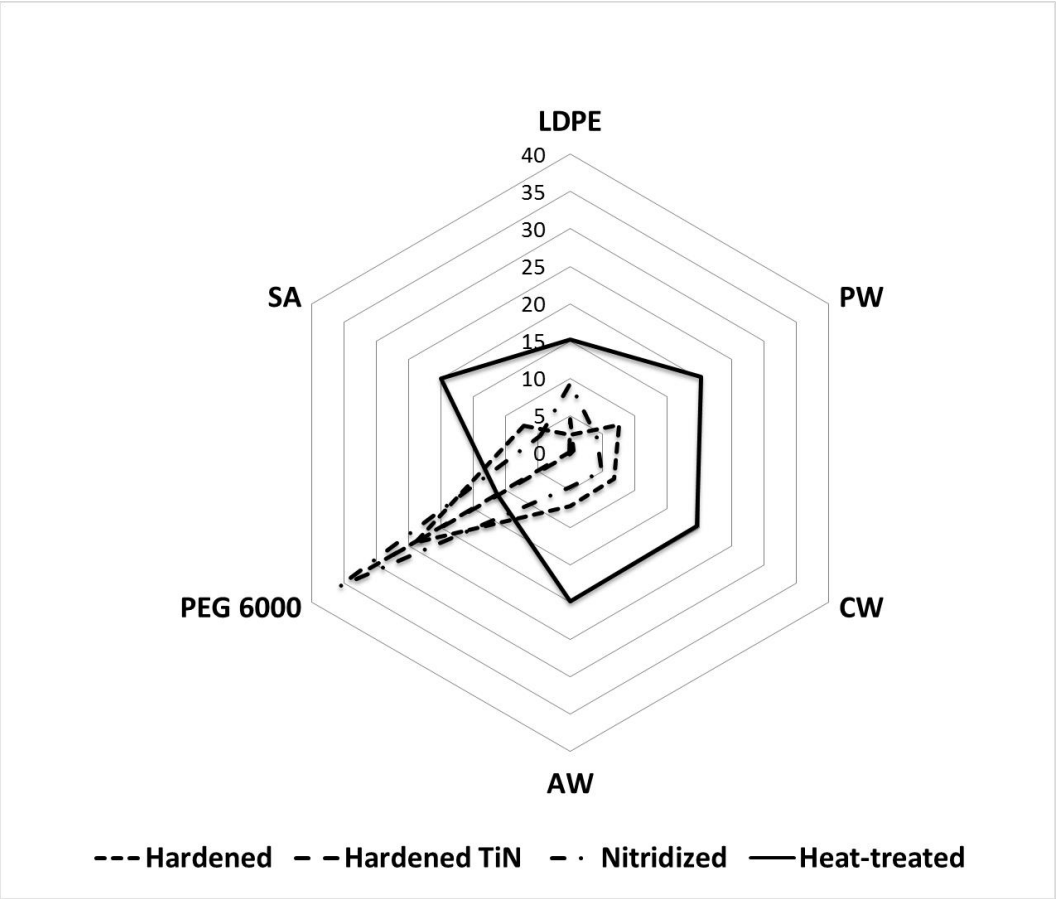

Fig. 1 The differences of $\gamma^{(total)}$ between polymer binders and mold materials.

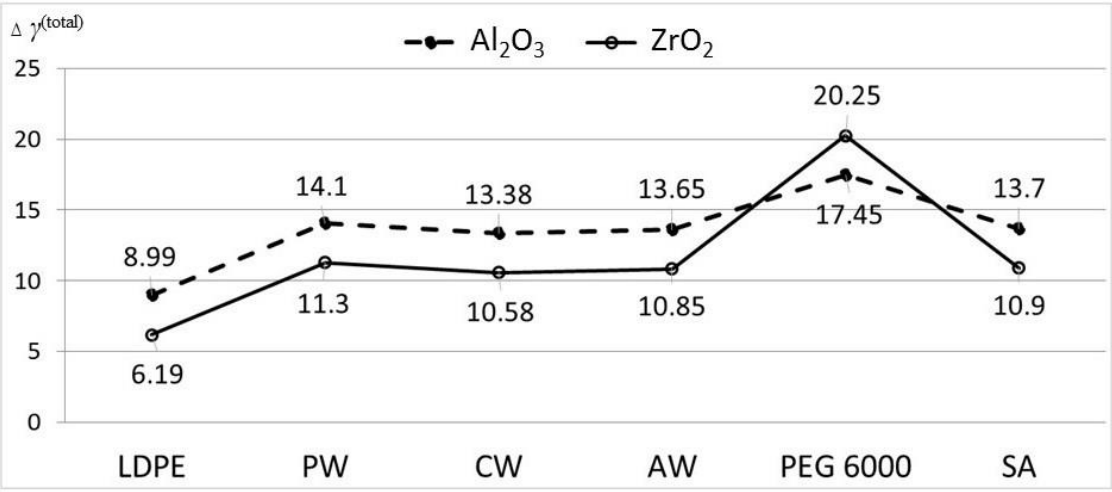

Fig. 2 The differences of $\gamma^{(total)}$ between polymer binders and ceramic powders.

PAPER V

ČESKÁ REPUBLIKA
ÚŘAD PRŮMYSLOVÉHO VLASTNICTVÍ

OSVĚDČENÍ

O ZÁPISU UŽITNÉHO VZORU

Josef Kratochvíl
předseda
Úřadu průmyslového vlastnictví

Úřad průmyslového vlastnictví

zapsal podle § 11 odst. 1 zákona č. 478/1992 Sb., v platném znění, do rejstříku

UŽITNÝ VZOR

číslo

27875

na technické řešení uvedené v přiloženém popisu.

ÚŘAD PRŮMYSLOVÉHO VLASTNICTVÍ

V Praze dne 2.3.2015

Za správnost:

Ing. Jan Mrva
vedoucí oddělení rejstříků

Číslo zápisu:	**27875**	Datum zápisu:	02.03.2015
Číslo přihlášky:	**2014-29955**	Datum přihlášení:	10.09.2014

MPT:
C 08 K 5/20 (2006.01)
C 08 L 91/06 (2006.01)
C 08 L 71/00 (2006.01)

Název: Nosné pojivo pro PIM technologie se zlepšenou adhezí

Majitel: Univerzita Tomáše Bati ve Zlíně, Zlín

Původce: prof. Ing. Berenika Hausnerová, Ph.D., Zlín
Ing. Davit Bleyan, Zlín

UŽITNÝ VZOR

(11) Číslo dokumentu:
27 875
(13) Druh dokumentu: **U1**
(51) Int. Cl.:

C08K 5/20	(2006.01)
C08L 91/06	(2006.01)
C08L 71/00	(2006.01)

(19) ČESKÁ REPUBLIKA

ÚŘAD PRŮMYSLOVÉHO VLASTNICTVÍ

(21) Číslo přihlášky: **2014-29955**
(22) Přihlášeno: **10.09.2014**
(47) Zapsáno: **02.03.2015**

(73) Majitel:
Univerzita Tomáše Bati ve Zlíně, Zlín, CZ

(72) Původce:
prof. Ing. Berenika Hausnerová, Ph.D., Zlín, CZ
Ing. Davit Bleyan, Zlín, CZ

(74) Zástupce:
UTB ve Zlíně, Ing. Dana Kreizlová, Nám. T. G. Masaryka 5555, 760 01 Zlín

(54) Název užitného vzoru:
Nosné pojivo pro PIM technologie se zlepšenou adhezí

CZ 27875 U1

Nosné pojivo pro PIM technologie se zlepšenou adhezí

Oblast techniky

Technické řešení se týká nosné pojivové složky pro PIM aplikace. Řešení je uplatnitelné při zpracování keramických i kovových prášků technologií PIM.

Dosavadní stav techniky

Technologie PIM se těší značné pozornosti v oblasti výroby vysoce přesných výrobků pro medicínu, letecký a automobilový průmysl, kde jsou požadovány vysoké objemy výroby s nízkou zpracovatelskou cenou a vysokou produktivitou.

Během procesu se keramický nebo kovový prášek směšuje s polymerními substancemi za vytvoření homogenní suroviny, která je po peletizaci tvářena do žádaného tvaru. S cílem následného odstranění polymerního pojiva se takto získané výrobky v následné fázi zpracovávají chemicky (rozpouštědlem) a tepelně, načež jsou v závěrečné etapě porézní výrobky slinovány do hustoty blízké teoretické.

Tento několikastupňový proces nutně klade často protichůdné požadavky na skladbu pojivového systému, který musí zajišťovat stejnoměrnou distribuci práškových částic bez aglomerace v polymerní surovině během míchání a poskytnout surovinu s viskozitou vhodnou pro proces vstřikování. Pak během uvolňování musí mít pojivový systém vlastnosti umožňující postupný degradační proces a dostatečné napětí k zachování tvaru výrobku až do začátku procesu slinování.

Dalšími benefity jsou pak úspory energie a materiálu v průběhu míchacího a tvářecího procesu.

Nedostatečné splnění kteréhokoliv z těchto požadavků může vést k tvorbě trhlin, dutin, zborcení, nestejnoměrného smrštění a deformací finálního výrobku. Aby mohla být surovina přizpůsobena na míru požadavkům procesu, je vhodné použít vícekomponentní pojivový systém. Typický pojivový systém zahrnuje polyolefiny jako nosné pojivo a zpracovatelská činidla, zejména parafinický vosk. Zpracovávané práškové materiály mají polární charakter, avšak polyolefiny i parafinické vosky jsou nepolární. Z tohoto důvodu je nutné pro zajištění dostatečné adheze mezi částicemi prášku a pojivem používat surfaktanty - např. kyselinu stearovou, a též polární polymery jako další složku polymerního pojiva - např. kopolymery na bázi polyetylenu s vinylacetátem apod. Snahou je nalézt a prověřit pojivovou složku, která při dodržení všech ostatních zpracovatelských parametrů a požadavků vykazuje zlepšené interakce pojivového systému bez použití surfaktantů.

Podstata technického řešení

Uvedené nevýhody a nedostatky dosud známých polymerních pojivových systémů pro PIM aplikace do značné míry odstraňuje nosné pojivo pro PIM technologie se zlepšenou adhezí podle technického řešení. Toto nosné pojivo pro PIM technologie obsahuje 40 až 60 % hmotn. polyetylenglykolové složky, sestávající z jednoho nebo více polyetylenglykolů (PEG) o rozdílných molekulových hmotnostech, a 60 až 40 % hmotn. voskové složky. Podstata technického řešení spočívá v tom, že vosková složka obsahuje 70 až 100 % hmotn. acrawaxu a do 30 % hmotn. parafinického vosku. Acrawax je syntetický vosk na bázi N,N'-ethylen-di(stearamidu) s obsahem N,N'-ethan-1,2-diylbishexadecan-1-amidu.

Výhodou nosného pojiva pro PIM technologii podle technického řešení je především skutečnost, že umožňuje zpracování (míchání, vstřikování) bez přídavku složek zlepšujících adhezi polymerního pojiva k prášku (zpracovatelská činidla tzv. smáčedla či surfaktanty typu kyselina stearová). Další výhodou nosného pojiva podle technického řešení je použití environmentálně benigních složek, z nichž některé jsou rozpustné ve vodě, což přináší další zefektivnění procesu i další energetické úspory. Acrawax vosky zlepšují zpracovatelnost PIM suroviny v důsledku své zvýšené interakce s práškem, čímž zabraňují možné separaci a agregaci částic prášku od pojiva během míchání. Tyto vosky tedy zvyšují smáčivost zpracovávaného prášku a zajišťují rovnoměrné

potažení částic, a tím následně zlepšují úroveň mechanických vlastností získaného materiálu ve srovnání s polyolefiny jako typickým pojivem dosavadních pojivových systémů pro PIM aplikace.

Příklady provedení technického řešení

Příklad 1

Bylo připraveno nosné pojivo pro PIM technologie, které obsahovalo 35 % hmotn. acrawaxu, 15 % hmotn. parafinického vosku, 25 % hmotn. PEG6000 (číselný údaj značí molekulovou hmotnost), 25 % hmotn. PEG4000.

Tzv. self-interaction a asociační energie pro acrawax a polyetylenglykol byly stanoveny pomocí kalorimetrických měření. Též FTIR spektra vykazovala posuny píků odpovídajících C–O, C=O, O–H a N–H vazbám v intervalu od 5.2 do 9.1 cm^{-1}. Z kombinace těchto dvou analýz je patrno, že interakce mezi polyetylenglykolem a acrawaxem jsou více než 2× silnější než při použití předchozí složky - karnaubského vosku.

Příklad 2

Bylo připraveno nosné pojivo pro PIM technologie, které obsahovalo 40 % hmotn. acrawaxu, 20 % hmotn. PEG6000, 20 % hmotn. PEG4000 a 20 % hmotn. PEG1000. Toto nosné pojivo obsahuje pouze acrawaxovou složku na úkor nepolární parafinické, přičemž je nárůst viskozity způsobený úplnou absencí parafinické složky kompenzován nízkomolekulárním polyetylenglykolem PEG1000. Tím se dosáhne potřebné nízké viskozity. Výhodou acrawaxu oproti nepolárnímu parafinickému vosku je právě jeho polarita, a také má lepší interakce s PEG, které u takto nastaveného složení směsi dosahují ve výsledku stejných hodnot jako u příkladu 1.

Příklad 3

Bylo připraveno nosné pojivo pro PIM technologie, které obsahovalo 55 % hmotn. acrawaxu a 45 % hmotn. PEG6000. Toto nosné pojivo je určeno pro případy zpracování prášků s kritickou charakteristikou, kde je i na úkor optimální viskozity nutné maximální posílení vzájemných interakcí mezi pojivem a práškem i mezi složkami pojiva navzájem. Tímto složením nosného pojiva se dosáhne nejlepších výsledků z hlediska adheze PEG a voskové složky pojiva.

Průmyslová využitelnost

Nosné pojivo pro PIM technologie podle technického řešení je využitelné při zpracování keramických i kovových prášků technologií PIM, umožňující získání vysoce přesných výrobků pro medicínu, letecký a automobilový průmysl, kde jsou požadovány vysoké objemy výroby s nízkou zpracovatelskou cenou a vysokou produktivitou.

NÁROKY NA OCHRANU

1. Nosné pojivo pro PIM technologie se zlepšenou adhezí, obsahující 40 až 60 % hmotn. polyetylenglykolové složky, sestávající z jednoho nebo více polyetylenglykolů o rozdílných molekulových hmotnostech, a 60 až 40 % hmotn. voskové složky, **vyznačující se tím**, že vosková složka obsahuje 70 až 100 % hmotn. syntetického vosku na bázi N,N'-ethylen-bis(stearamidu) - acrawaxu - a do 30 % hmotn. parafinického vosku.

Konec dokumentu